

## Advances in 3C-3D design for converted waves

Don C. Lawton, Robert R. Stewart, Andreas Cordsen<sup>1</sup>, and Stacey Hrycak<sup>2</sup>

### ABSTRACT

New developments in 3C-3D survey design for converted waves are shown, using the Blackfoot 3C-3D survey design as an example. The initial Blackfoot design showed high frequency  $P$ - $S$  fold variations when a bin-centred  $P$ - $P$  reflection point acquisition geometry design was used. Asymptotic  $P$ - $S$  fold is smoother when a bin fractionation design is followed. In this case, the Flexi-bin® approach was used to assist in the design of the final survey. The survey consists of 1395 sourcepoints and 903 receivers, recorded in 2 fixed patches with up to 700 receivers per patch. The survey hence can be considered as two, overlapping subsurveys with a number of shots common to both patches. Depth-variant fold mapping capabilities have been developed which show that the actual fold distribution at target horizons will vary significantly with the choice of  $V_p/V_s$ .

### INTRODUCTION

In this paper, we show new developments in the design of 3C-3D surveys for converted waves ( $P$ - $S$ ) and illustrate these ideas using the design plan for the Blackfoot 3C-3D survey. Previously, design of 3C-3D surveys for converted waves (Lawton, 1994) used the asymptotic location of the conversion point with respect to the source-receiver offset; i.e. that the conversion point is depth (time)-invariant and located at a position corresponding to a large depth-to-offset ratio. This work has now been extended to show how bin fractionation using, for example, the Flexi-bin® approach, results in a smooth asymptotic  $P$ - $S$  fold distribution. Also, code has been developed to enable depth-variant fold to be evaluated, based on a user-defined  $V_p/V_s$ . Planning of the Blackfoot survey was based primarily on the asymptotic fold mapping, and a comparison is made with full depth-variant analysis which has recently been completed.

### $P$ - $S$ asymptotic fold distribution

In previous studies (Lawton, 1993, 1994) it was shown that empty bins occur for asymptotic  $P$ - $S$  mapping when  $V_p/V_s = 2$  and if the shot-line spacing is an even integer spacing of the group interval. In this case, empty bins occur in every fourth row in the crossline direction; i.e. parallel to the shot lines. We developed the concept of the *optimum bin size*, based on the natural separation of conversion points at the reflector. This bin dimension,  $\Delta r$ , is given by  $\Delta r = \Delta g / (1.0 + V_s/V_p)$ , where  $\Delta g$  is the

<sup>1</sup> Geophysical Exploration and Development Company Ltd.

<sup>2</sup> Boyd Exploration Consultants Ltd.

Note: Colour versions of figures appear at the end of this document.

group interval. As an example, for  $V_p/V_s = 2$  and  $\Delta g = 60\text{m}$ , the normal CMP bin dimension for  $P$ - $P$  data would be 30m, whereas the optimum bin dimension for  $P$ - $S$  data would be 40m. While this provides smooth  $P$ - $S$  fold with no empty bins, it is undesirable to have different numbers of traces in the  $P$ - $P$  and  $P$ - $S$  data volumes for interpretation, particularly when trace-by-trace correlations are undertaken. It was found that it was also possible to avoid empty bins by setting the shot line interval to an odd integer multiple of the group interval. This was shown (Lawton, 1994) to produce a high frequency variation in the fold and that the fold in adjacent bins oscillated about the mean  $P$ - $P$  fold for equivalent bins.

All of the designs used previously and discussed above used bin-centred  $P$ - $P$  reflection points, in which the reflection points all cluster at the centre of the bin. With the geometries used,  $P$ - $S$  conversion points are distributed within the bins, but at separations which are not a simple fraction of the regular bin size (for  $P$ - $P$  bin dimensions).

An alternative design strategy using the Flexi-bin® concept has recently been proposed by Geophysical Exploration and Development Corporation (GEDCO), in which the conversion points are distributed at even 10m intervals in both the in-line and cross-line directions. This approach results in a more even fold distribution for  $P$ - $S$  data with asymptotic conversion points. However, it does also result in distributed midpoints for  $P$ - $P$  data. An example of this design approach is shown later in the discussion of the Blackfoot survey.

### **Depth-variant $P$ - $S$ fold distribution.**

The asymptotic approximation for mapping  $P$ - $S$  conversion points is adequate when the source-receiver offset is less than about half the target depth. However, as the offset-to-depth ratio increases, the conversion point moves closer toward the receiver location. For  $V_p/V_s = 2$ , the displacement of the conversion point from the asymptotic location is about 3.5% when the source-receiver offset is equal to the reflector depth. Hence for a depth of 1500m, the conversion point will be displaced about 52m from the asymptotic location point. Although this value is not large, it will result in the trace being moved 1 or 2 bins. However, this displacement will increase at greater source-receiver offsets and will also be affected by the rms  $P$ -wave and  $S$ -wave velocities above the reflector.

The 3C-3D design software developed within CREWES now includes a simple raytracing routine which computes depth-variant conversion points for a specified acquisition geometry and a simple velocity model. These conversion point coordinates are then used to display fold, offset and azimuth information within each bin in the data volume.

### **Offset distribution quality factor**

Work has also continued on a colour-coded display showing the quality of the offset distribution within each bin. At present the ideal model is one in which the source-receiver offsets within a bin are equally distributed between the minimum and maximum specified offsets. The offset distribution quality factor developed is defined as the linear regression correlation coefficient between the model and actual offsets, weighted by the slope of the cross-plot between the model and actual data. Hence, a perfect offset distribution with a cross-plot slope of 45 degrees would have a quality factor of unity. Colour displays of the quality factor provide a semi-quantitative evaluation of the offset distribution over the entire survey area. The display can also be limited to show only bins which have a fold which exceed a user-defined threshold.

## **BLACKFOOT 3C-3D SEISMIC SURVEY**

### **Introduction**

In the spring of 1995, Boyd Exploration Consultants Ltd and the CREWES Project proposed a 3C-3D seismic survey to evaluate the effectiveness of integrated *P-P* and *P-S* surveys for improved hydrocarbon exploration. The objectives are to demonstrate that 3C-3D seismic data can build on and improve conventional 3D *P*-wave data, provide additional stratigraphic and structural images of the subsurface, discriminate lithology, and test for anisotropy which may be caused by fracturing and regional stress directions. A number of proposals for the location of the survey were submitted from industry, and the site chosen was over the Blackfoot field near Strathmore Alberta (Township 23, Range 23 W4M). A stratigraphic column of Cretaceous rocks in this area is shown in Figure 1. The primary target horizon of the 3C-3D survey is the Glauconitic Member of the Mannville Group. Glauconitic sandstones and shales fill valleys which were incised into the regional Lower Mannville stratigraphy. In particular, the Ostracod and Bantry Shale Members of the Lower Mannville Formation were truncated by the valleys. Older valley-fills also occur in the Sunburst and Detrital Members (Figure 1). The Glauconitic reservoir sands occur at a depth of 1550 m.

In the Blackfoot area, a Glauconitic valley-fill was interpreted from wells and a previous 3D *P*-wave seismic survey conducted by PanCanadian Petroleum Ltd. The interpreted trend of the valley, based on the well information, is shown in Figure 2. Good channel sands were encountered in wells in the southern part of the area shown (e.g. 08-08 well), but the channel-fill facies appears to be a shale plug to the north at the 12-16 well. Prime objectives of the 3C-3D survey are to discriminate channel and regional seismic signatures, and to distinguish between sand-fill and shale-fill within the channel. A secondary objective of the 3C-3D survey is to characterise the *P-S* response of deeper Paleozoic carbonates

(Beaverhill Lake Fm) around the location of a deep well slightly to the east of the channel trend shown in Figure 2.

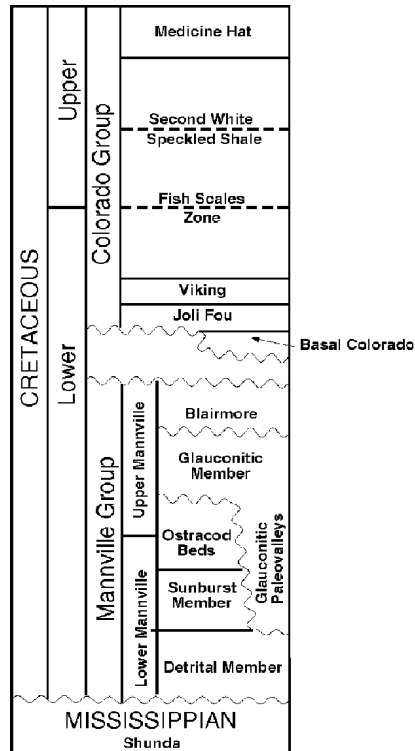


Fig 1. Stratigraphic column of Cretaceous rocks in the Blackfoot area.

### Broad-band 3C-2D survey

The CREWES Project recorded a line 4 km long across part of the Blackfoot field during the summer of 1995. The purpose was to compare characteristics of various types of multicomponent geophones as well as to obtain a template multicomponent seismic line which could be used for planning the 3C-3D survey. Results from this survey are contained in other papers in this Research Report, with a preliminary interpretation of some of the *P-P* and *P-S* data presented by Miller et al. (this volume).

Common offset stacks of the *P-P* and *P-S* data from the broad-band survey are shown in Figures 3 and 4 respectively. The outside mute pattern used during processing is shown on these plots and show the effective offset range that will contribute to the final stacks. Shallow (Glauconitic) and deep (Beaverhill Lake) targets are indicated on these sections. Effective offset ranges are shown in Table 1.

Table 1. Effective offset ranges for Blackfoot 3C-3D survey

Glauconic ( <i>P-P</i> )	0 - 1500 m
Glauconic ( <i>P-S</i> )	300 - 1700 m
Beaverhill Lake ( <i>P-P</i> )	0 - 2700 m
Beaverhill Lake ( <i>P-S</i> )	400 - 2900 m

The near offset limit for *P-S* data is due to the fact that there is no conversion at zero offset and that the converted-wave amplitude builds with increasing offset. Evaluation of the 2D data also showed that subsurface coverage in excess of about 35 fold is required to properly image the target horizons for both *P-P* and *P-S* data

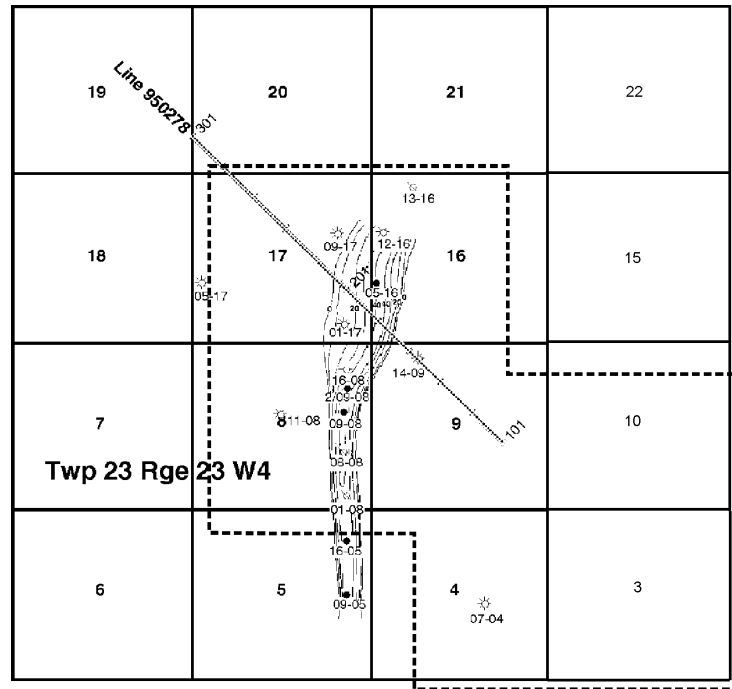


Fig 2. Base map of Blackfoot area. The 3C-3D survey area is shown by the dashed line.

**Design 1: Bin-centred geometry**

Table 2 shows the acquisition parameters for design option 1. The acquisition geometry was established in order to obtain about 40 fold over the Glauconic channel using the effective offsets shown in Table 1. It was also recommended that the maximum bin dimension should be 30 m in order to have an adequate number of bins located within the Glauconic channel. The receiver effort was reduced over the deeper target area in order to cut down on the total number of receivers that were required for the program.

This geometry would require 2907 live channels and the layout of source and receiver lines is shown in Figure 5. *P-P* fold for offsets limited from 0 to 1500 m is shown in Figure 6. It is smooth over the target areas, with 40 fold over the Glauconitic channel and about 22 around the deep target (14-3 well). Asymptotic *P-S* fold is shown in Figure 7 for offsets between 300 m and 17 00 m. It shows the expected high frequency fold variations between adjacent bins, ranging between 40 and 80 fold over the area of the Glauconitic channel, and between about 20 and 40 around the 14-3 well. Increasing the bin dimension to the optimum size (40 m x 40 m) results in smoother *P-S* fold of up to 80 over the channel and 40 fold at the 14-3 well.

Table 2. Acquisition parameters for design option 1.

*Source parameters:*

Line orientation:	North-south
Source interval:	60 m
Source line interval:	180 m
Number of source lines:	26
Total number of sourcepoints:	1504

*Receiver parameters:*

Line orientation:	East-west
Receiver interval:	60 m
Receiver line interval:	240 m (Glauconitic); 480 m (Beaverhill Lake)
Number of receiver lines:	19
Total number of receivers:	969

*Patch:*

All receivers live for all shots

However, the total cost for this proposed program was in excess of the budget available so it was necessary to reduce the total number of sourcepoints and required channel capacity. Also, there were only slightly over 700 3-component geophones available, so it was also required to reduce the number of live geophones being recorded for each shot. Reduction in patch size to 700 live receivers (2100 recording channels) would not compromise patch quality significantly since source-receiver offsets in excess of 2900 m would not contribute significantly to the final data volumes.

### P-P common-offset stacks

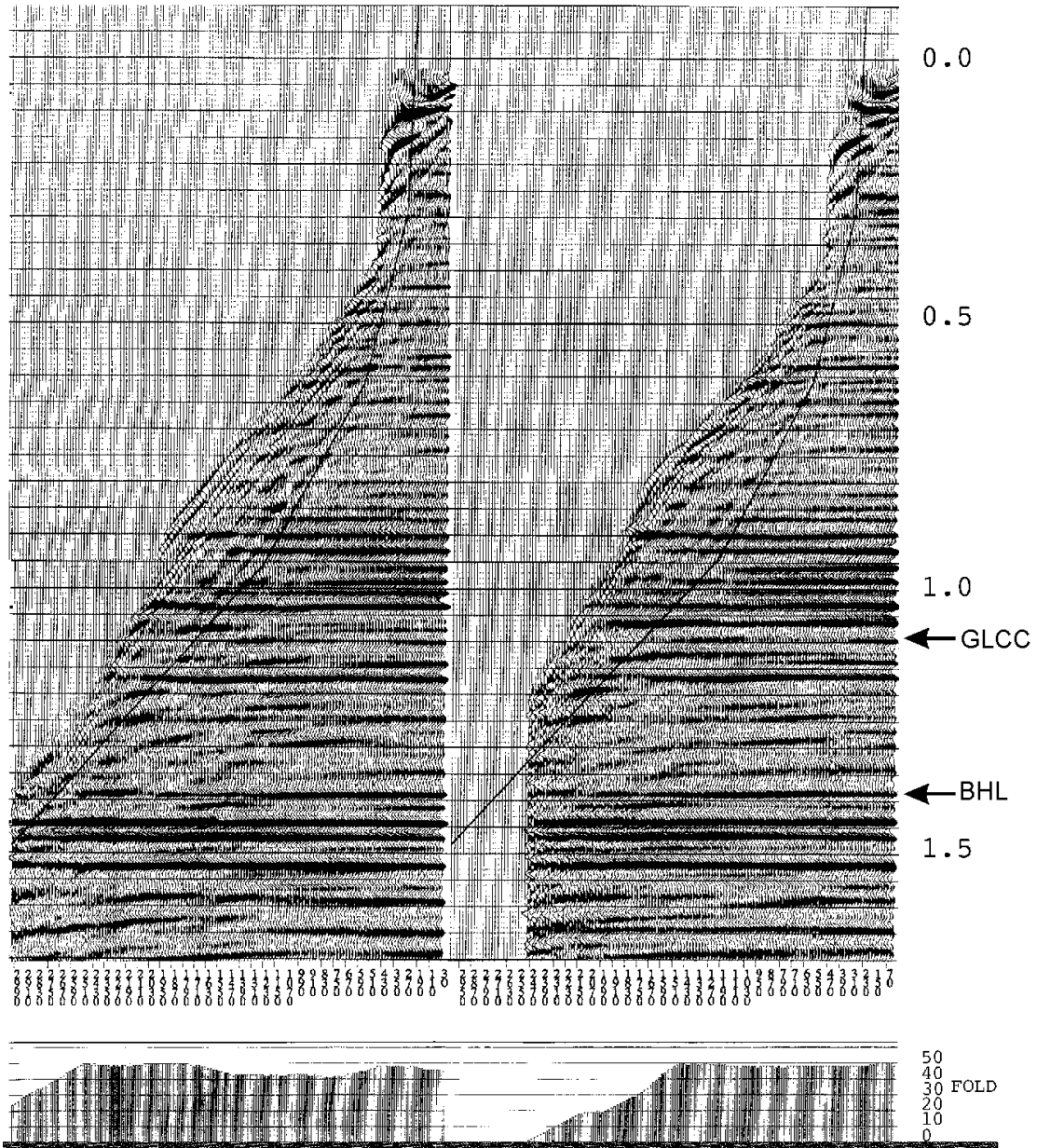


Fig 3. P-P common offset stack from Blackfoot 3C-2D line. Target levels are indicated (GLCC = Glauconitic; BHL = Beaverhill Lake). Outside mute pattern is shown by line.

### P-S common-offset stacks

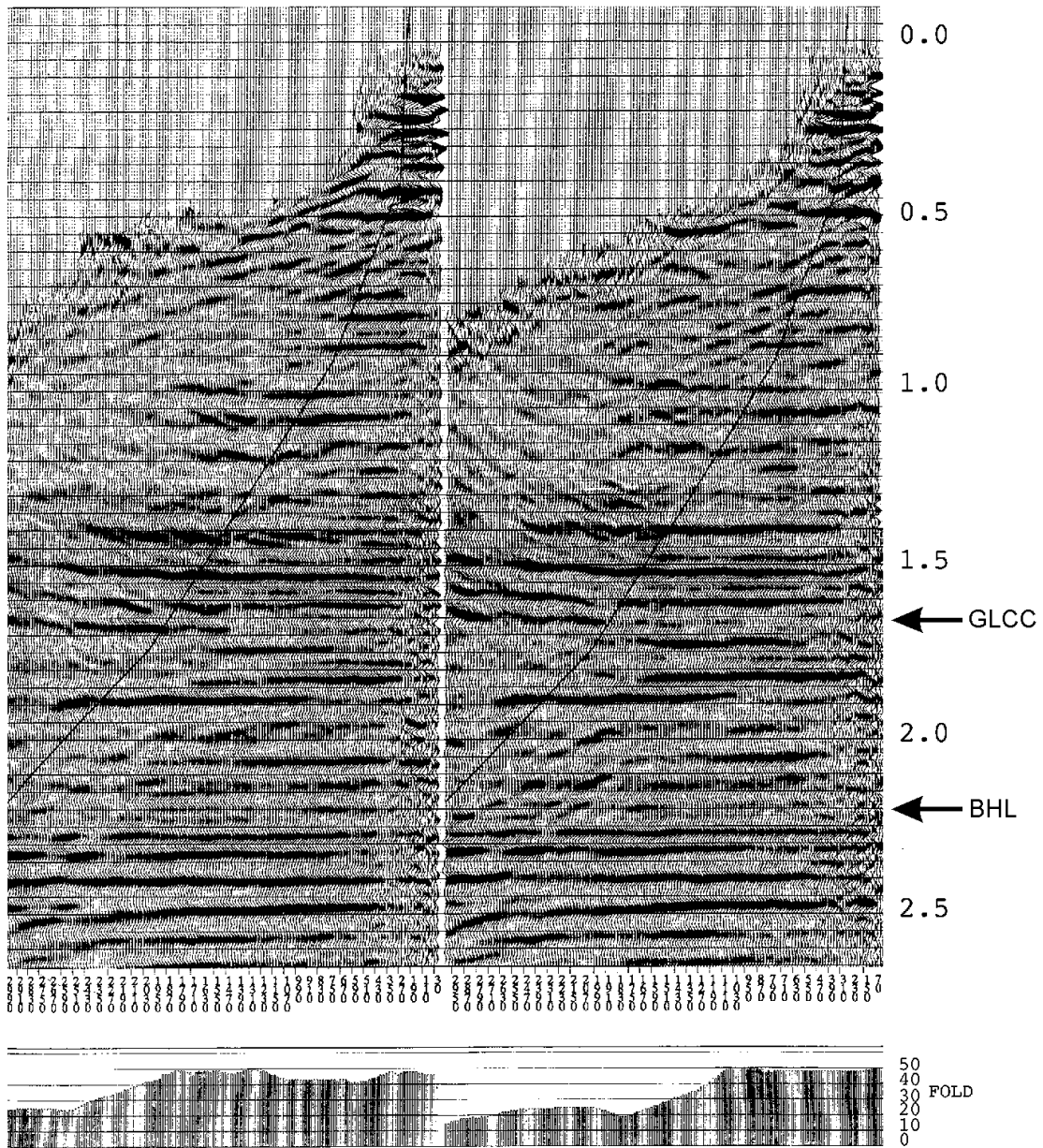


Fig 4. P-S common offset stack from Blackfoot 3C-2D line. Target levels are indicated (GLCC = Glauconitic; BHL = Beaverhill Lake). Outside mute pattern is shown by line.

**Design 2: Distributed reflection/conversion points (Flex-bin®)**

Table 3 shows the acquisition parameters for design option 2. The acquisition geometry was established in order to reduce the number of sourcepoints to less than 1400, and record an active patch of up to 700 geophones (2100 channels). An additional benefit of this geometry was that it provides smooth asymptotic fold for *P-S* data using the standard 30 m x 30 m bin dimension, with an average fold of 36 at the Glauconitic level. The receiver effort was still reduced over the deeper target area in order that imaging of the Glauconitic target was not compromised with the available budget.

Table 3. Acquisition parameters for design option 2.

*Source parameters:*

Line orientation:	North-south
Source interval:	60 m
Source line interval:	210 m
Number of source lines:	24
Total number of sourcepoints:	1395

*Receiver parameters:*

Line orientation:	East-west
Receiver interval:	60 m
Receiver line interval:	255 m (Glauconitic); 495 m (Beaverhill Lake)
Number of receiver lines:	18
Total number of receivers:	903

*Patch:*

Number of patches:	2
Live geophones/ patch:	up to 700.

The survey layout for this design is shown in Figure 9. Because of the extra care required to lay out 3-component geophones, it has been decided to not have a rolling patch, but to shoot the survey into two patches, one over the Glauconitic target (“Glauconitic patch”) and the other over the deeper carbonate target (“BHL patch”). *P-P* fold for offsets limited from 0 to 1500 m is shown in Figure 10. It is quite smooth over the target areas, with 36 fold over the Glauconitic patch and about 15 within the BHL patch. Asymptotic *P-S* fold is shown in Figure 11 for source-receiver offsets of between 300 m and 1700 m. Fold averages about 40 within the Glauconitic patch and

about 22 over the BHL patch. The distribution of near offsets for  $P$ - $S$  data is shown in Figure 11 and is seen to be close to the desired value of 300 m over the Glauconitic patch. East-west stripes with larger near offsets (about 550 m) occur between receiver lines over the BHL patch, due to the increased receiver line spacing in this area. Distribution of far offsets for the  $P$ - $S$  data is displayed in Figure 13 and is seen to be close to the desired value of 1700 m over most of the survey area. Total offset range is displayed in Figure 14. Stripes occur in the BHL patch due to the larger near offsets along these bins.

It is useful to evaluate which offsets contribute most to bin fold, since  $P$ - $S$  amplitudes are not constant across the entire range of offsets captured. Figures 15 through 17 show  $P$ - $S$  fold for near (300-700 m), middle (700-1200 m) and far offset (1200 - 1700 m) ranges, respectively. For the Glauconitic patch, the near offset range contributes mostly to bins between the receiver lines, whereas the middle offset range contributes mostly to bins clustered near the receiver lines. The far offsets contribute quite smoothly to all bins across the Glauconitic patch, with a slight increase in contribution along the receiver lines. The offset distribution quality factor for all offsets in the 300-1700 m offset range, and for bins with fold greater than 15, is shown in Figure 18. Consistent factors of between 0.8 and 0.9 are obtained over the Glauconitic patch, indicating that the offset distribution in this part of the survey is good. The quality factor is lower over the BHL patch, as expected, since the survey design for this patch was optimised for the deeper target.

Azimuthal distribution for asymptotic  $P$ - $S$  data is best evaluated by examining fold for the full offset range within limited source-receiver azimuth apertures. Figures 19 through 22 show asymptotic  $P$ - $S$  fold for azimuths divided into 4 quadrants, each spanning 90°. These displays show similar fold distributions for the 4 azimuths over the Glauconitic patch. Note that the area of maximum coverage within each display is displaced in the direction of the average azimuth because of the asymmetry in the  $P$ - $S$  raypath.

### **Depth-variant analysis**

The Blackfoot survey was also modelled using a depth-variant conversion point. A  $V_p/V_s$  ratio of 1.9 was used as this is an average value for the Upper Mannville interval determined from dipole sonic logs and interpretation of the 3C-2D data (Miller et al., this volume). Figure 23 displays  $P$ - $S$  fold for offsets from 300 m to 1700 m, and shows that the fold distribution is not quite as even as that determined using the asymptotic approach (Figure 11). Fold varies from about 35 to 50 over the central part of the Glauconitic patch, and generally is highest between receiver lines. Figures 24 through 26 show fold for the same limited offset ranges as shown for asymptotic modelling in Figures 15 through 18. Examination of Figures 24 through 26 show that for the near and far offset ranges, the highest fold bins cluster between the receiver lines, whereas in the mid-offset ranges, the highest fold clusters along the receiver lines.

Several tests showed that the actual fold pattern which develops is quite sensitive to  $V_p/V_s$ , so that comprehensive knowledge of this ratio is important for optimum design. The offset distribution quality for conversion point modelling is shown in Figure 27 and is similar to that determined using the asymptotic assumption (Figure 18).

Fold and offset distribution for the deeper Paleozoic target were also determined. Figures 28 and 29 show  $P-P$  and  $P-S$  fold respectively, for source-receiver offsets of 0-2700 m for the  $P-P$  data, and 400-2900 m for the  $P-S$  data. The  $P-P$  fold around the 14-3 well in the BHL patch is about 60, increasing to over 100 within the Glauconitic patch. The  $P-S$  asymptotic fold (Figure 29) oscillates between 30 and 50 within the BHL patch, with stripes parallel to the receiver lines. Figure 30 shows that the  $P-S$  offset range is excellent over the Glauconitic patch, and acceptable over the BHL patch. Offset distribution quality (Figure 31) shows some significant stripes within the BHL patch, although it is good at the 14-3 well.

Depth-variant  $P-S$  fold distribution was also undertaken for the deeper target, at a depth of 2370 m and assuming  $V_p/V_s = 2$ . Figure 32 shows that the  $P-S$  fold over the BHL patch is less uniform than that obtained using asymptotic mapping, with the highest fold being generated along the receiver lines. It is clear that the wide receiver line spacing in this part of the survey is not optimum. Total offset range (Figure 33) is excellent over the Glauconitic patch, but still shows a striped pattern over the BHL patch, with rather poor values at the 14-3 well location. Offset distribution quality is generally not as good as that determined with asymptotic mapping.

## CONCLUSIONS

This paper illustrates the approach used to design a 3C-3D survey for converted waves using the Blackfoot survey as an example. Asymptotic fold mapping shows high frequency  $P-S$  fold variations when a bin-centred  $P-P$  reflection point acquisition geometry design is used. Asymptotic  $P-S$  fold is smoother when a bin fractionation design is followed. In this case, the Flexi-bin® approach was used to assist in the design of the final survey. Depth-variant fold mapping was also developed and shows that actual fold distribution at the target horizons will vary significantly with  $V_p/V_s$ .

## ACKNOWLEDGEMENTS

We thank the Technical Advisory Group of the Blackfoot Project for valuable input into the design parameters. These people are John Boyd, Louis Blinn, Zig Doborzynski, Larry Mewhort, Darren Kondrat and Garth Syhlonyk. PanCanadian Petroleum Ltd provided geological, well and seismic data from the project area which was useful for assisting in the 3C-3D survey design.

REFERENCES

- Lawton, D.C., 1994, Acquisition design for 3-D converted waves: CREWES Project, Annual Research Report, Volume 6, 23.1-23.23.  
 Lawton, D.C., 1993, Optimum bin size for converted-wave 3-D asymptotic mapping: CREWES Project, Annual Research Report, Volume 5, 28.1-28.16.

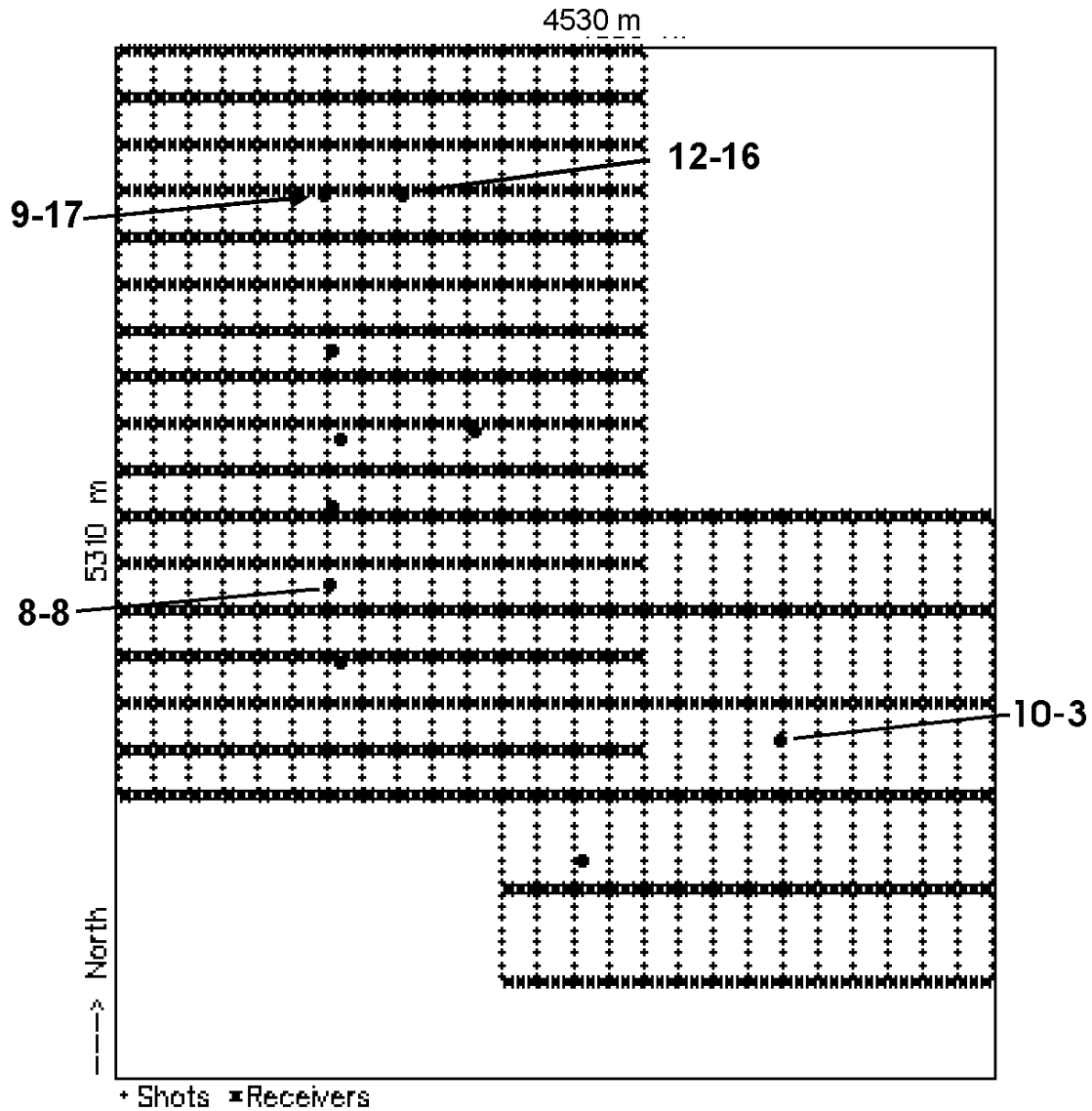


Fig. 5. Source and receive line geometry for design option 1. P-P midpoints are centred in each bin. Wells are shown by position only. Source line interval = 180 m; receiver line interval = 240 m over Glauconitic patch and 480 m over the BHL patch.

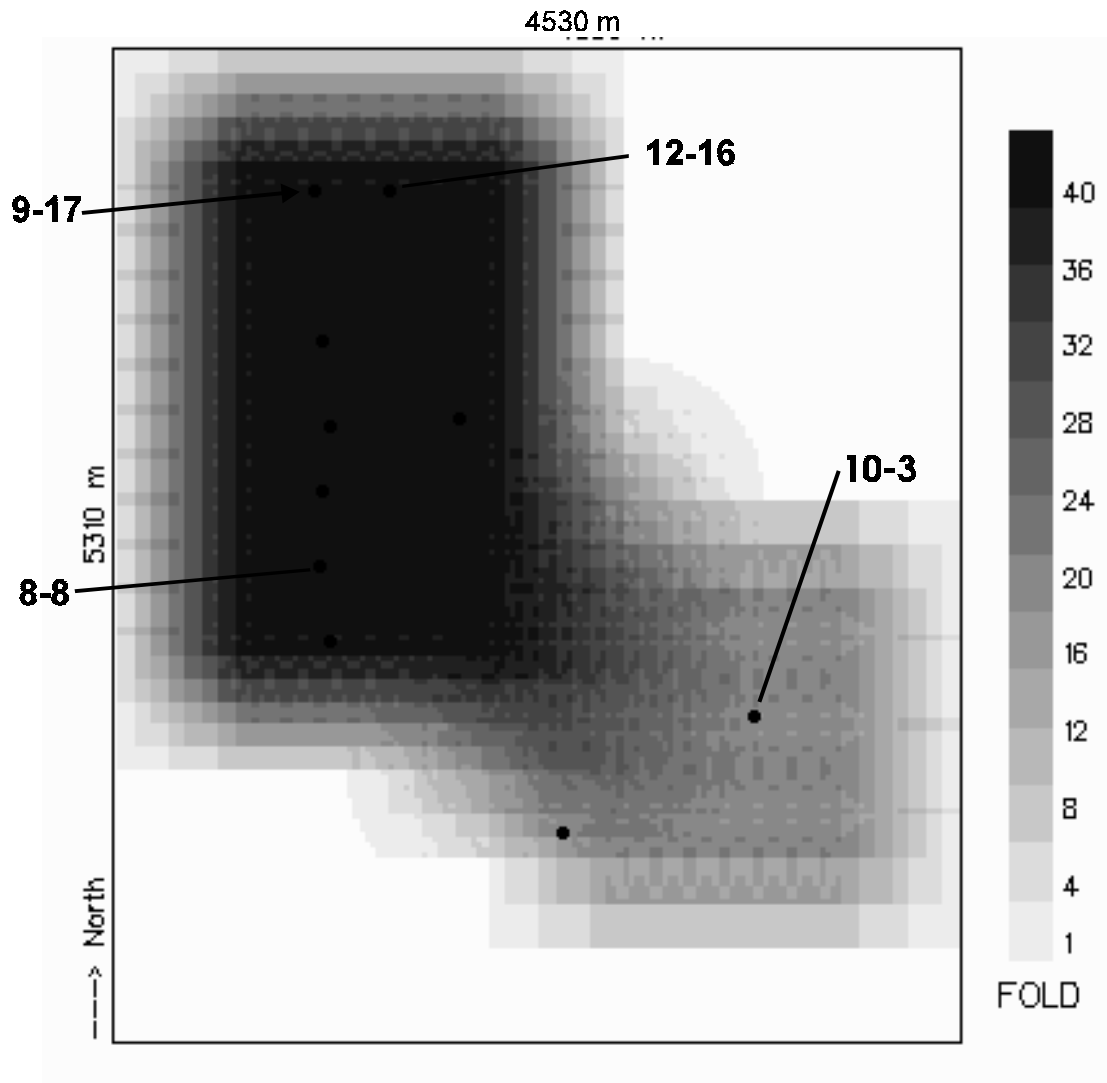


Fig. 6. P-P fold, Glauconitic target for design option 1. Offsets limited from 0 - 1500 m. Bin size is 30 m x 30 m.

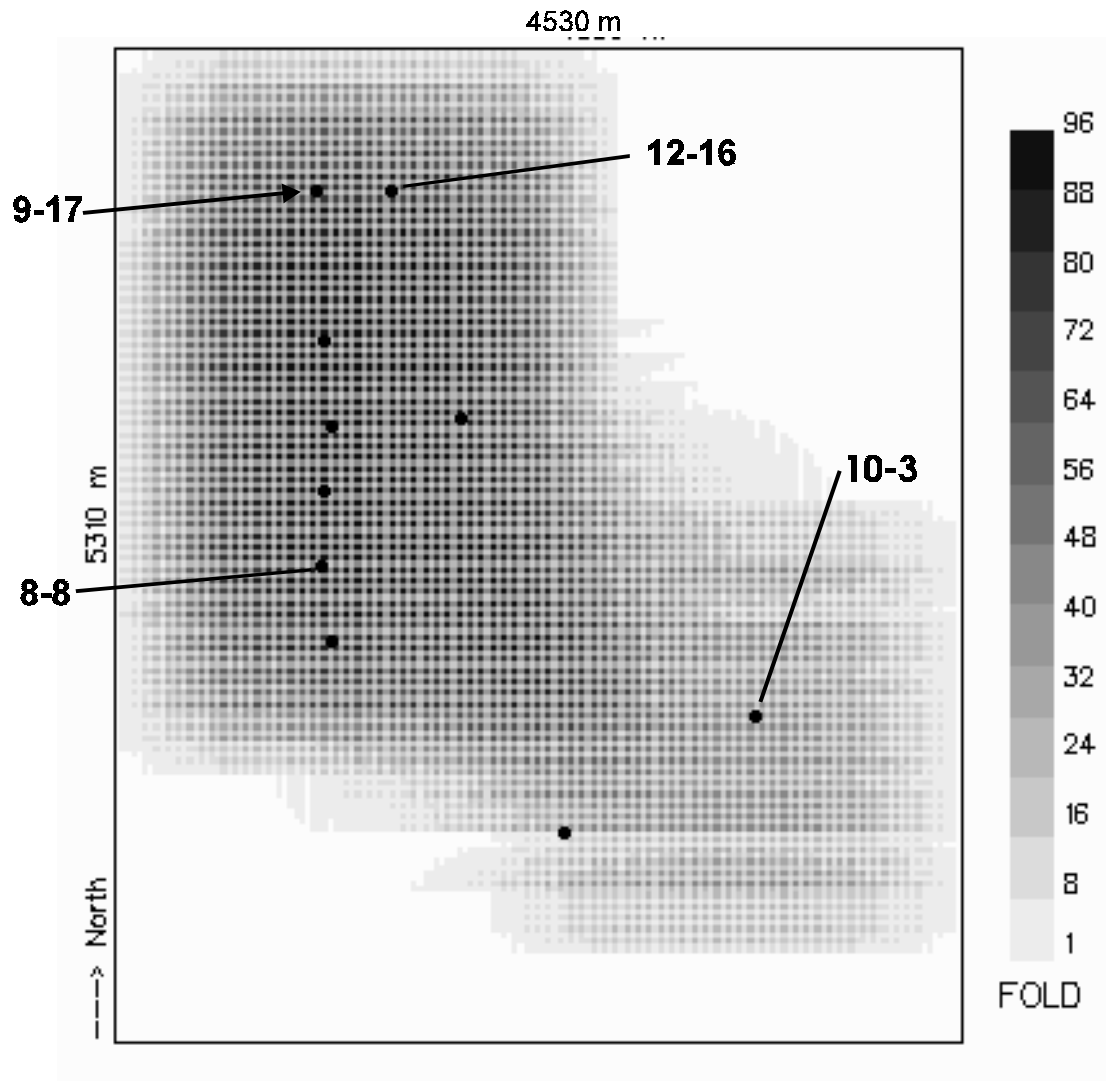


Fig. 7. Asymptotic P-S fold, Glauconitic target for design option 1. Offsets are limited from 300 -1700 m. Bin size is 30 m x 30 m.

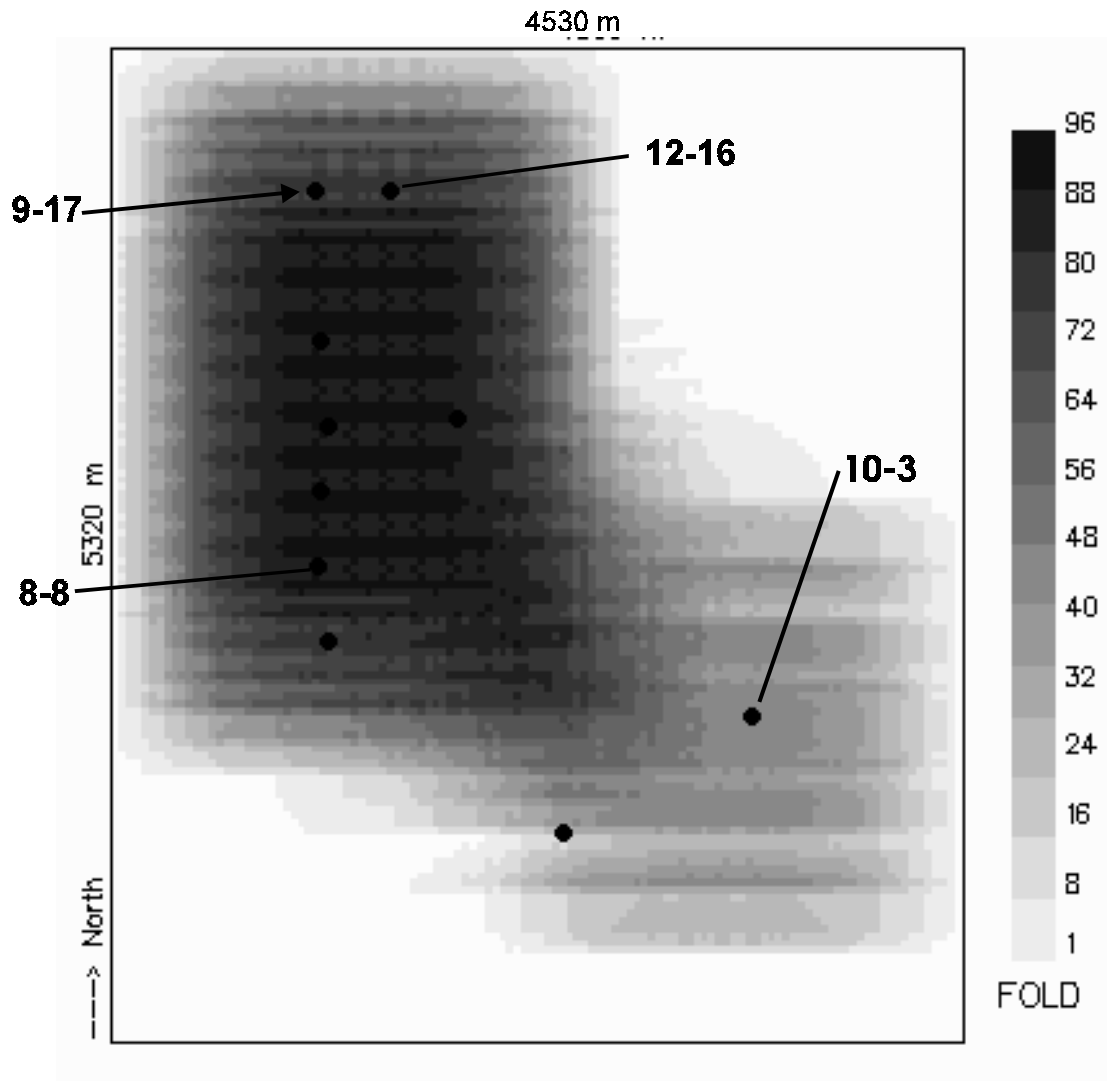


Fig. 8. Asymptotic P-S fold, Glauconitic target for design option 1. Offsets are limited from 300 - 1700 m, bin size of 40 m x 40 m.

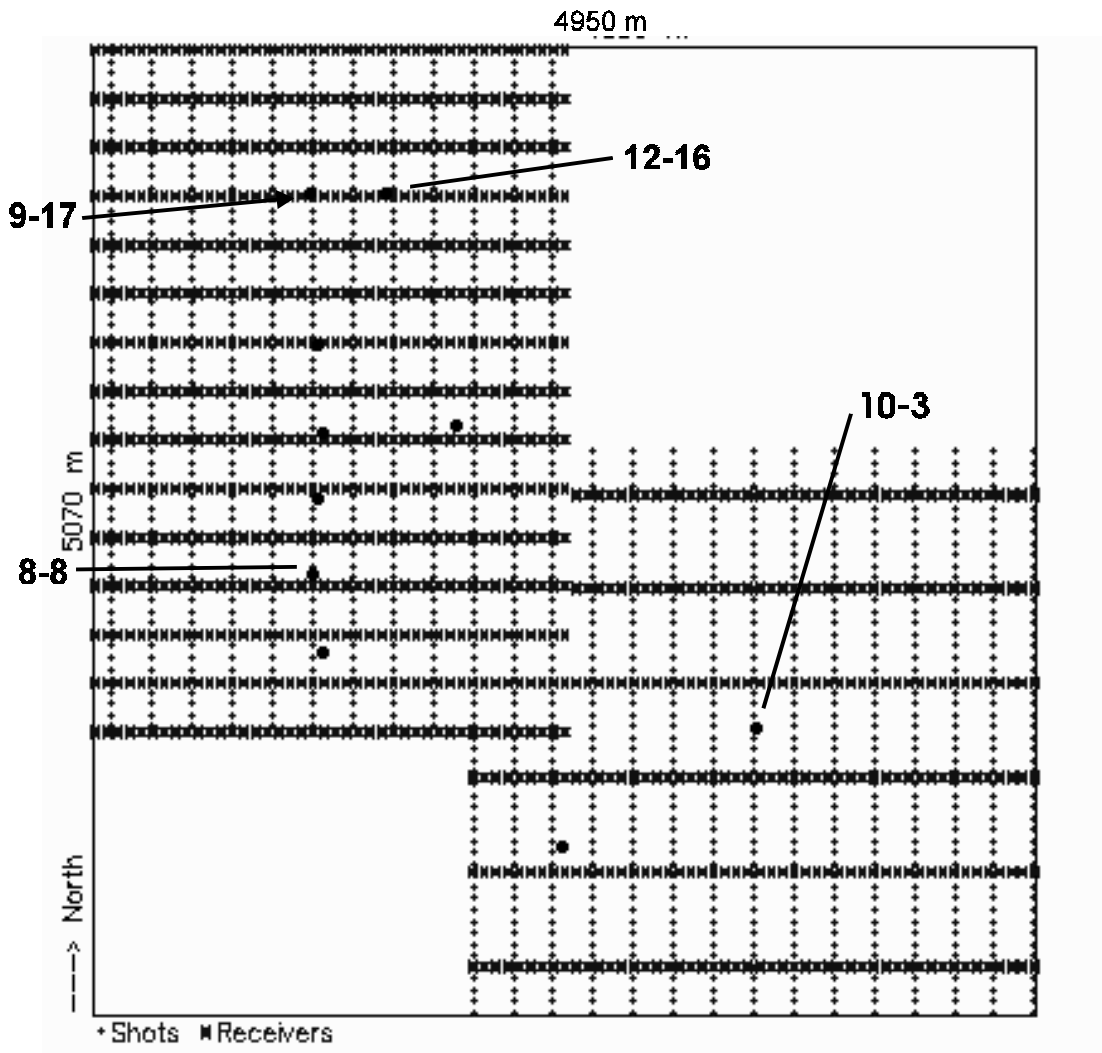


Fig. 9. Source and receiver line geometry for design option 2. P-P midpoints are distributed within each bin according to Flexi-bin design. Wells are shown by position only. Source line interval = 210 m; receiver line interval = 255 m over Glauconitic patch and 495 m over the BHL patch.

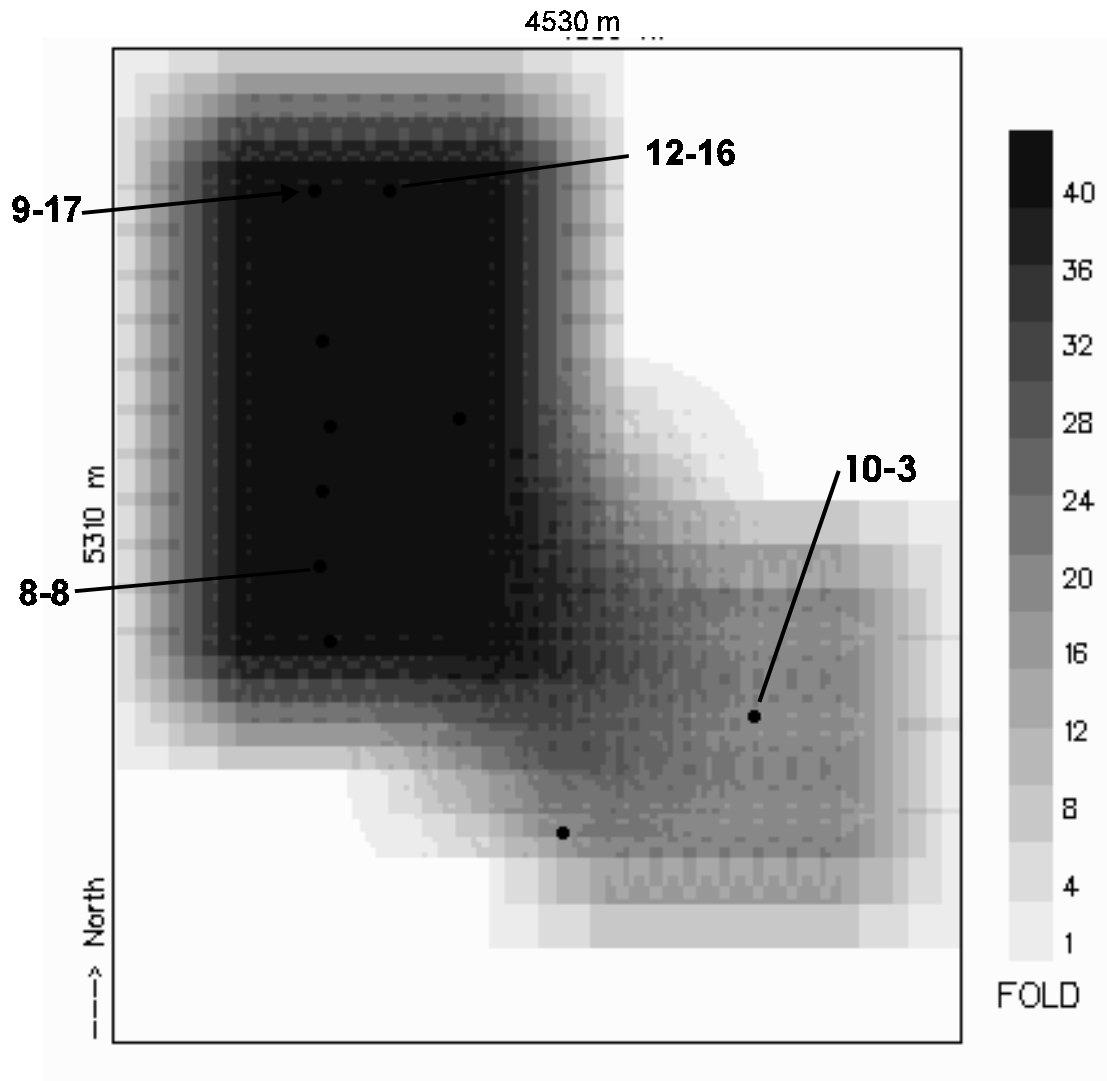


Fig. 10. P-P fold using Flexi-bin geometry, Glauconitic target for design option 2. Offsets limited from 0 - 1500 m. Bin size is 30 m x 30 m.

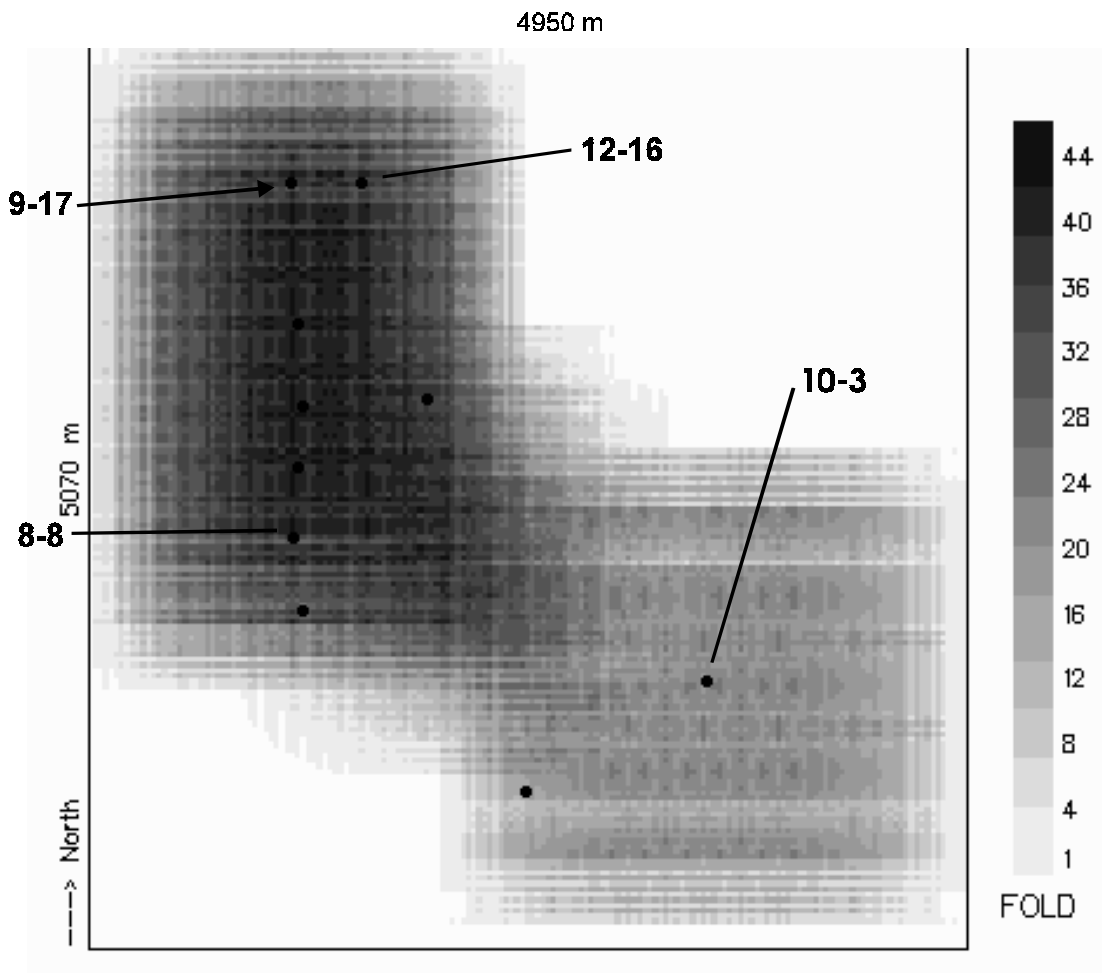


Fig. 11. Asymptotic P-S fold, Glauconitic target for design option 2. Offsets are limited from 300 -1700 m. Bin size is 30 m x 30 m.

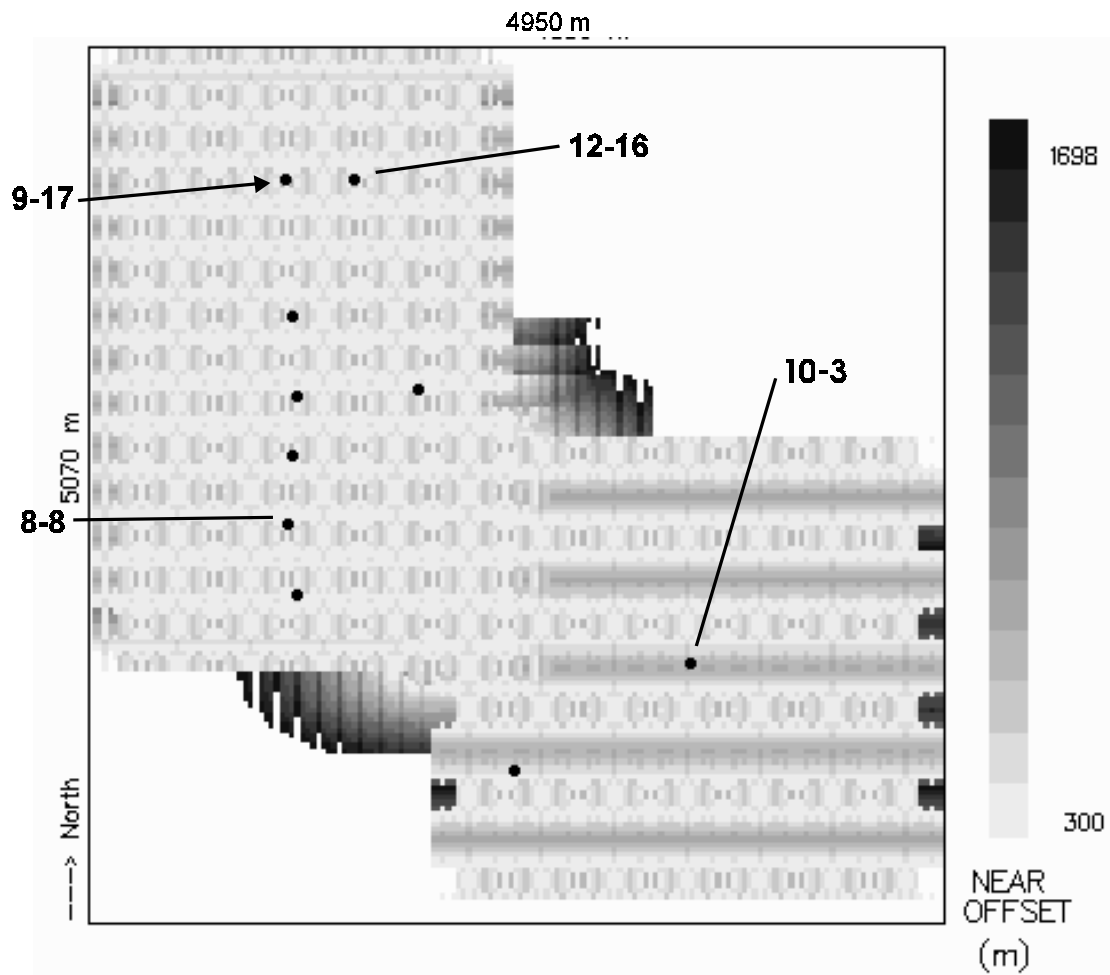


Fig. 12. Near offset distribution for asymptotic P-S fold, Glauconitic target for design option 2. Offsets are limited from 300 -1700 m. Bin size is 30 m x 30 m.

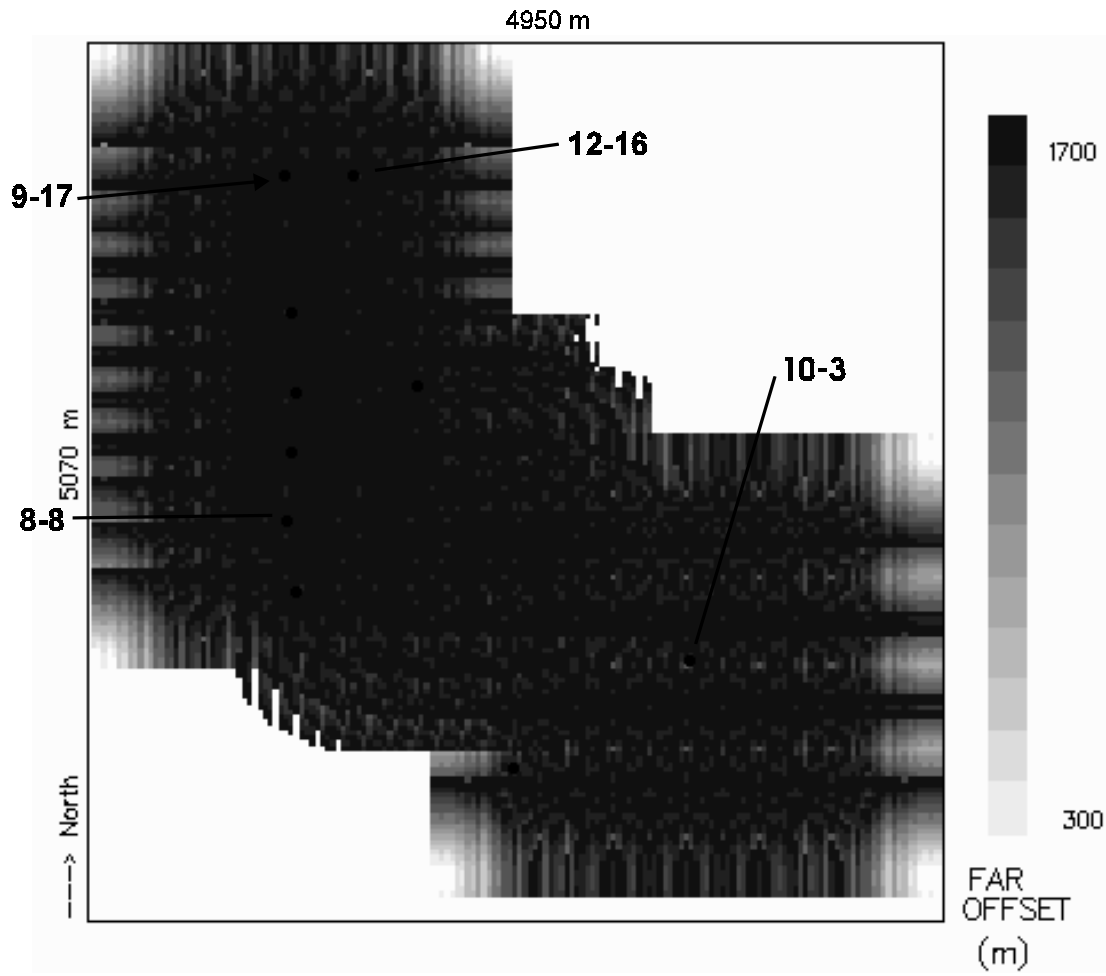


Fig. 13. Far offset distribution for asymptotic P-S fold, Glauconitic target for design option 2. Offsets are limited from 300 -1700 m. Bin size is 30 m x 30 m.

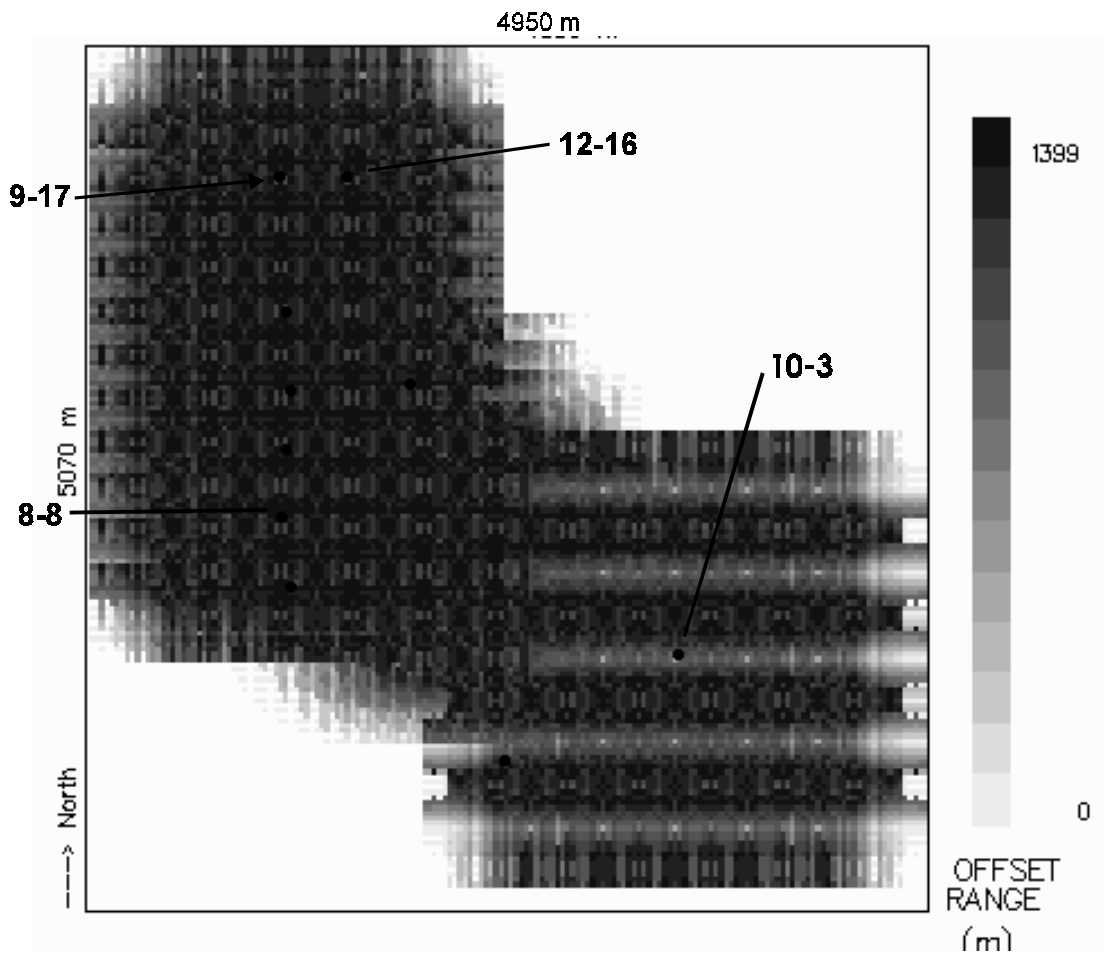


Fig. 14. Offset range for asymptotic P-S fold, Glauconitic target for design option 2. Offsets are limited from 300 -1700 m. Bin size is 30 m x 30 m.

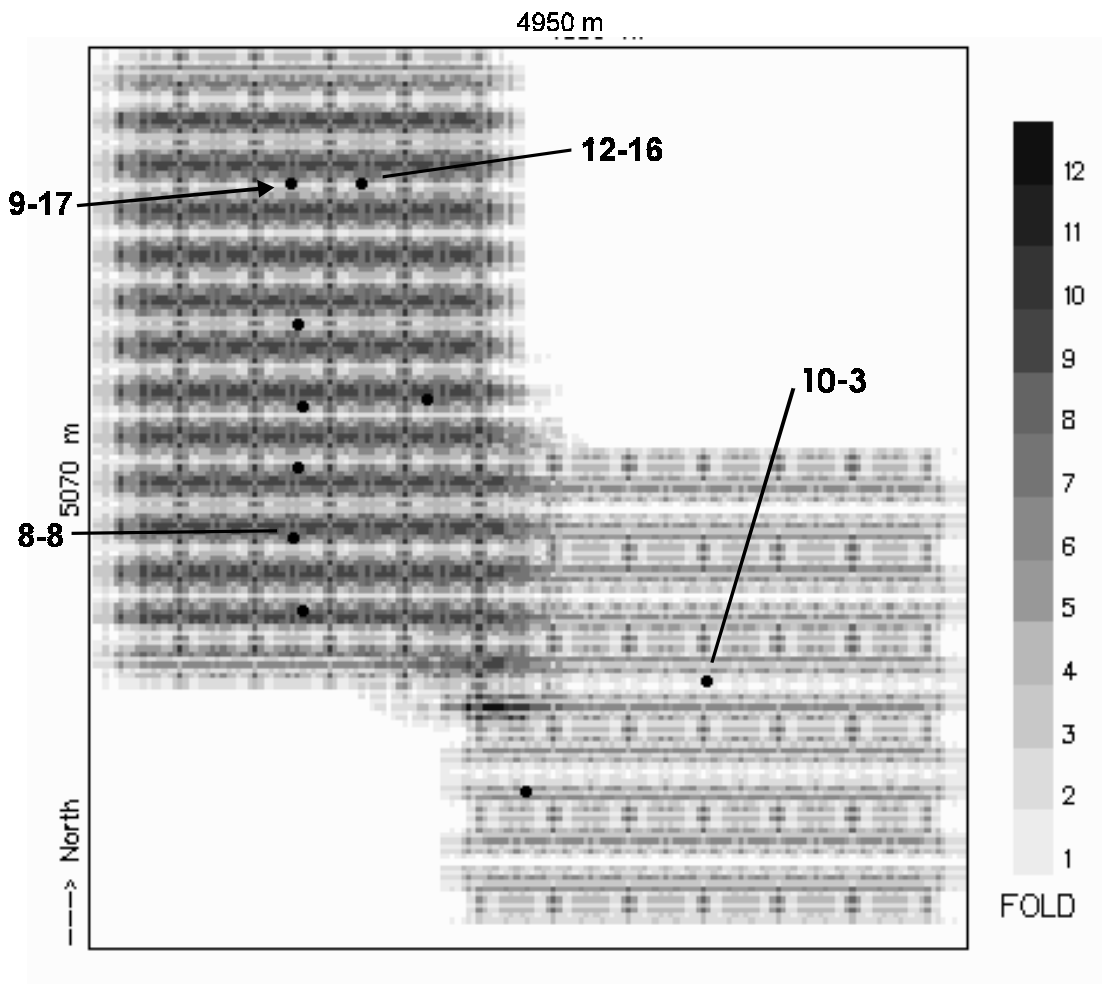


Fig. 15. Near offset fold for asymptotic P-S fold, Glauconitic target for design option 2. Offsets are limited from 300 - 700 m. Bin size is 30 m x 30 m.

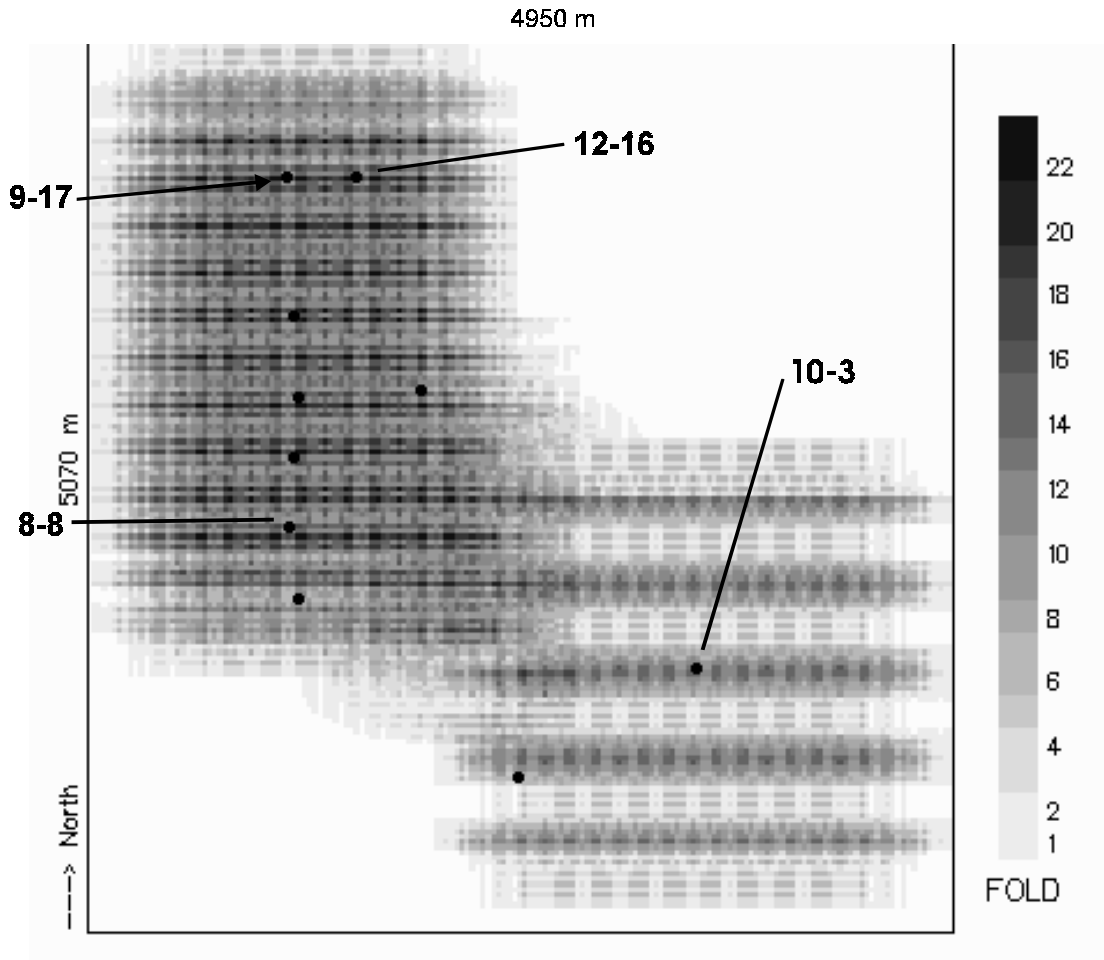


Fig. 16. Middle offset fold for asymptotic P-S fold, Glauconitic target for design option 2. Offsets are limited from 700 - 1200 m. Bin size is 30 m x 30 m.

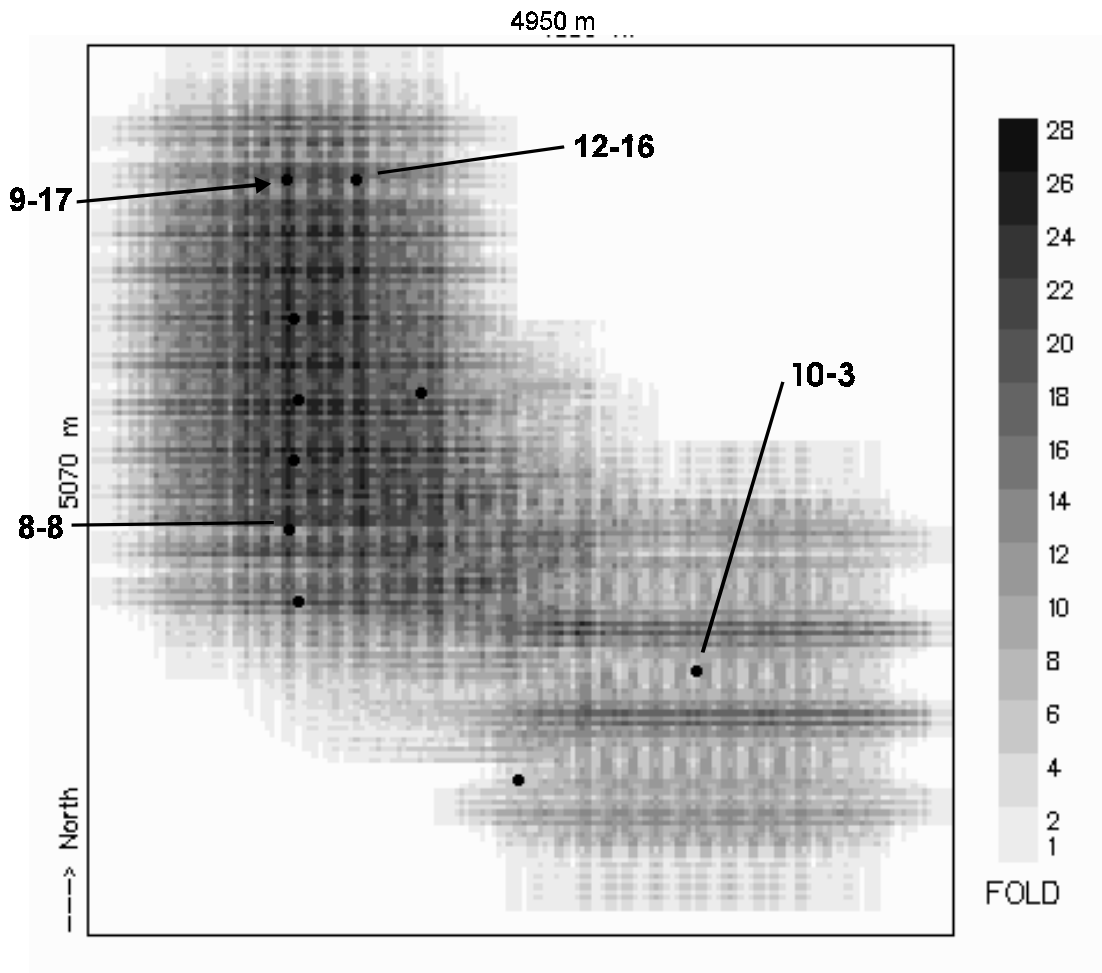


Fig. 17. Far offset fold for asymptotic P-S fold, Glauconitic target for design option 2. Offsets are limited from 1200 - 1700 m. Bin size is 30 m x 30 m.

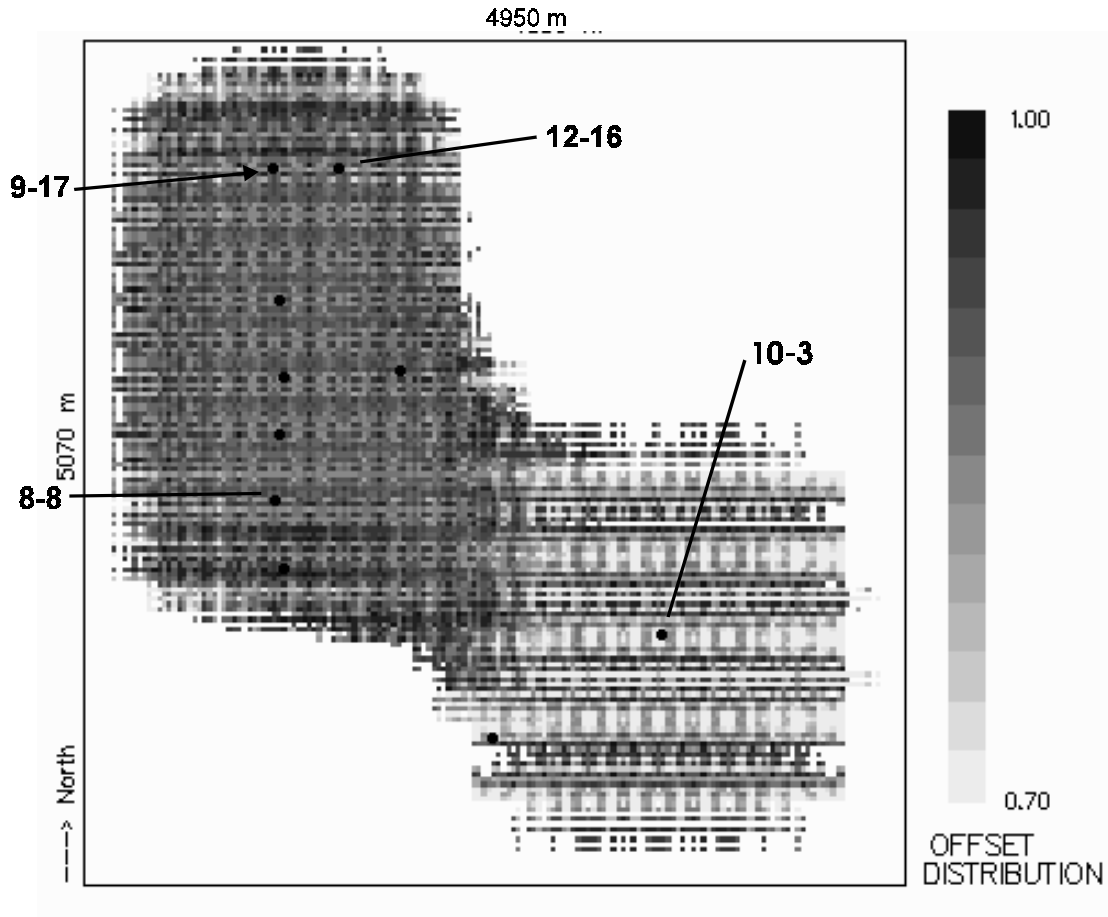


Fig. 18. Offset distribution quality factor for asymptotic P-S fold, Glauconitic target for design option 2. Offsets are limited from 300 - 1700 m. Bin size is 30 m x 30 m.

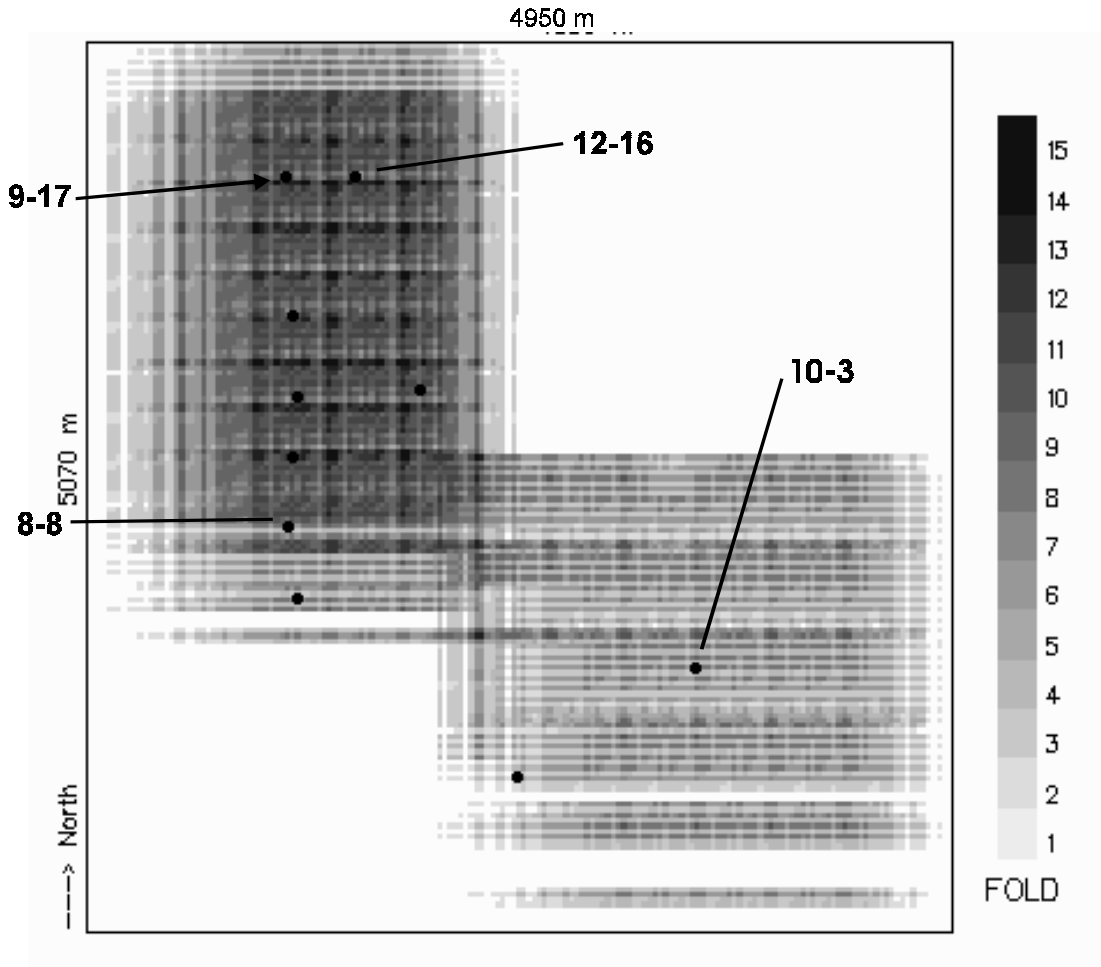


Fig. 19. Azimuthal fold distribution for asymptotic P-S fold, Glauconitic target for design option 2. Source-receiver azimuths are limited from 0 - 90 degrees. Bin size is 30 m x 30 m.

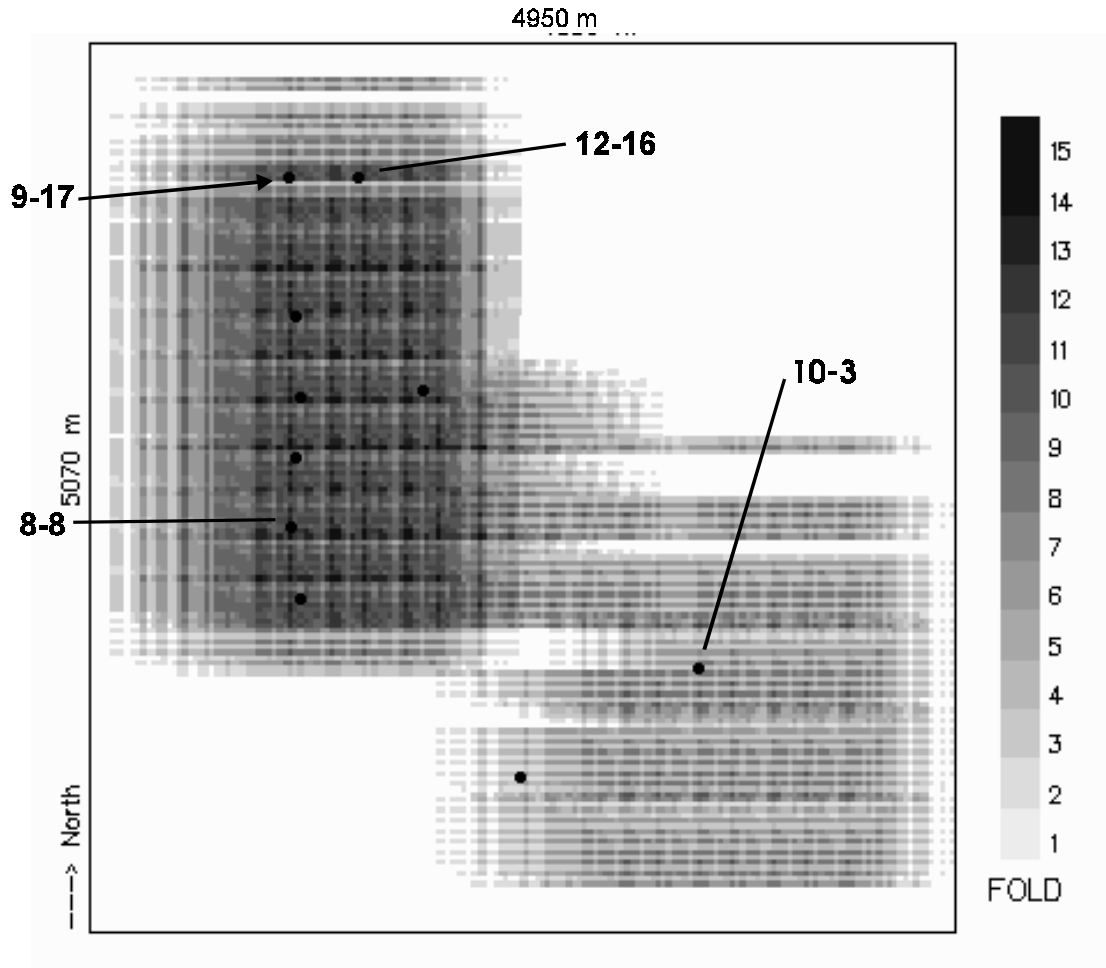


Fig. 20. Azimuthal fold distribution for asymptotic P-S fold, Glauconitic target for design option 2. Source-receiver azimuths are limited from 90 - 180 degrees. Bin size is 30 m x 30 m.

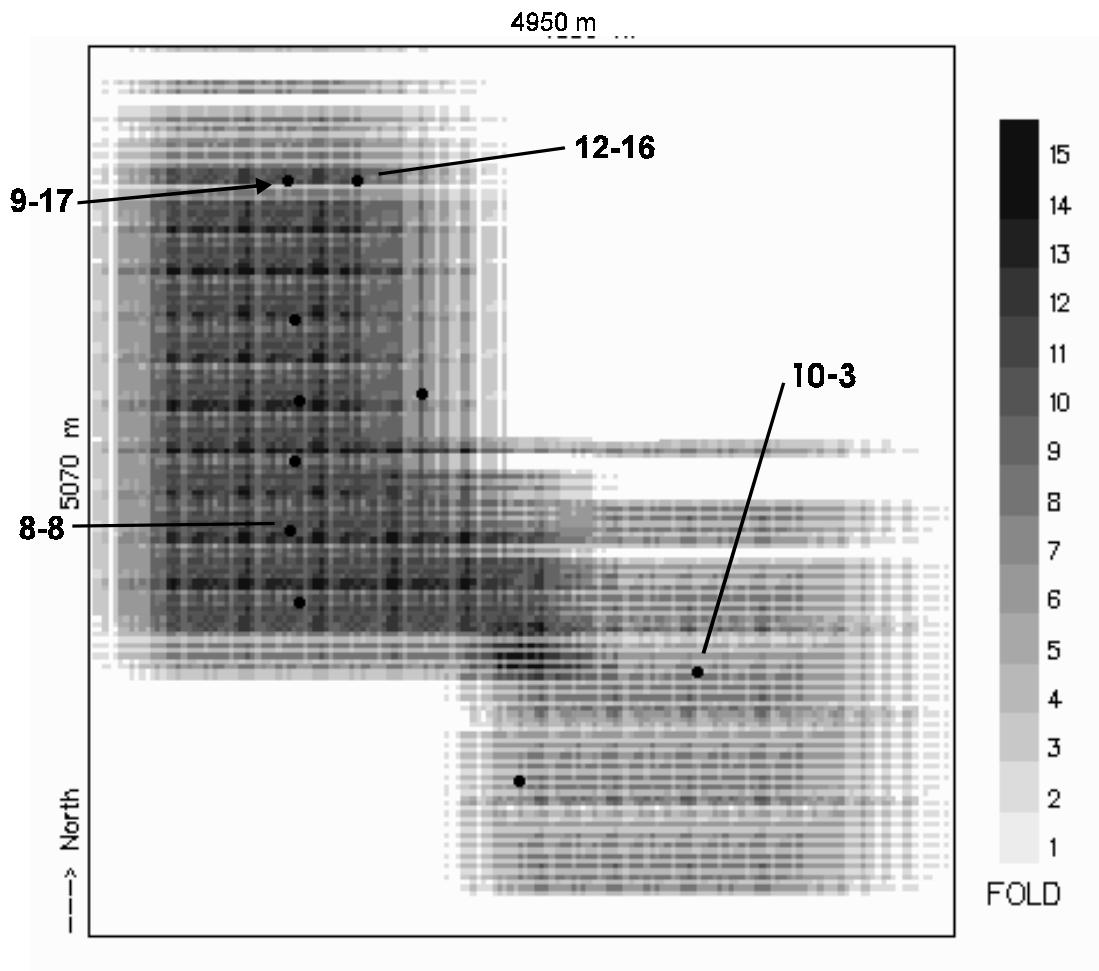


Fig. 21. Azimuthal fold distribution for asymptotic P-S fold, Glauconitic target for design option 2. Source-receiver azimuths are limited from 180 - 270 degrees. Bin size is 30 m x 30 m.

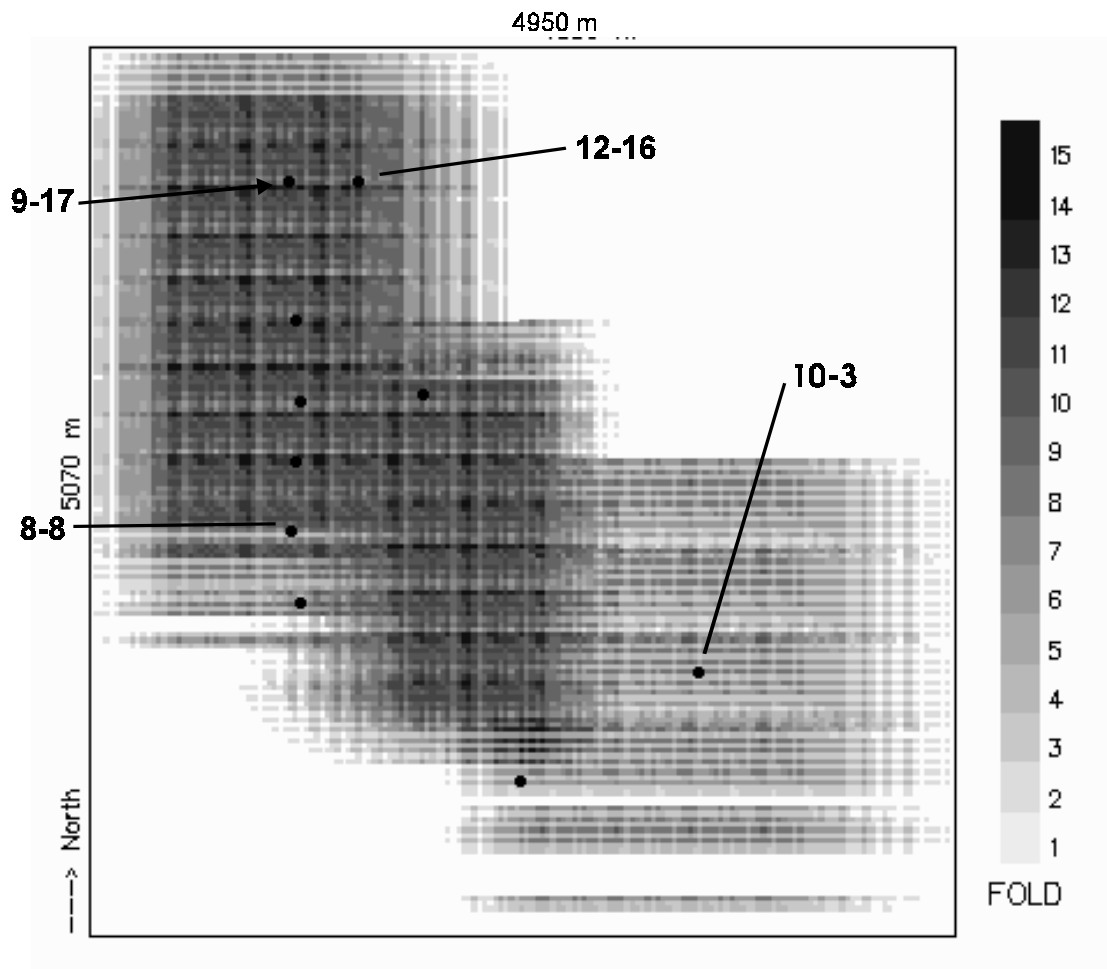


Fig. 22. Azimuthal fold distribution for asymptotic P-S fold, Glauconitic target for design option 2. Source-receiver azimuths are limited from 270 - 360 degrees. Bin size is 30 m x 30 m.

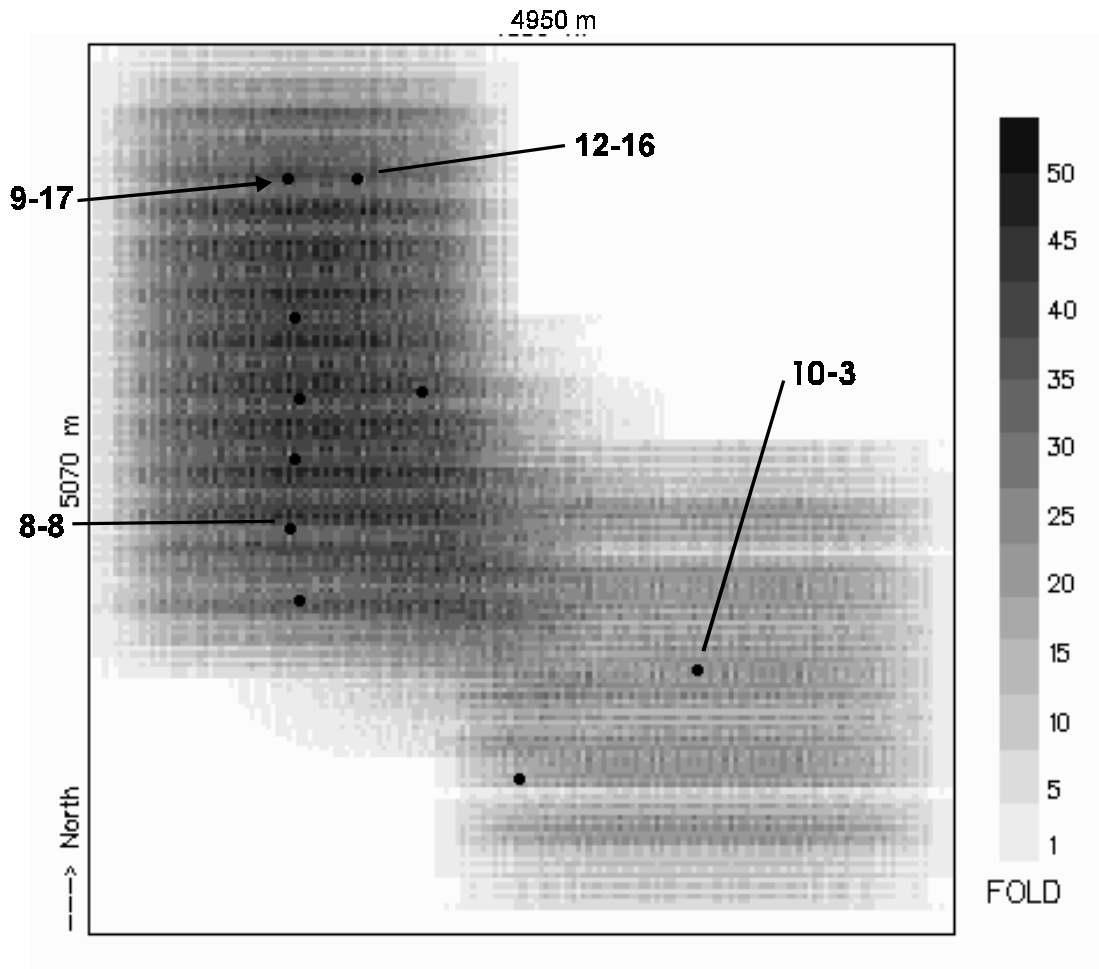


Fig. 23. Depth-variant P-S fold, Glauconitic target for design option 2. Offsets are limited from 300 -1700 m. Bin size is 30 m x 30 m.

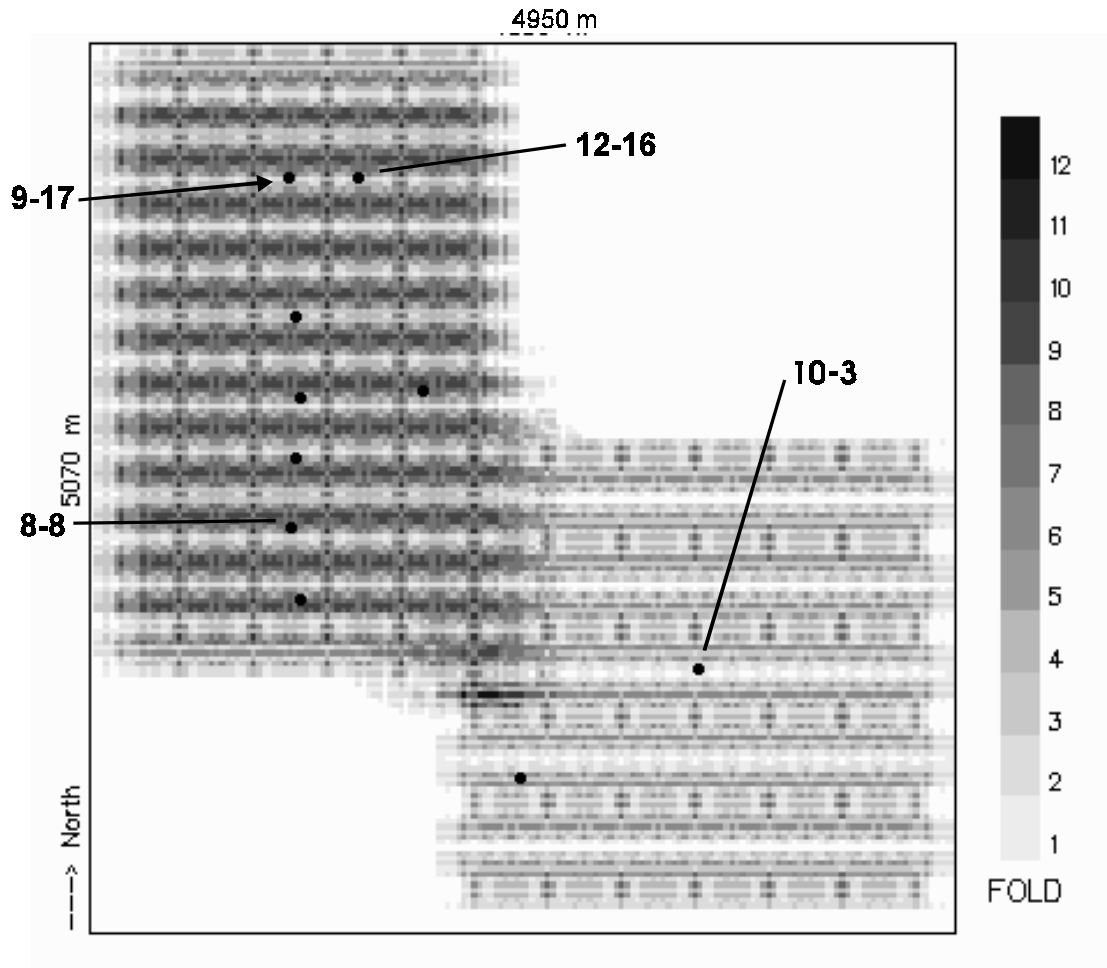


Fig 24. Depth-variant near offset P-S fold, Glauconitic target for design option 2. Offsets are limited from 300 -700 m. Bin size is 30 m x 30 m.

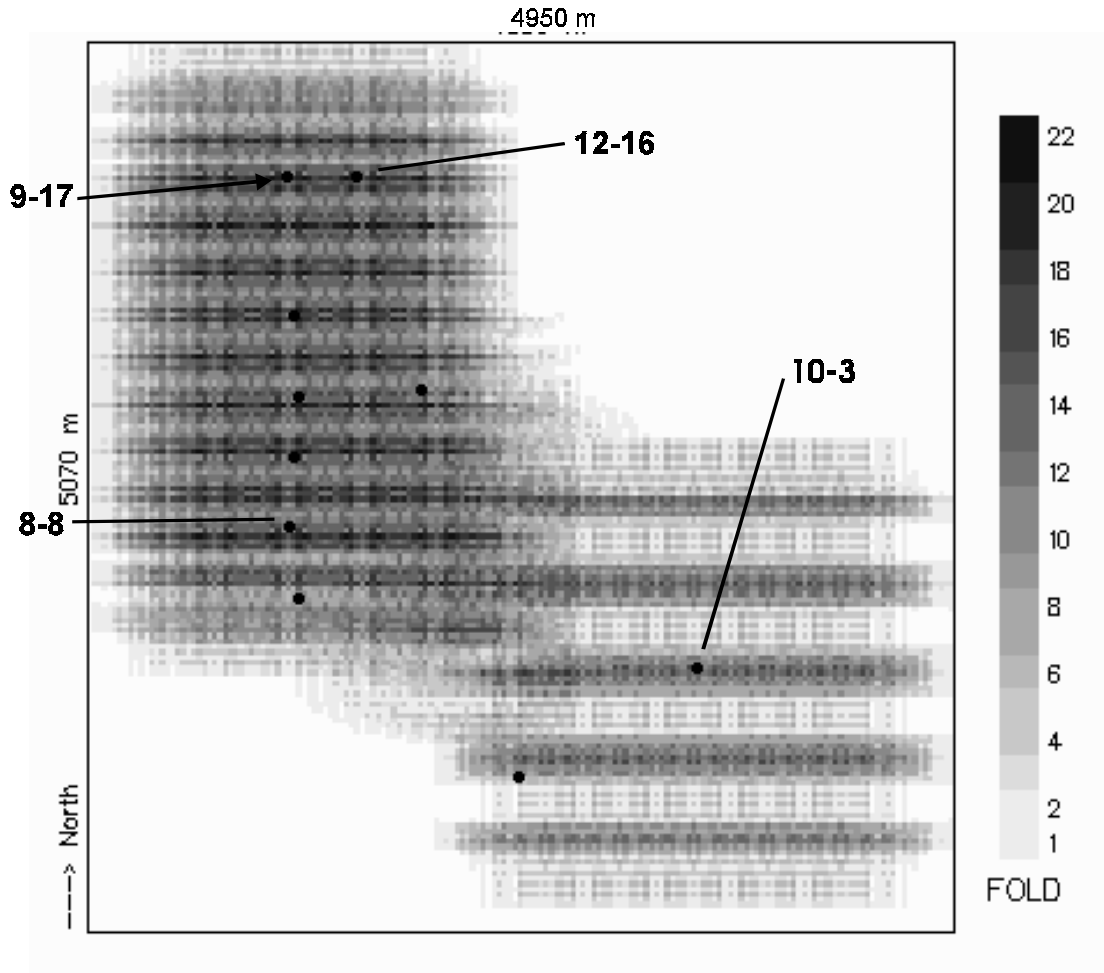


Fig 25. Depth-variant middle offset P-S fold, Glauconitic target for design option 2. Offsets are limited from 700 -1200 m. Bin size is 30 m x 30 m.

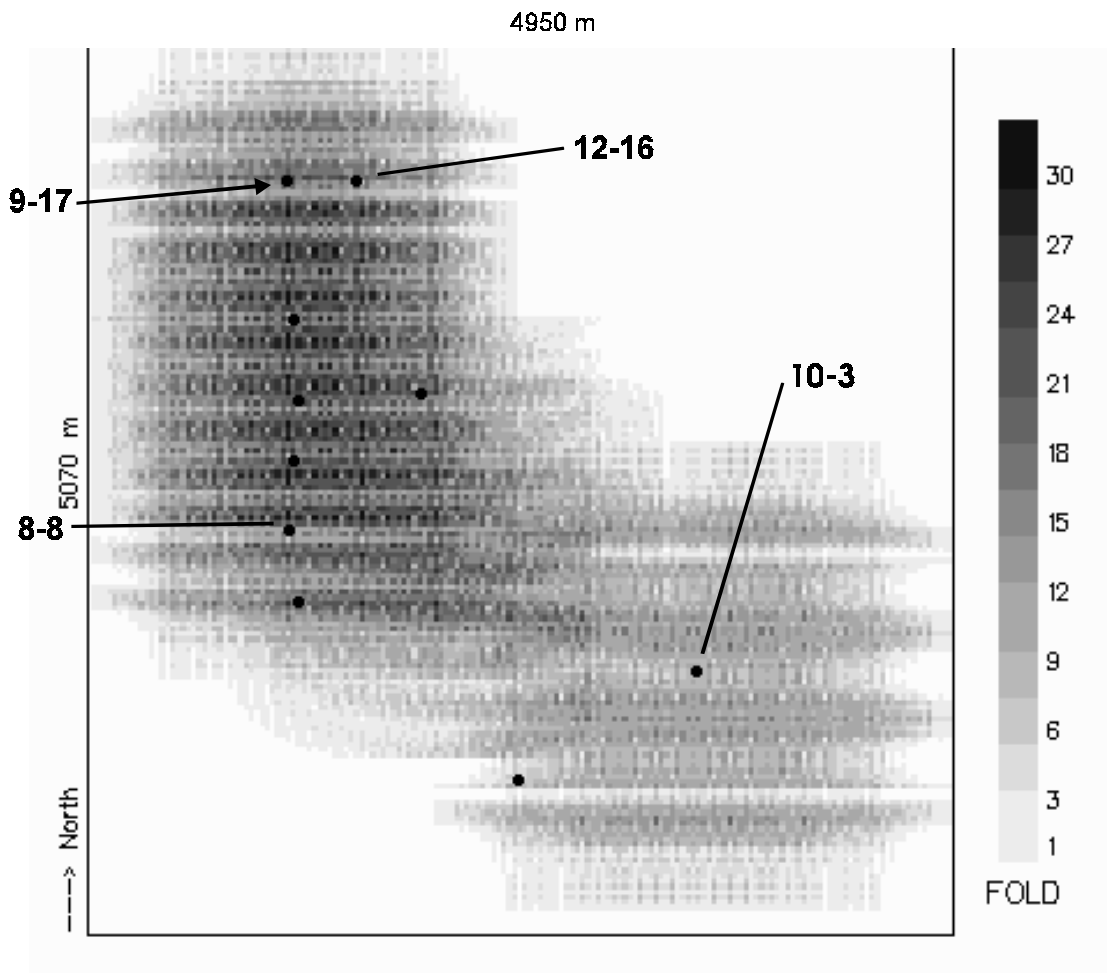


Fig 26. Depth-variant far offset P-S fold, Glauconitic target for design option 2. Offsets are limited from 1200 -1700 m. Bin size is 30 m x 30 m.

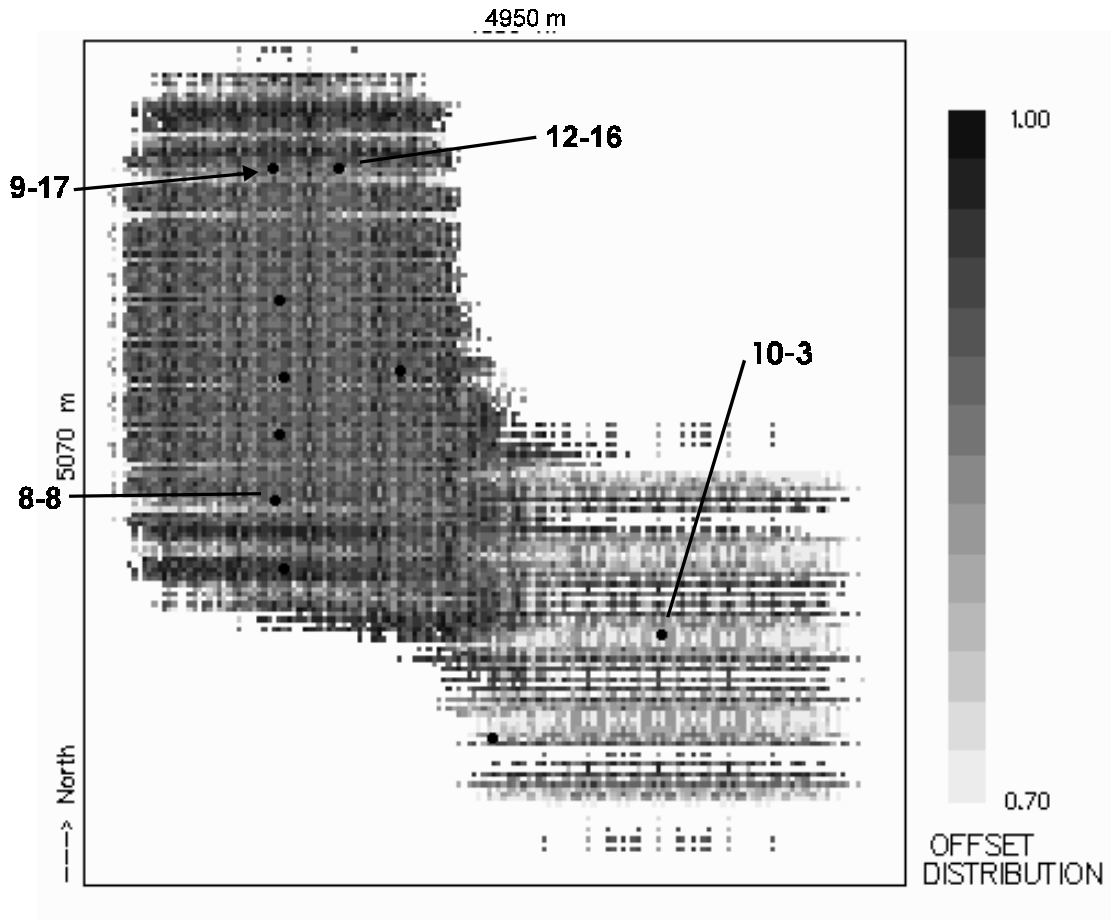


Fig. 27. Offset distribution quality factor for depth-variant P-S fold, Glauconitic target for design option 2. Offsets are limited from 300 - 1700 m. Bin size is 30 m x 30 m.

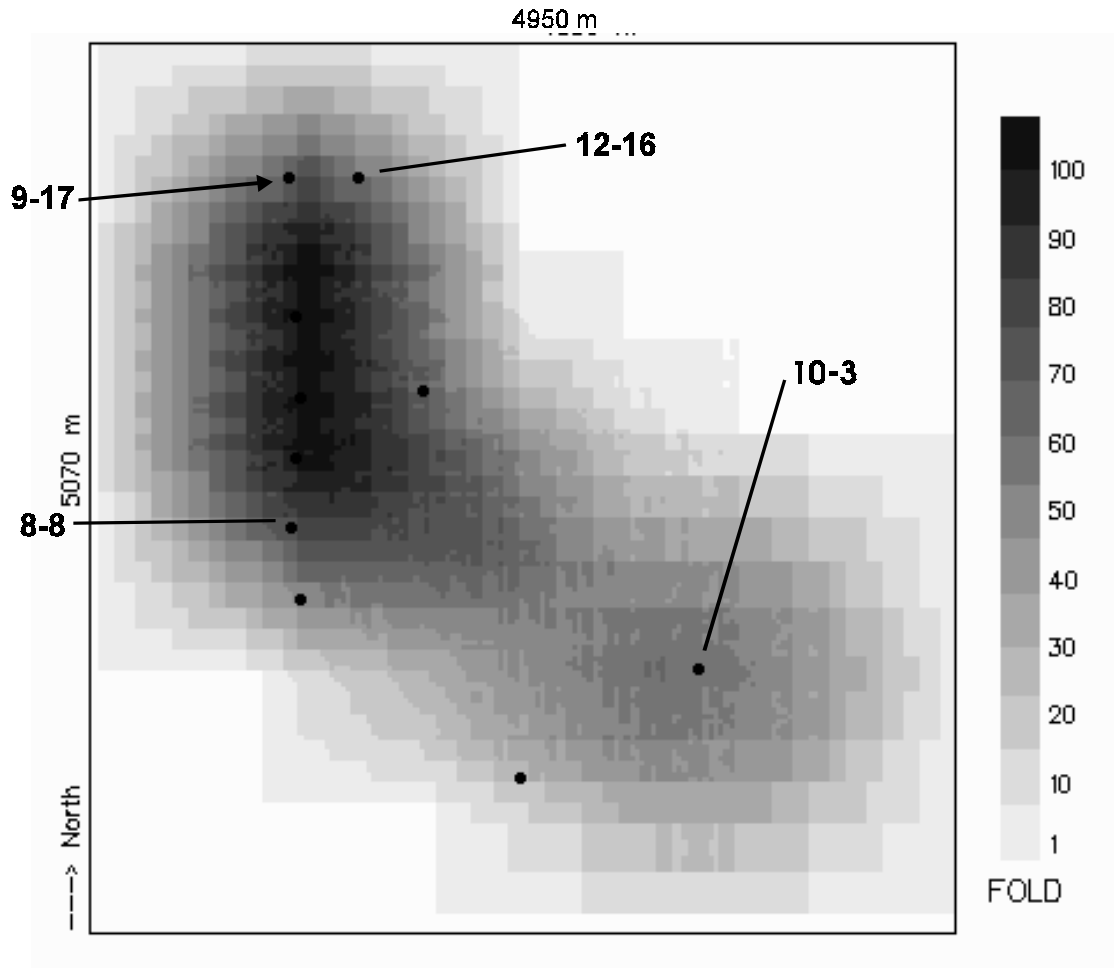


Fig 28. P-P fold, Beaverhill Lake target, design option 2. Offsets 0 - 2700 m.

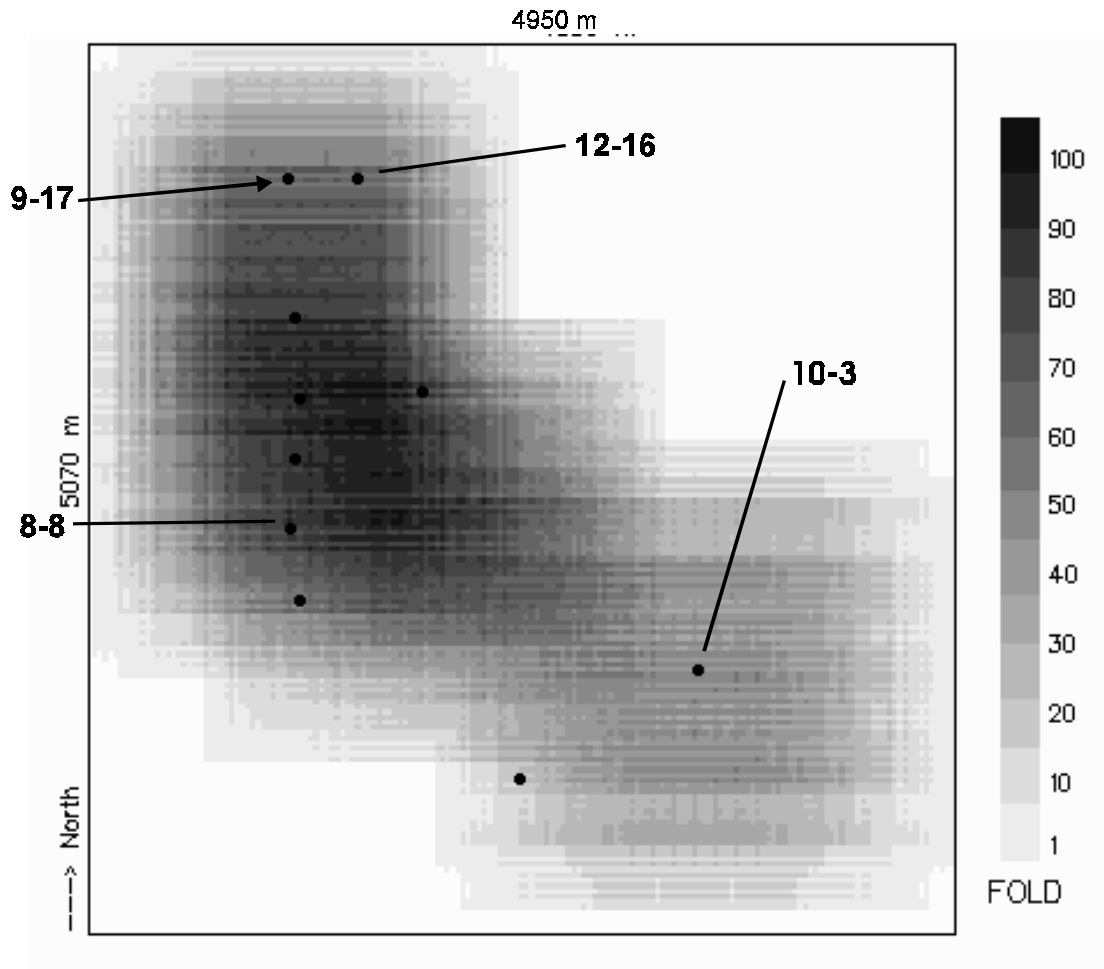


Fig. 29. Asymptotic P-S fold, Beaverhill Lake target, design option 2. Offsets 400 - 2900 m.

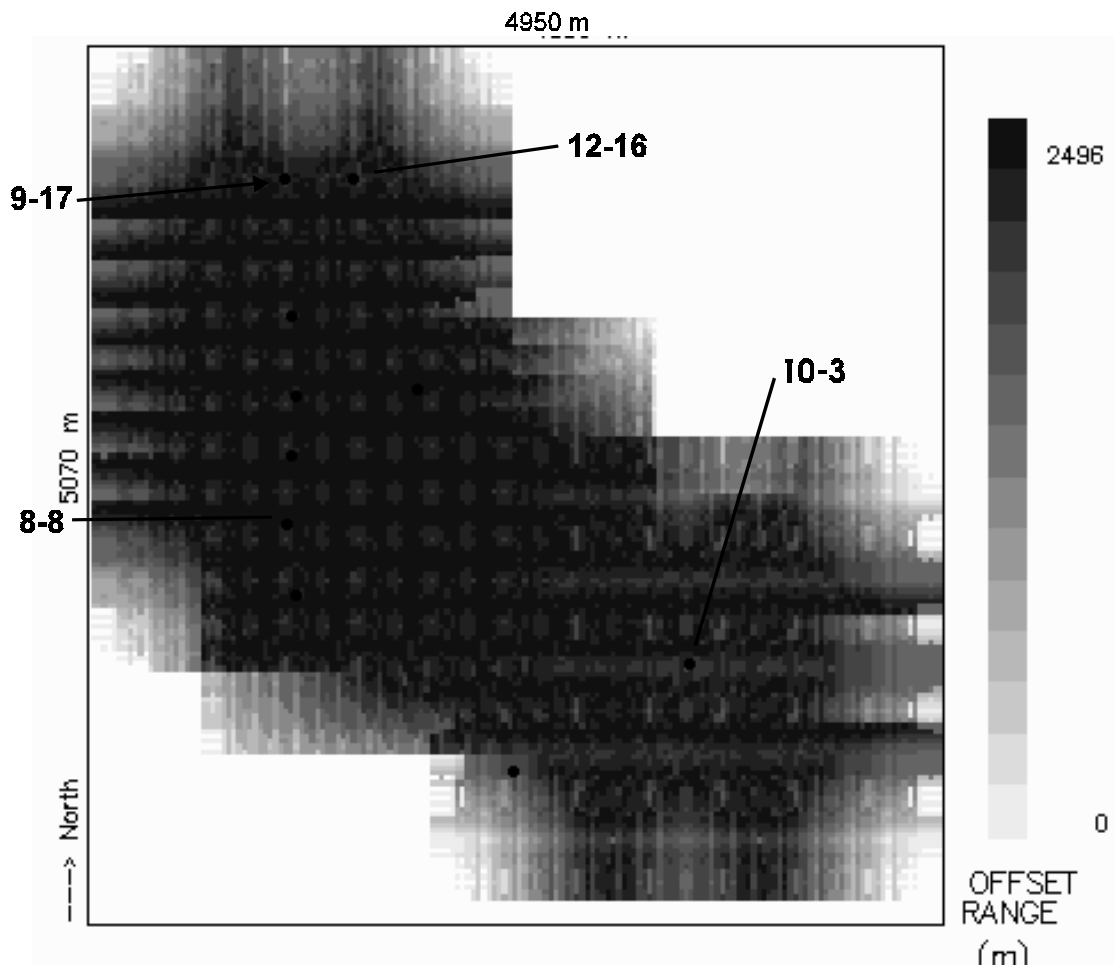


Fig. 30. Asymptotic P-S offset range, Beaverhill Lake target. Offsets 400 - 2900 m.

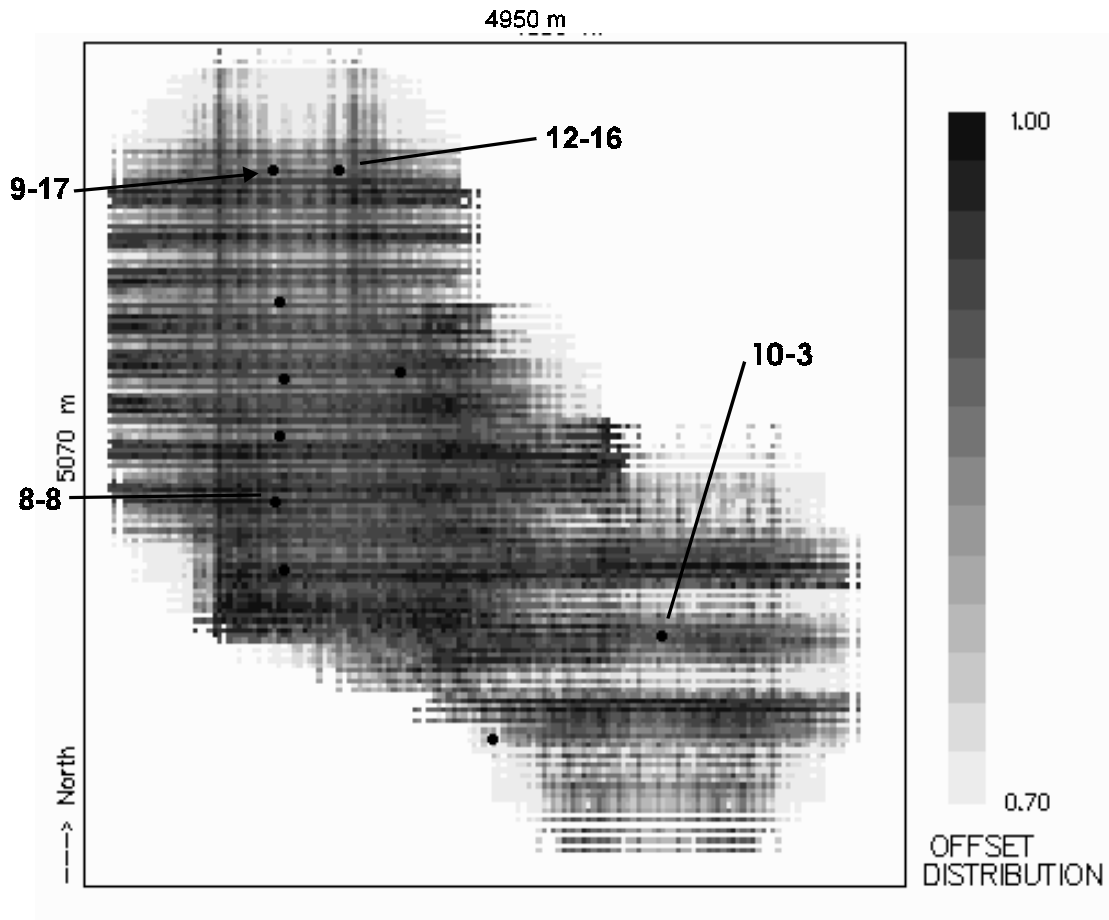


Fig. 31. Asymptotic P-S offset quality factor, Beaverhill Lake target, design option 2. Offsets 400-2900 m.

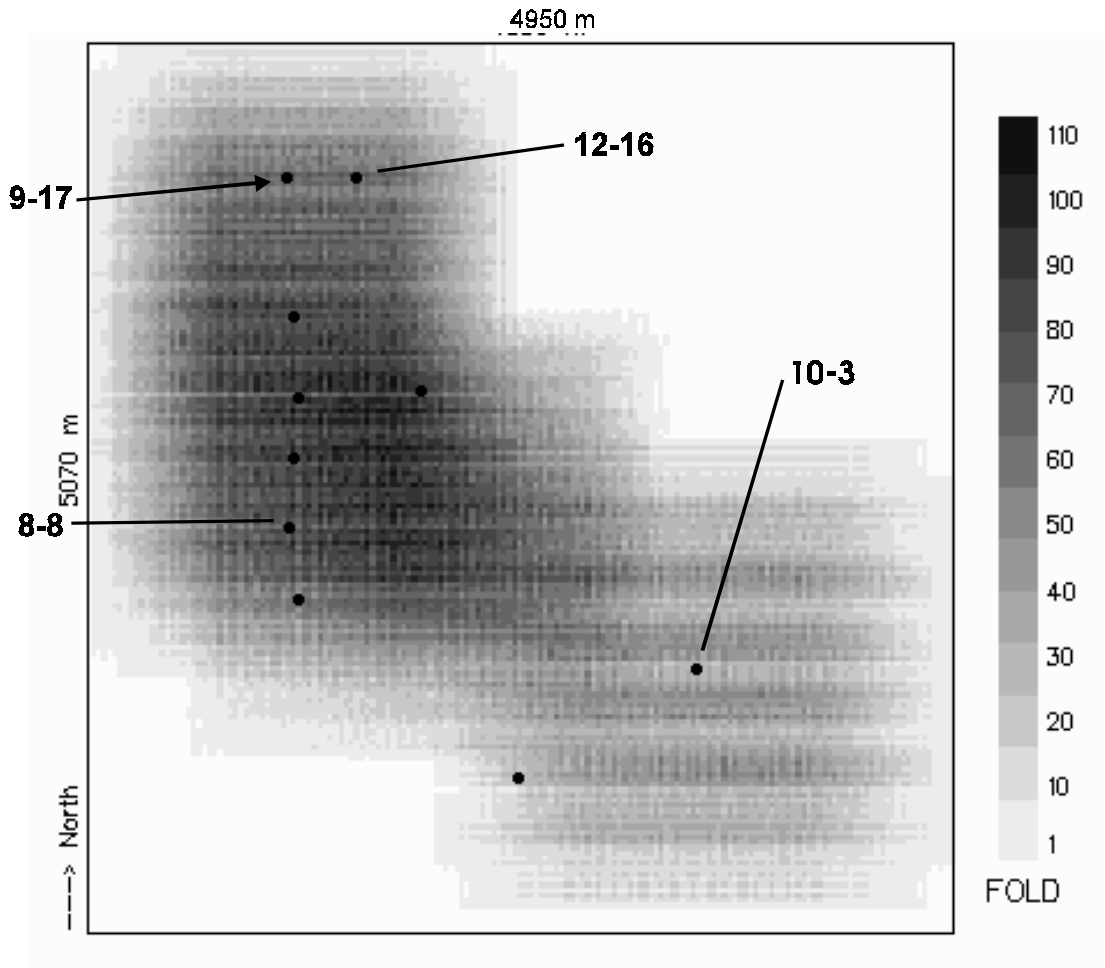


Fig. 32. Depth-variant P-S fold, Beaverhill Lake target, design option 2. Offsets 400 - 2900 m.

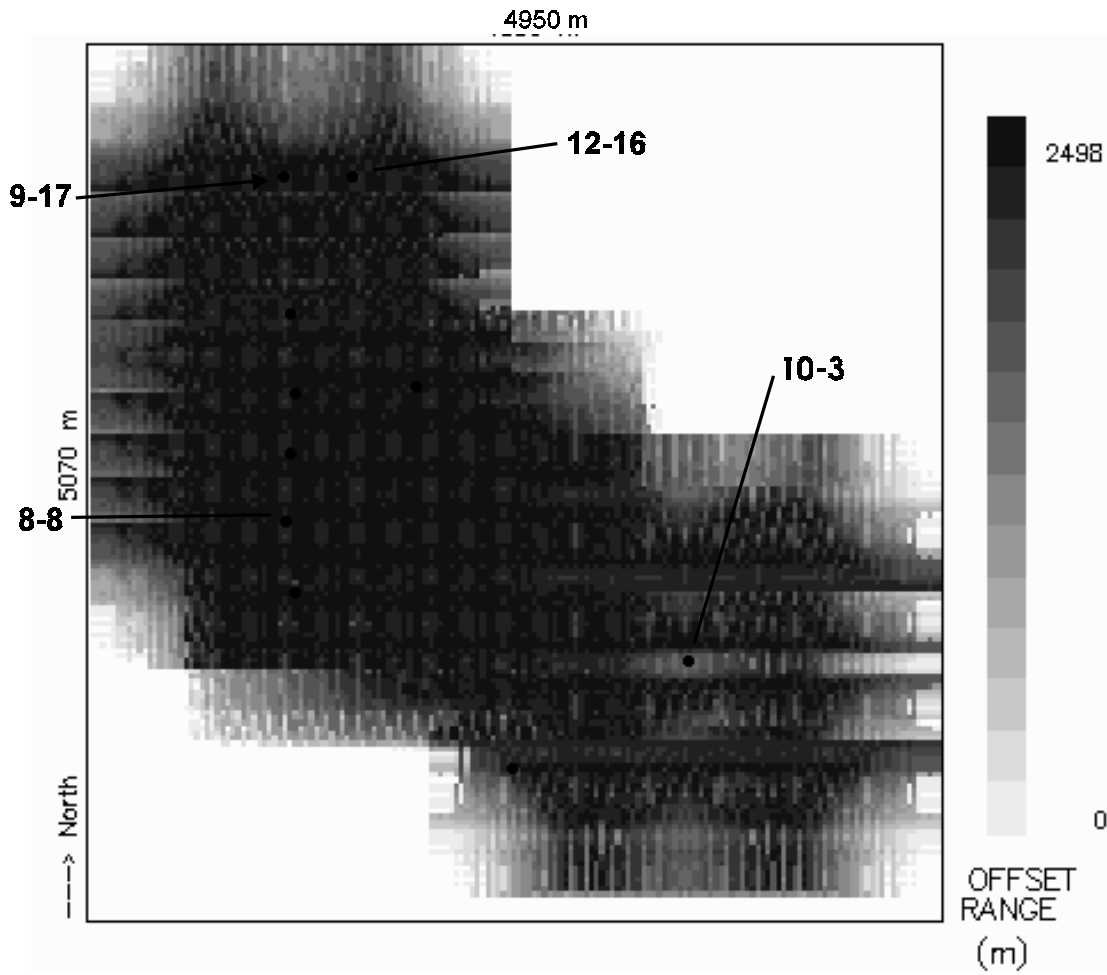


Fig. 33. Depth-variant P-S offset range, Beaverhill Lake target, design option 2. Offsets 400-2900m.

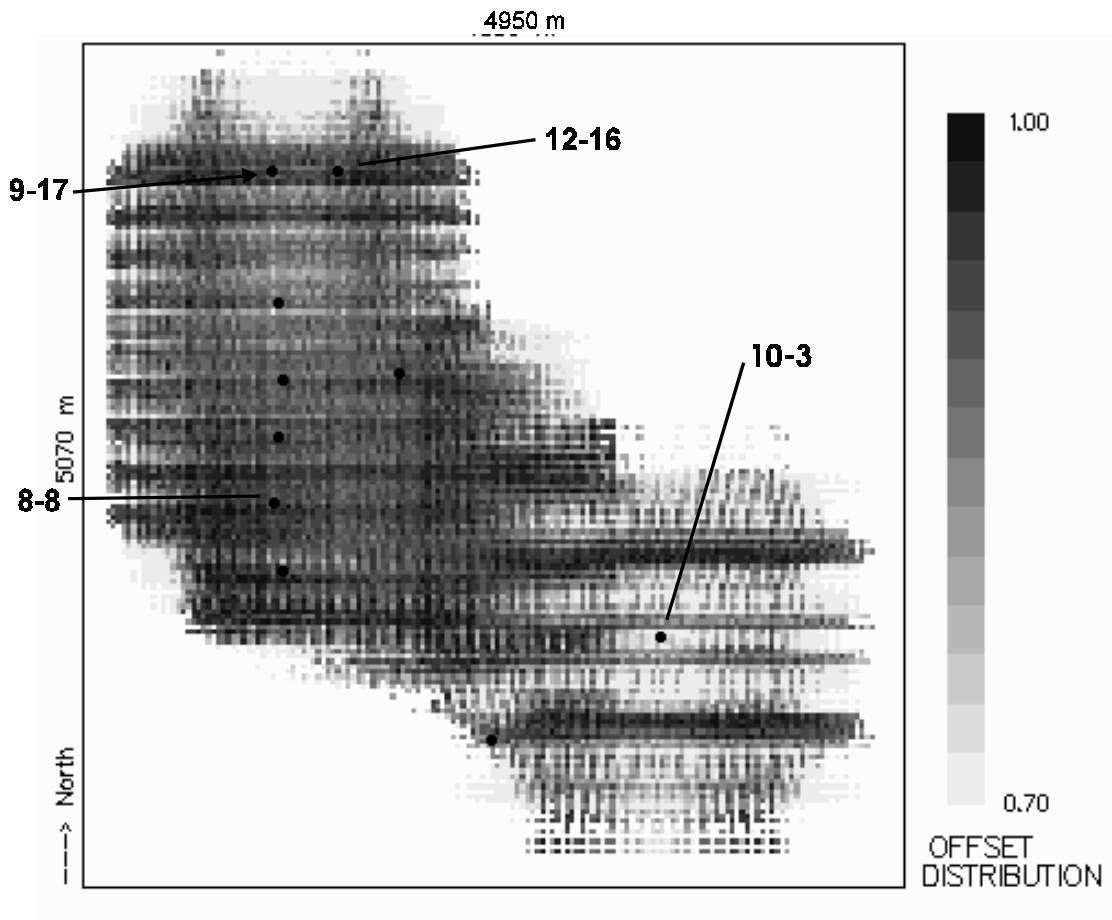


Fig. 34. Depth-variant P-S offset distribution quality, design option 2. Offsets 400-2900 m.

Figure 5

# BLACKFOOT 3C-3D DESIGN 1 BIN-CENTRED P-P MIDPOINTS

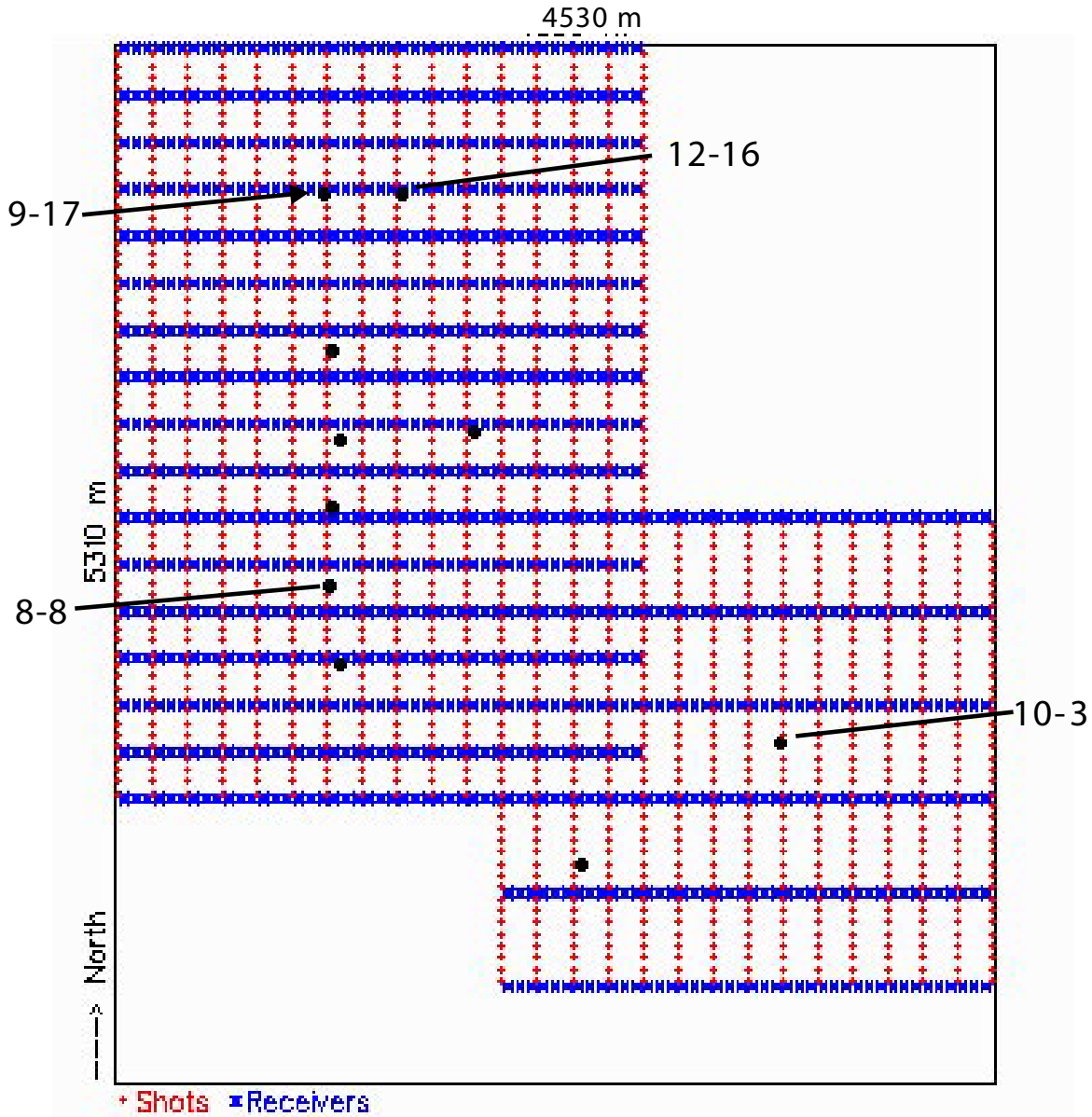


Figure 6

### P-P FOLD, 0-1500 m OFFSETS

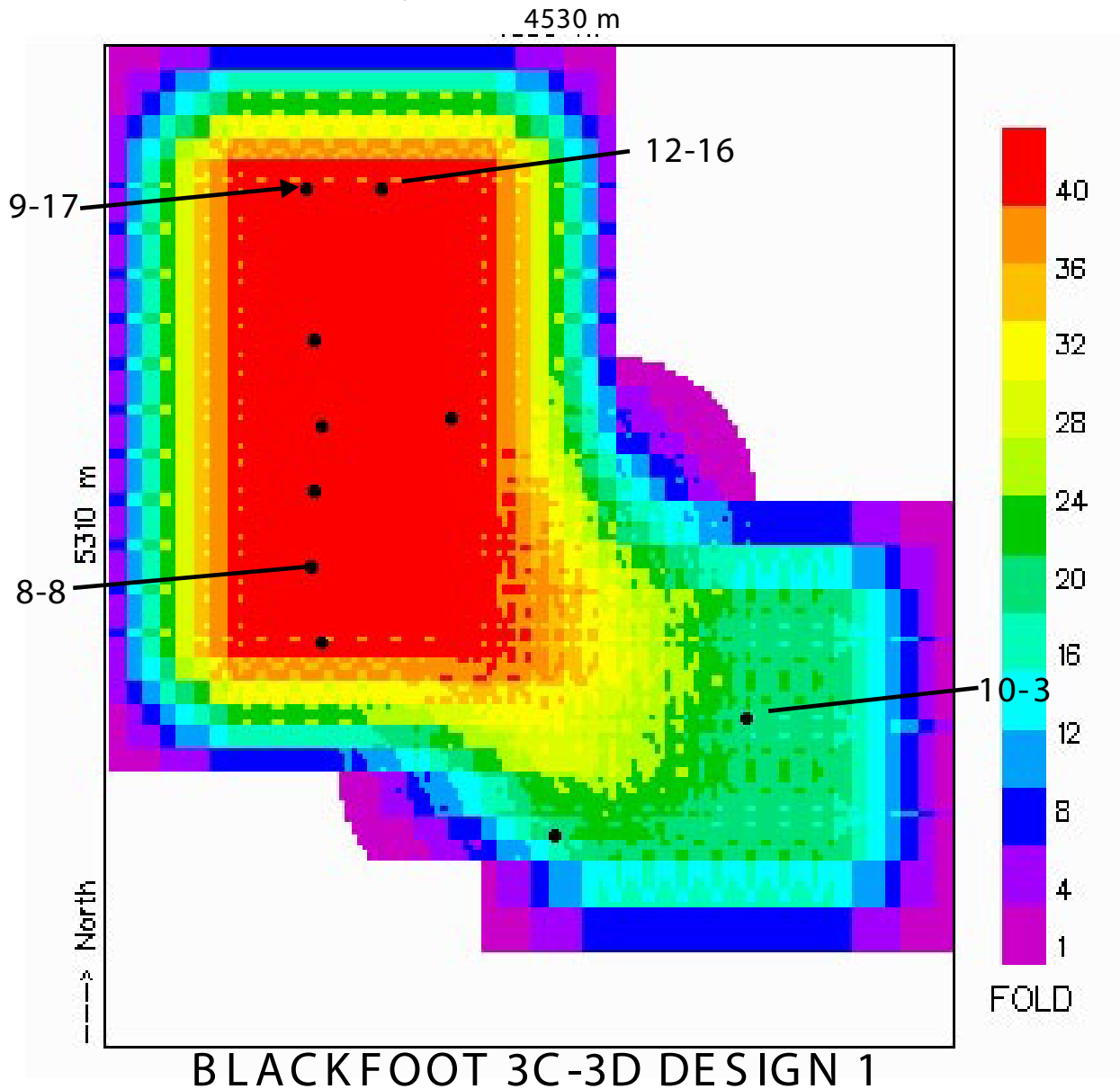


Figure 7

# ASYMPTOTIC P-S FOLD, 300-1700 m OFFSETS

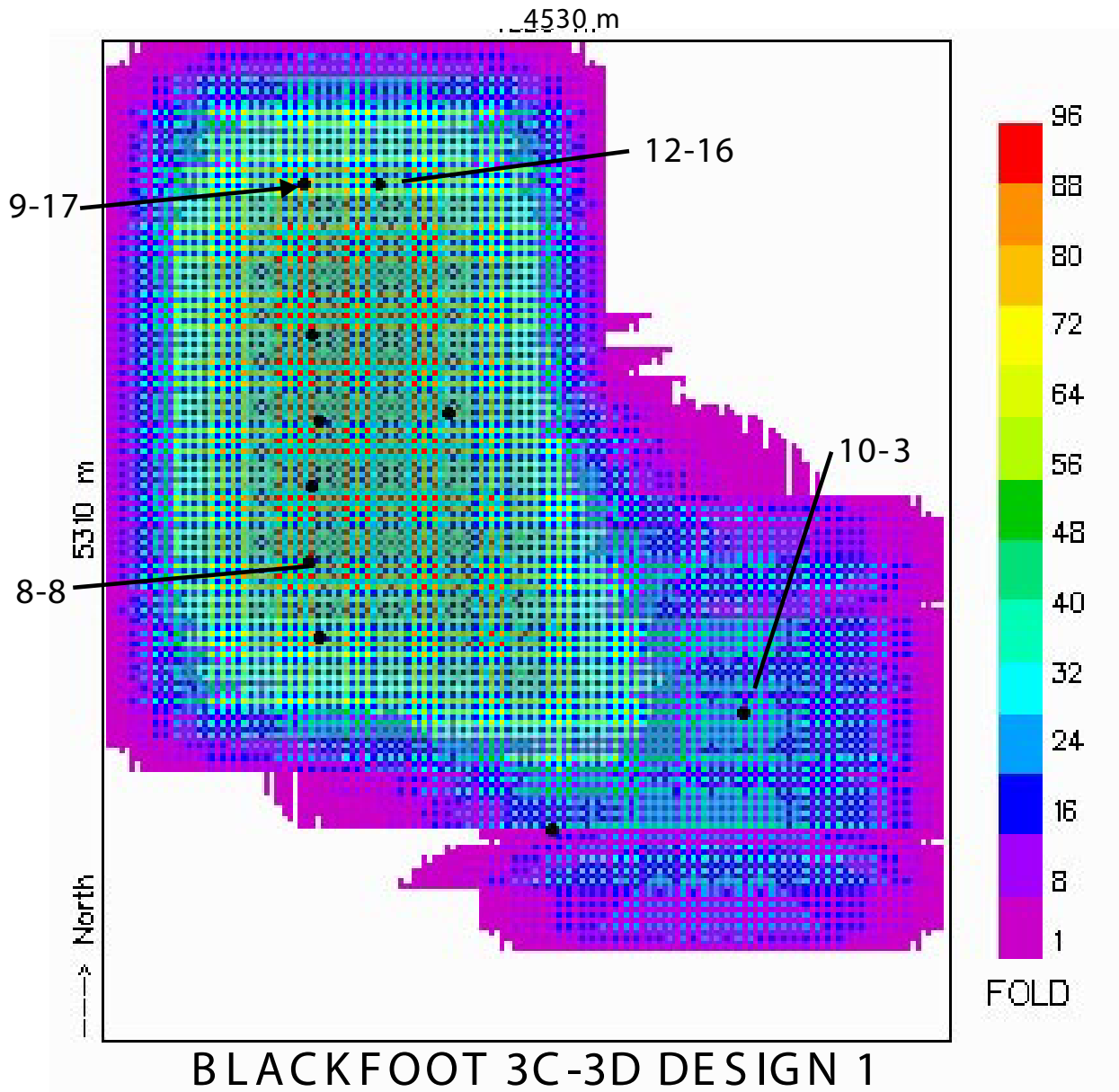


Figure 8

# ASYM. P-S FOLD, 300-1700 m OFFSETS, OBS

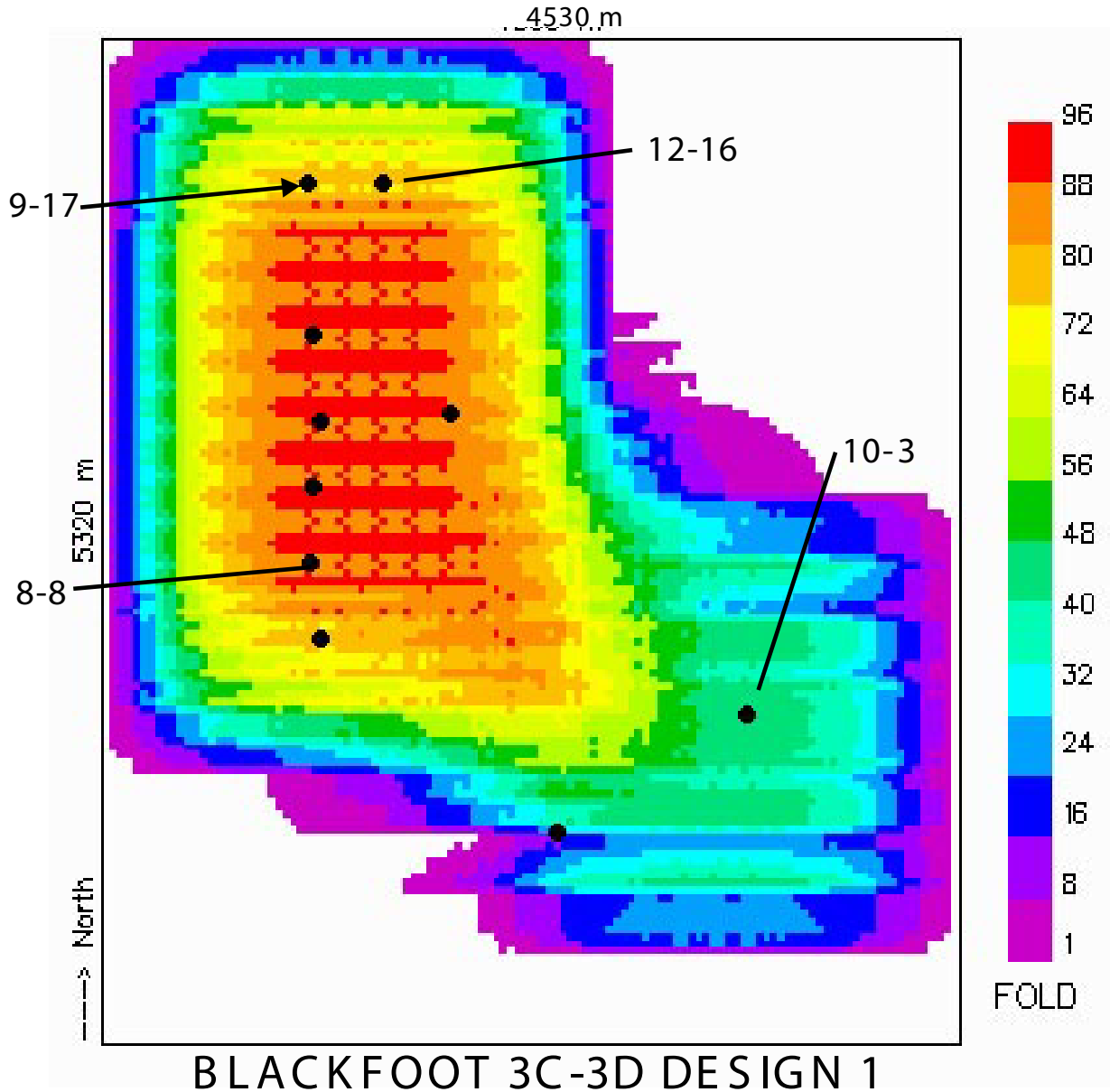


Figure 9

# BLACKFOOT 3C-3D DESIGN 2 DISTRIBUTED P-P MIDPOINTS (FLEXI-BIN)

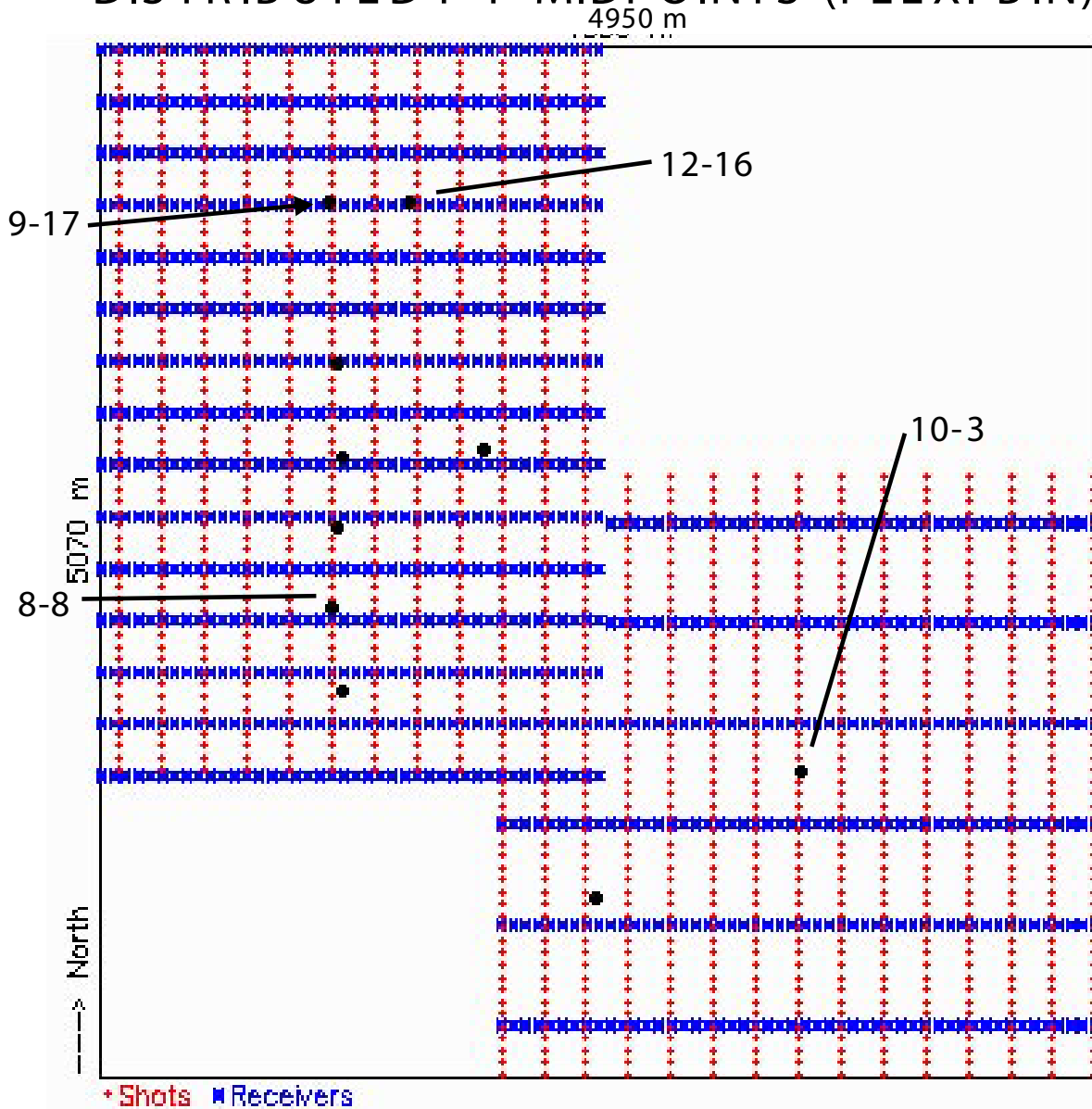


Figure 10

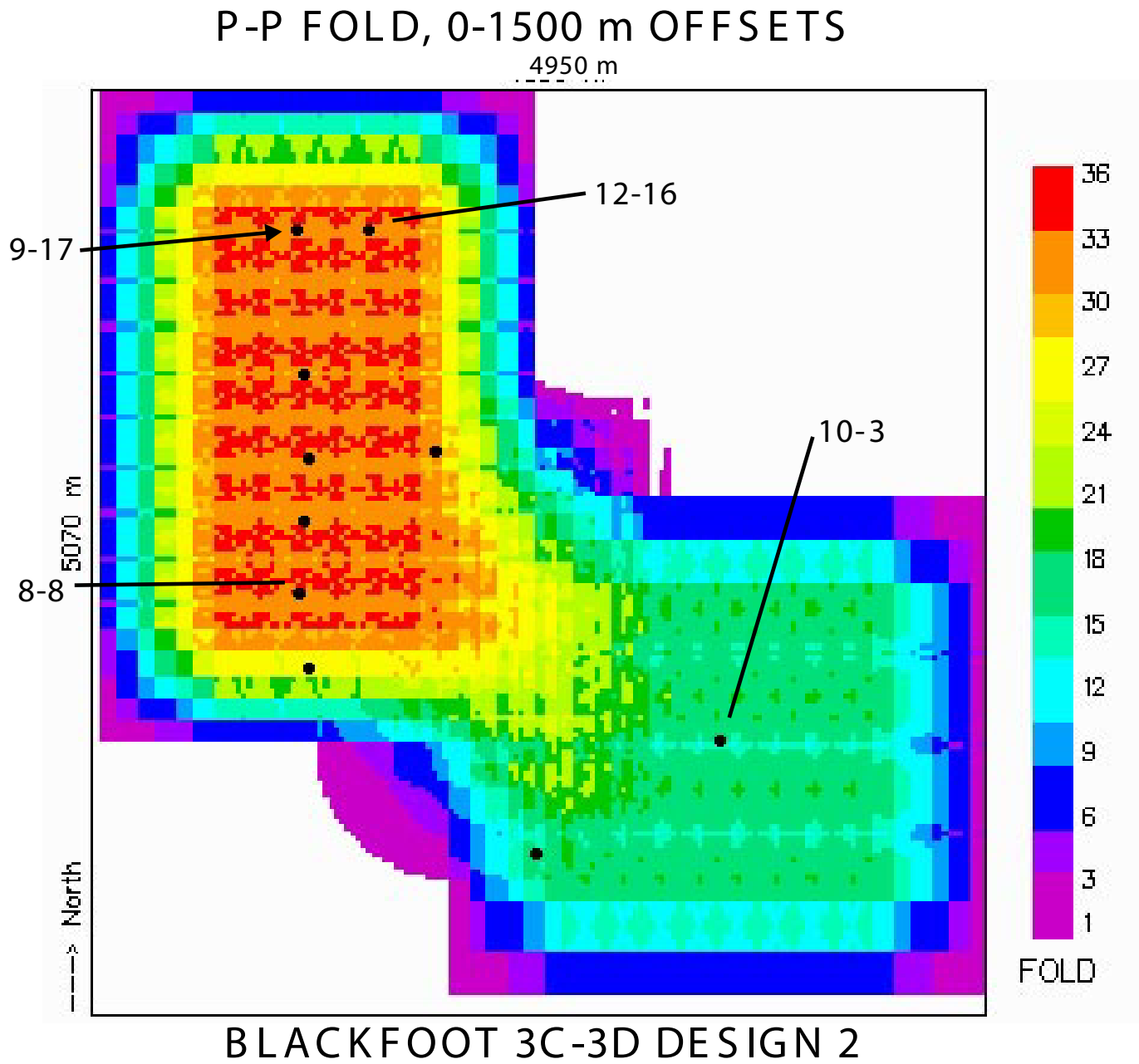
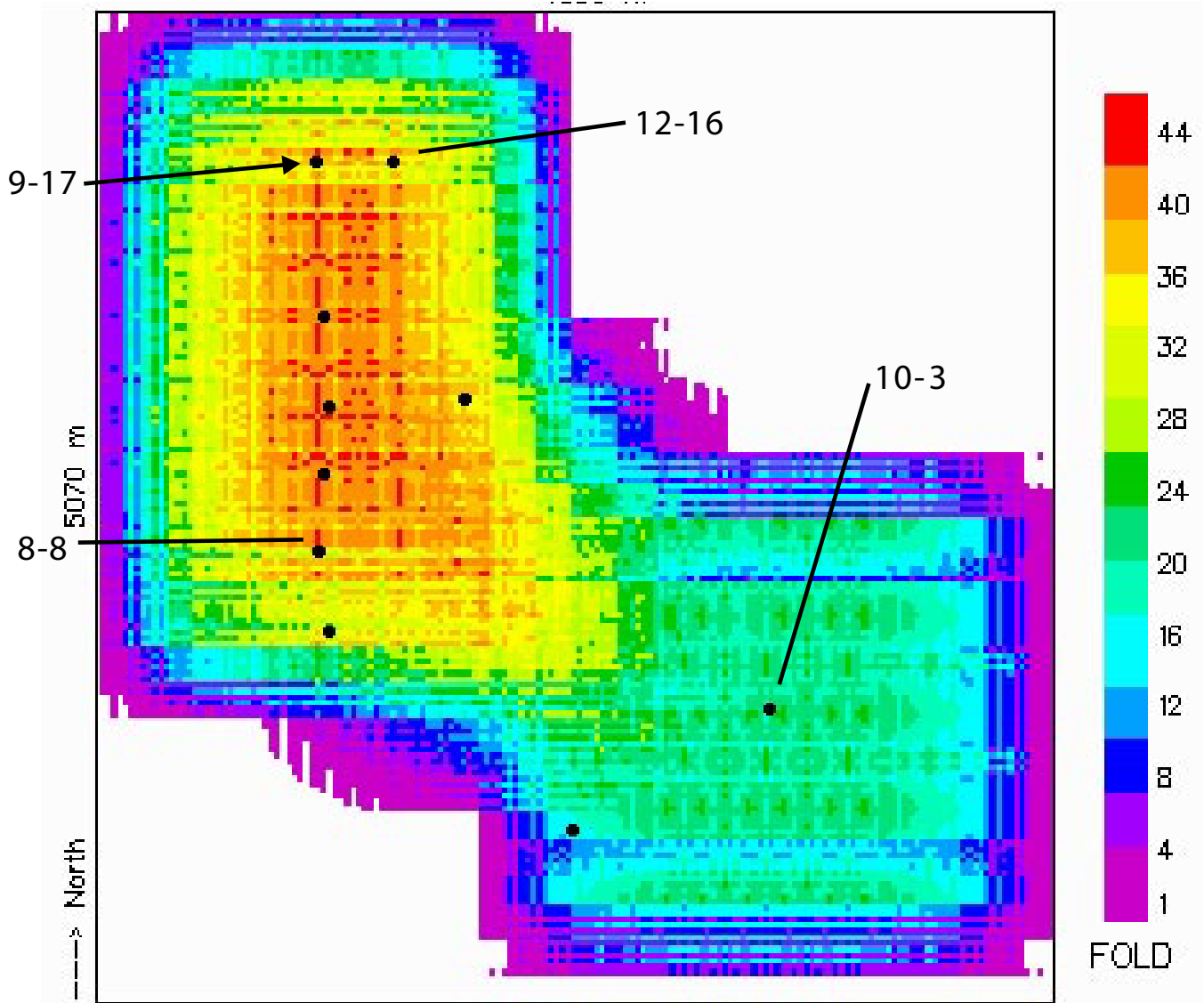


Figure 11

# ASYMPTOTIC P-S FOLD, 300-1700 m OFFSETS

4950 m



BLACKFOOT 3C-3D DESIGN 2

Figure 12

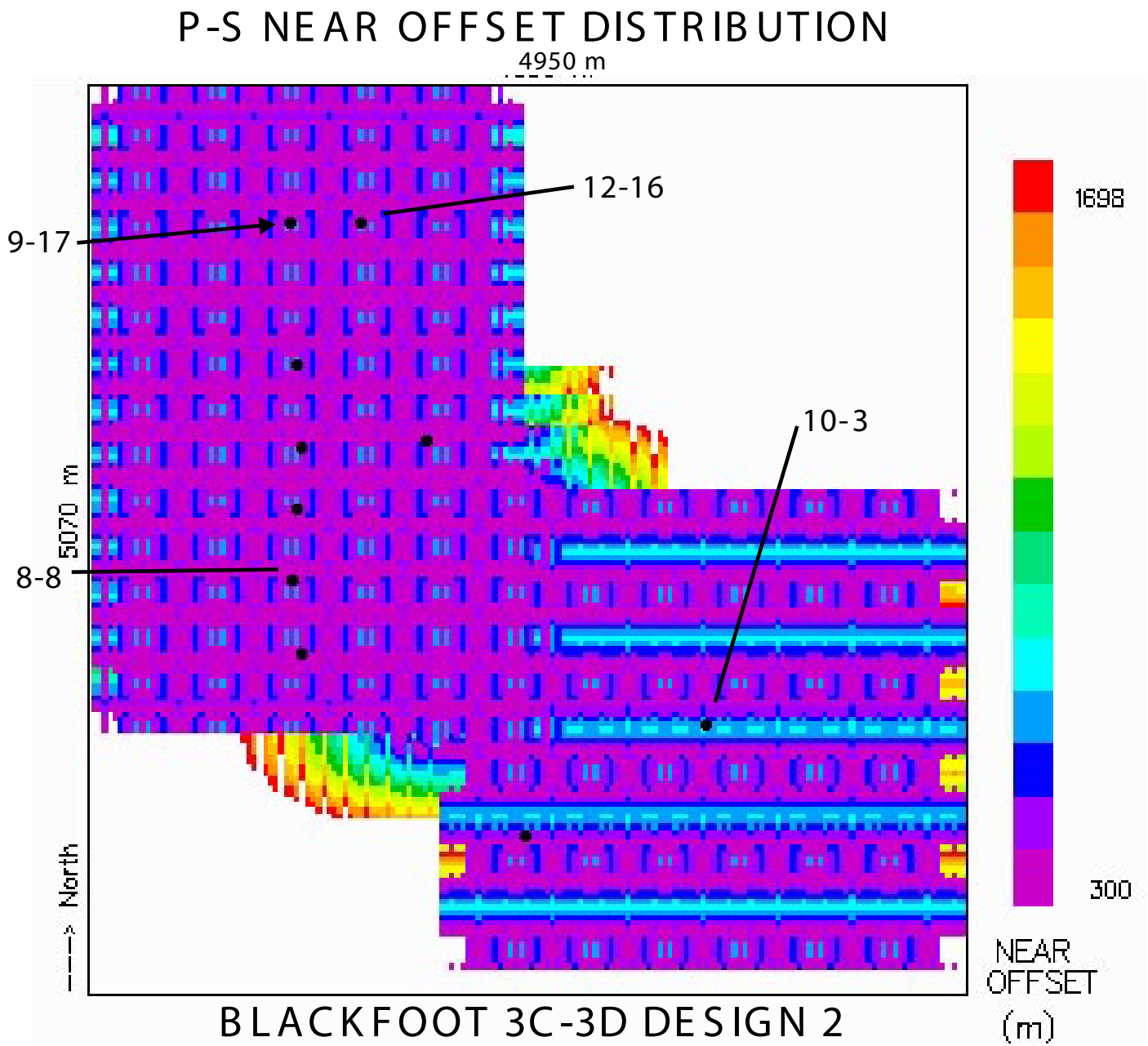


Figure 13

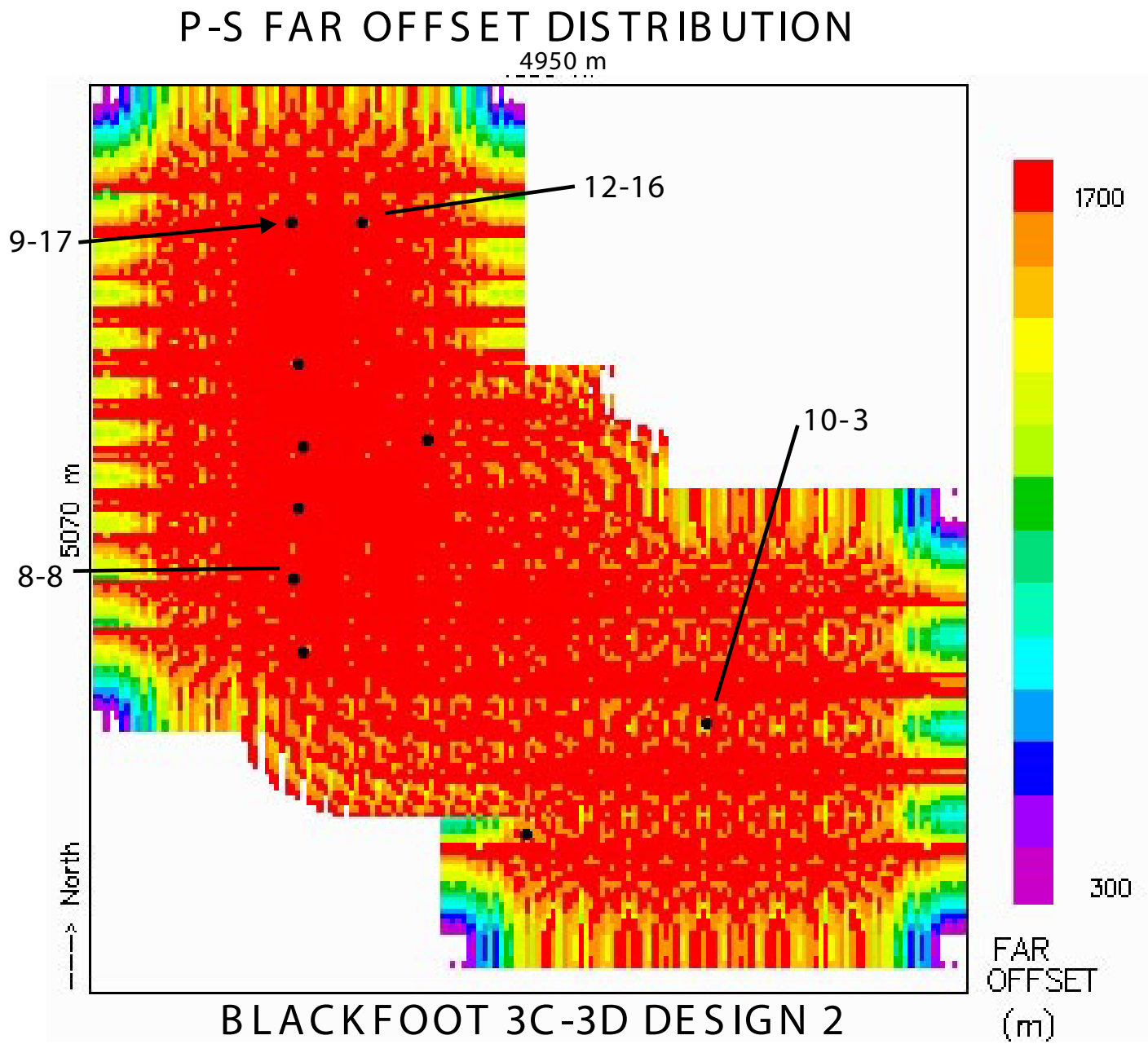


Figure 14

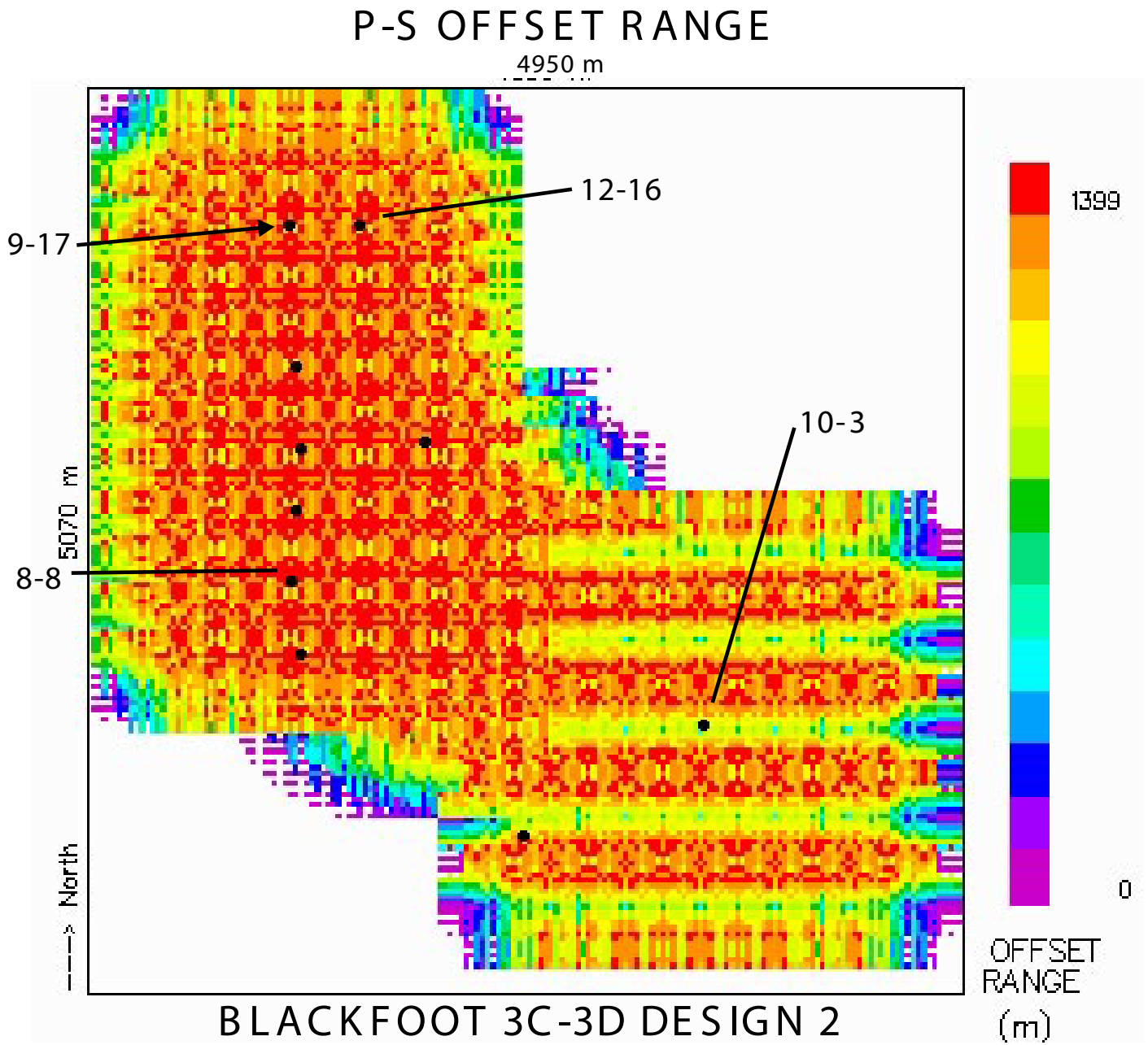
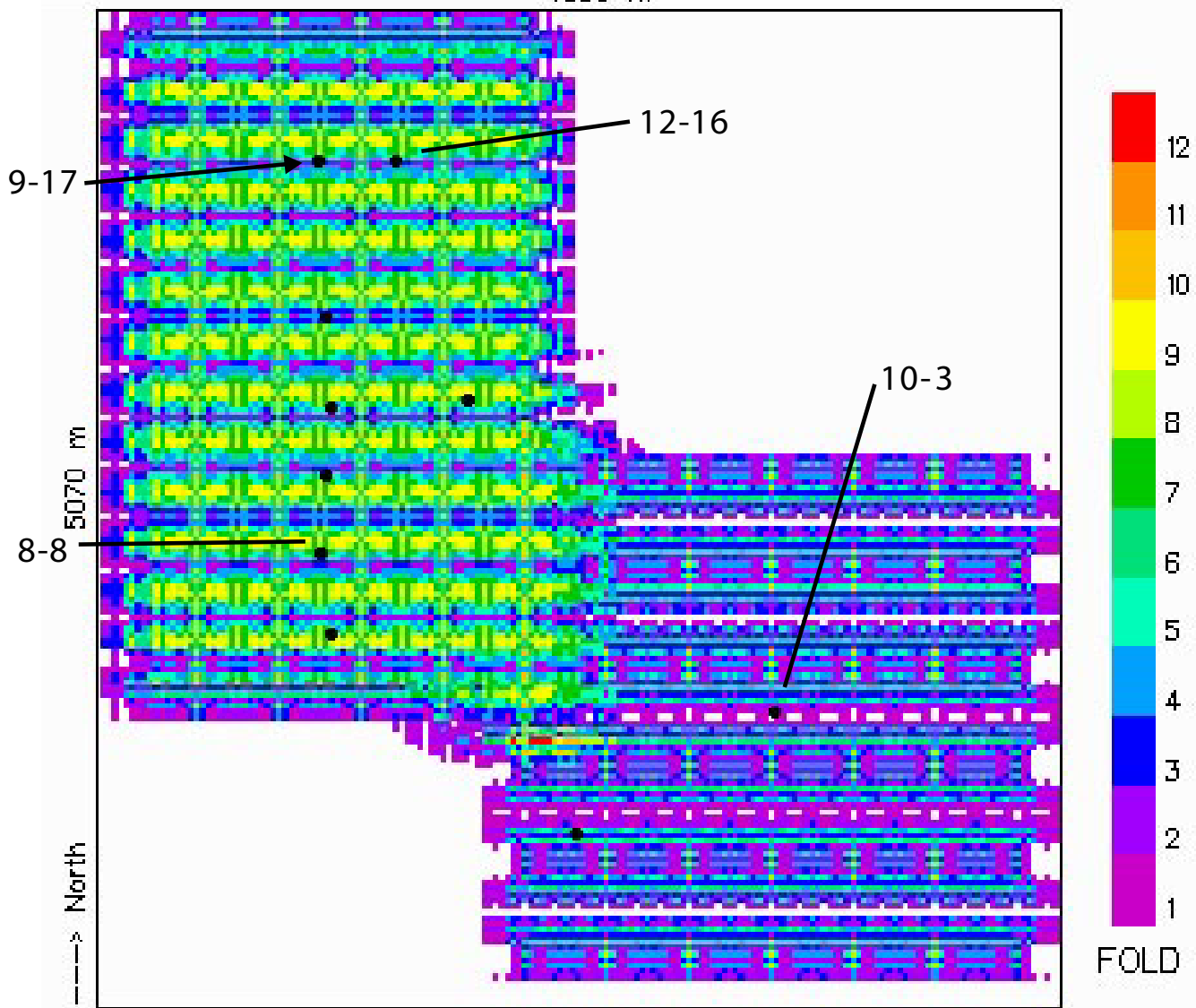


Figure 15

# ASYMPTOTIC P-S FOLD, OFFSETS 300-700 m

4950 m

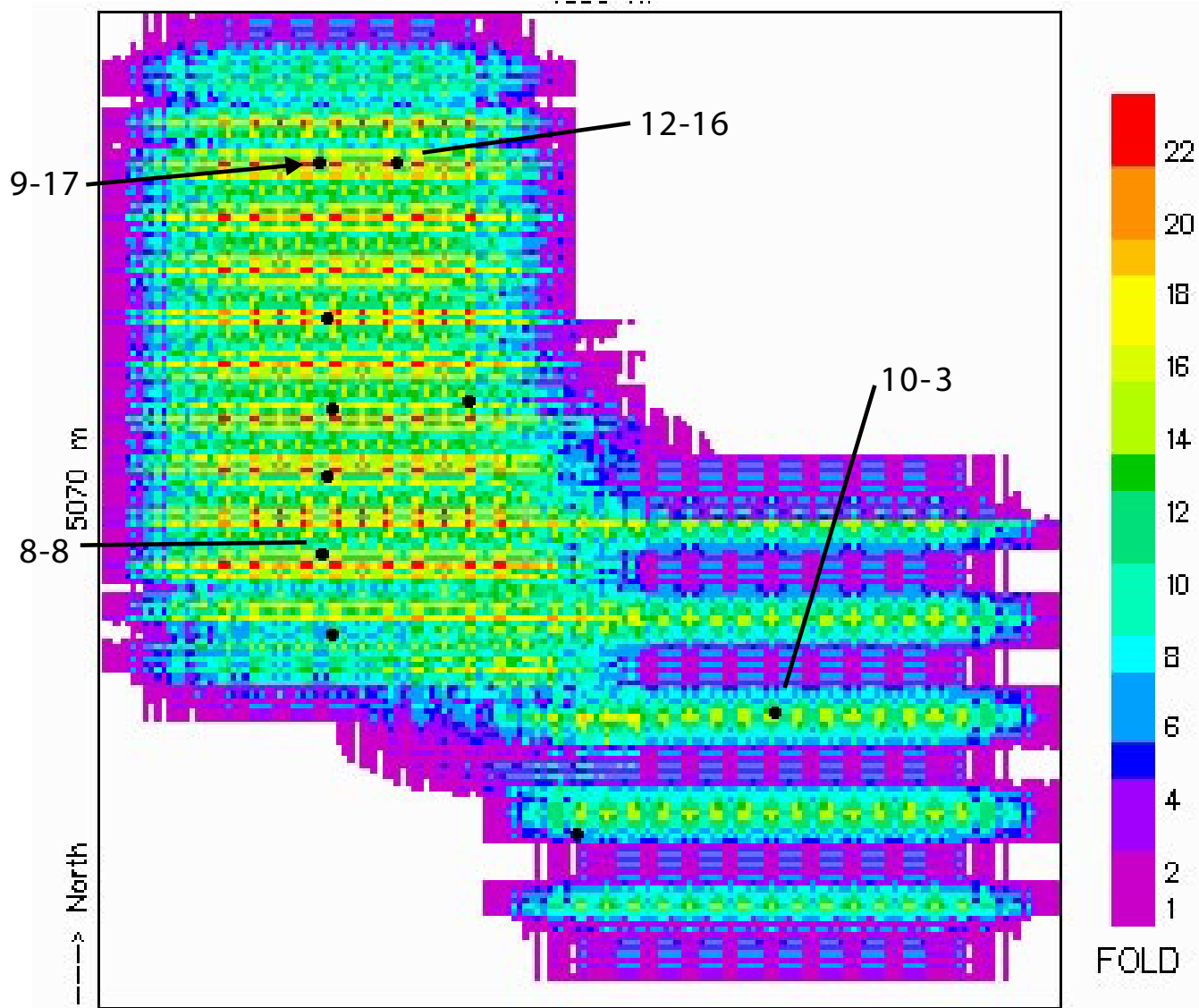


BLACKFOOT 3C-3D DESIGN 2

Figure 16

# ASYMPTOTIC P-S FOLD, OFFSETS 700-1200 m

4950 m

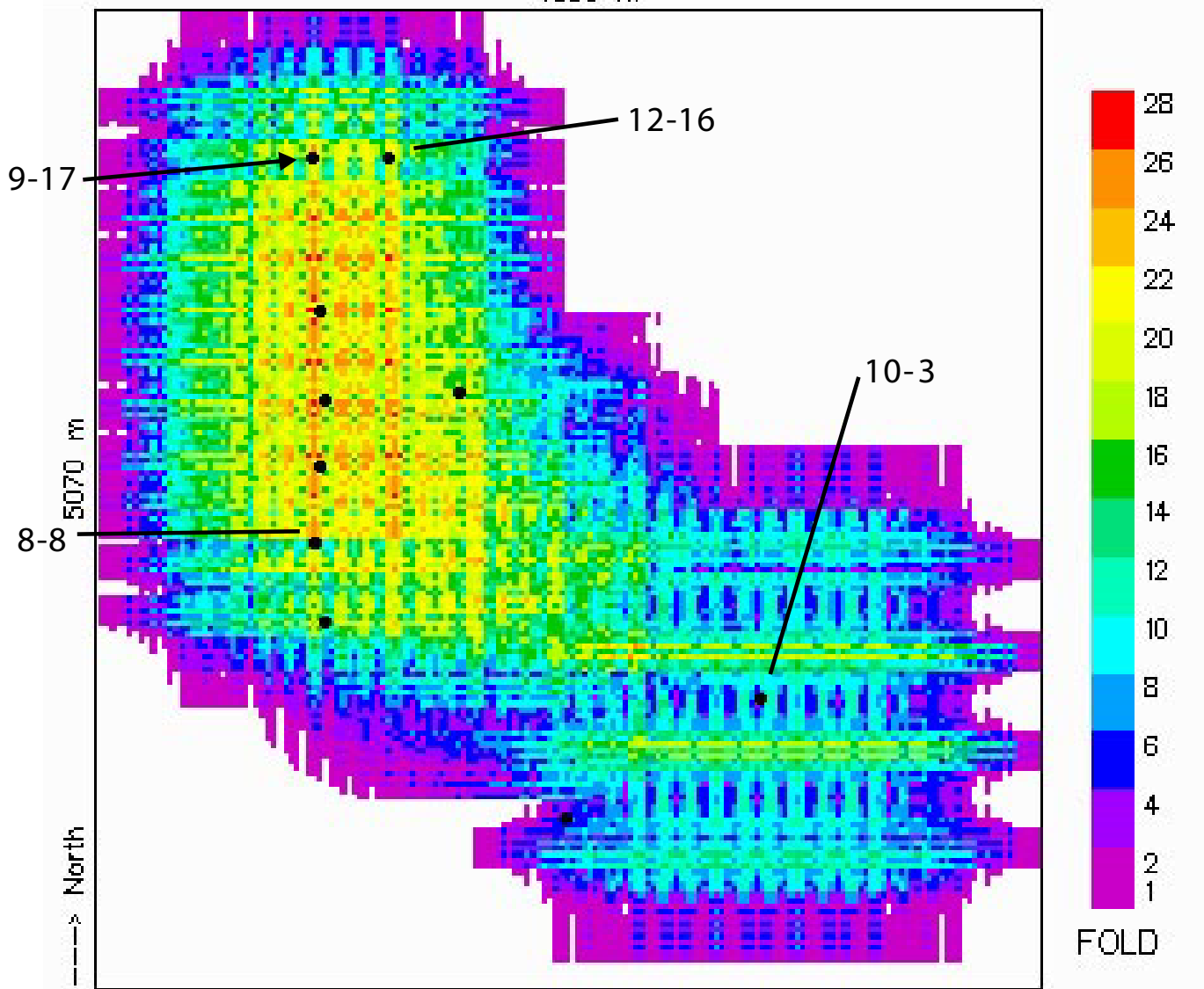


BLACKFOOT 3C-3D DESIGN 2

Figure 17

# ASYMPTOTIC P-S FOLD, OFFSETS 1200-1700 m

4950 m

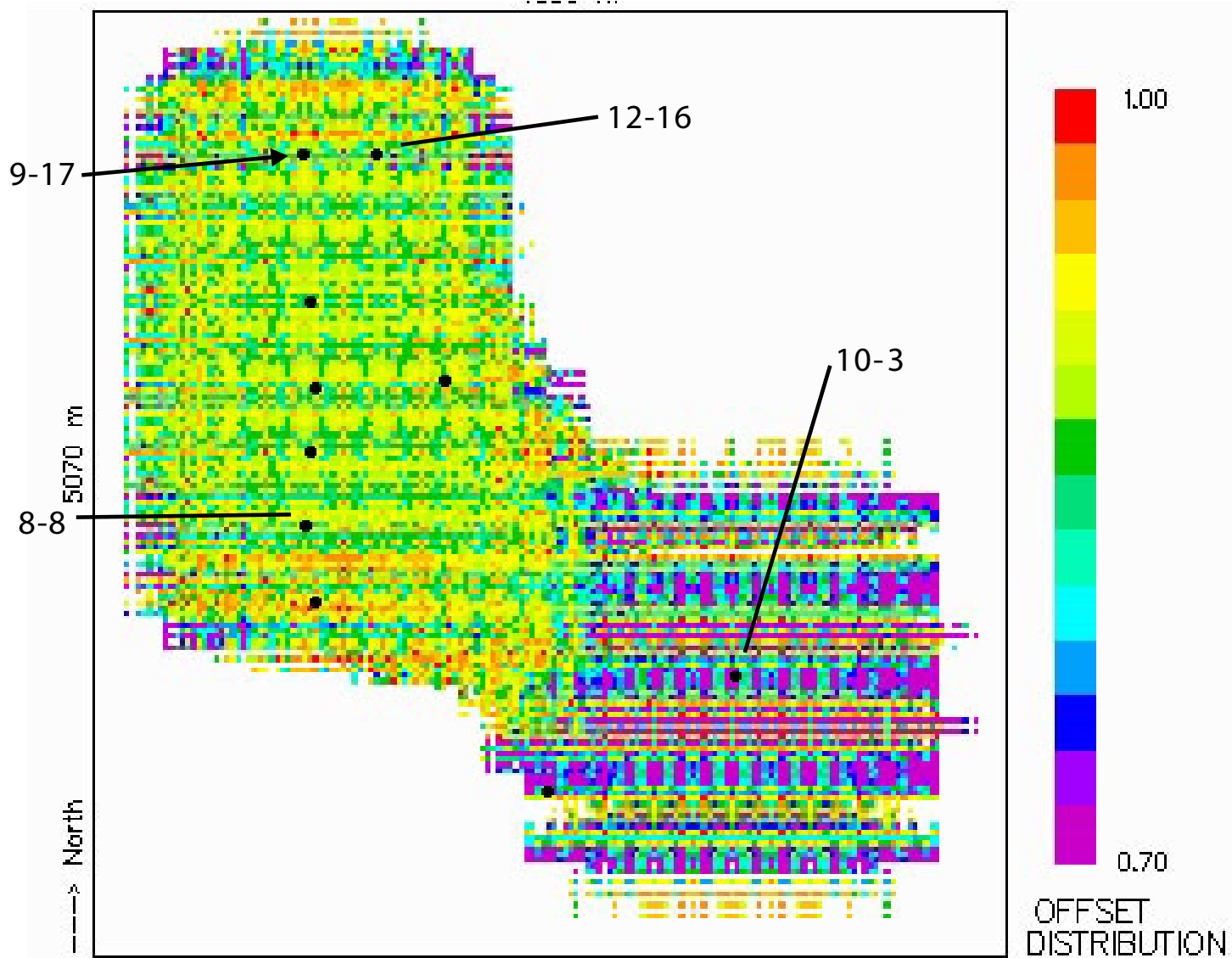


## BLACKFOOT 3C-3D DESIGN 2

Figure 18

# OFFSET DISTRIBUTION QUALITY, OFFSETS 300-1700 m

4950 m

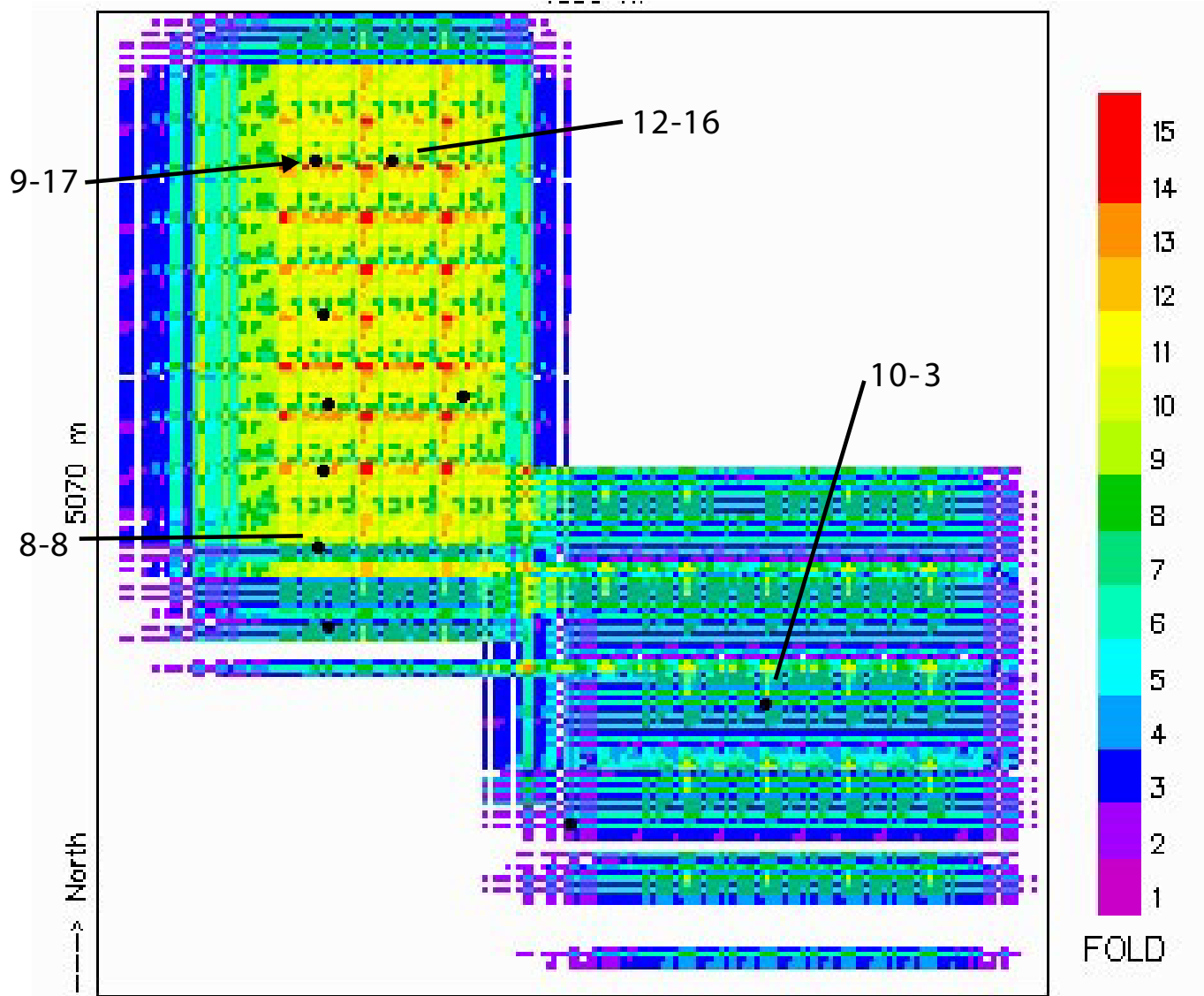


## BLACKFOOT 3C-3D DESIGN 2

Figure 19

P-S FOLD, AZIMUTHS 0 - 90 deg., OFFSETS 300-1700 m

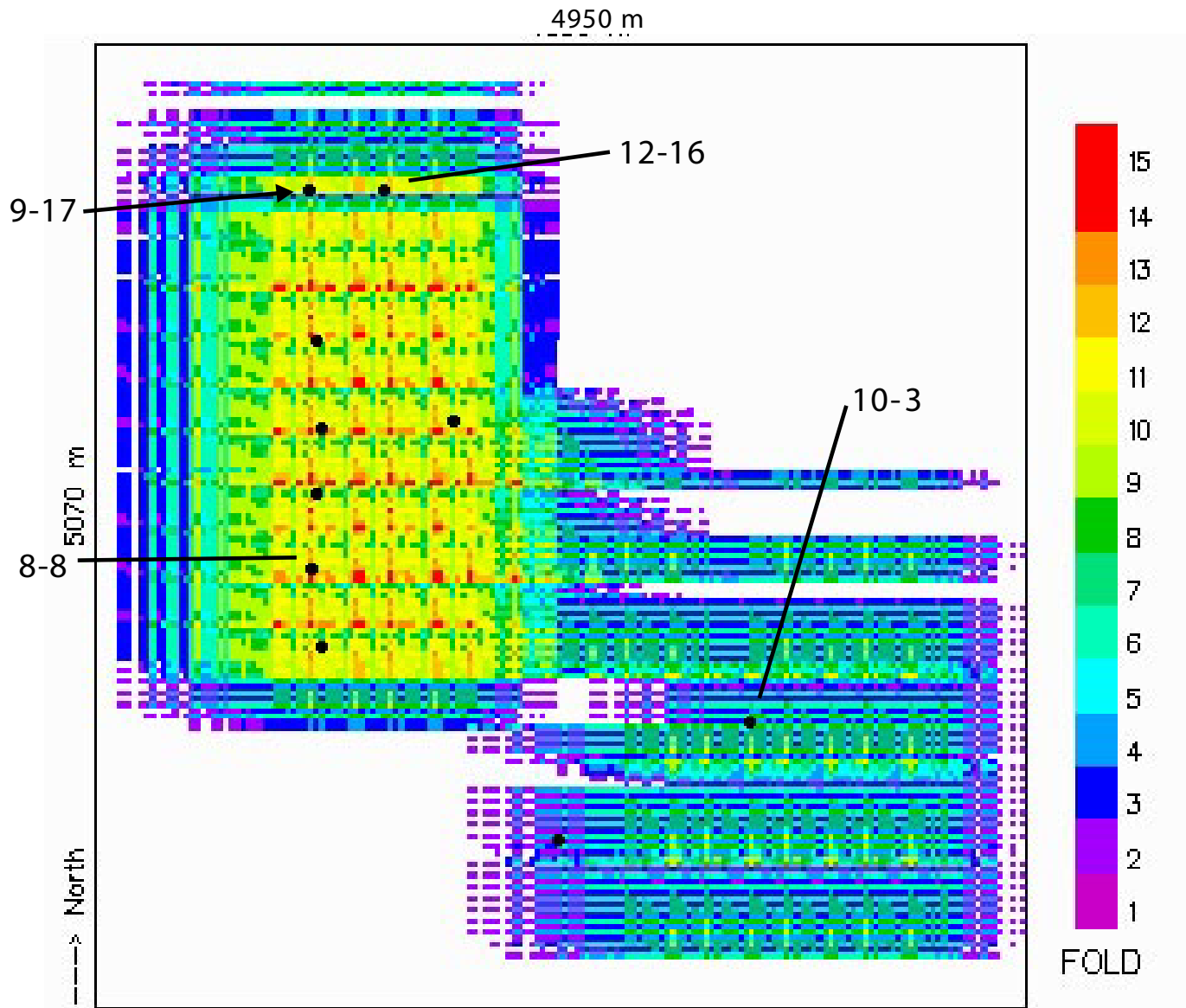
4950 m



BLACKFOOT 3C-3D DESIGN 2

Figure 20

P-S FOLD, AZIMUTHS 90 - 180 deg., OFFSETS 300-1700 m

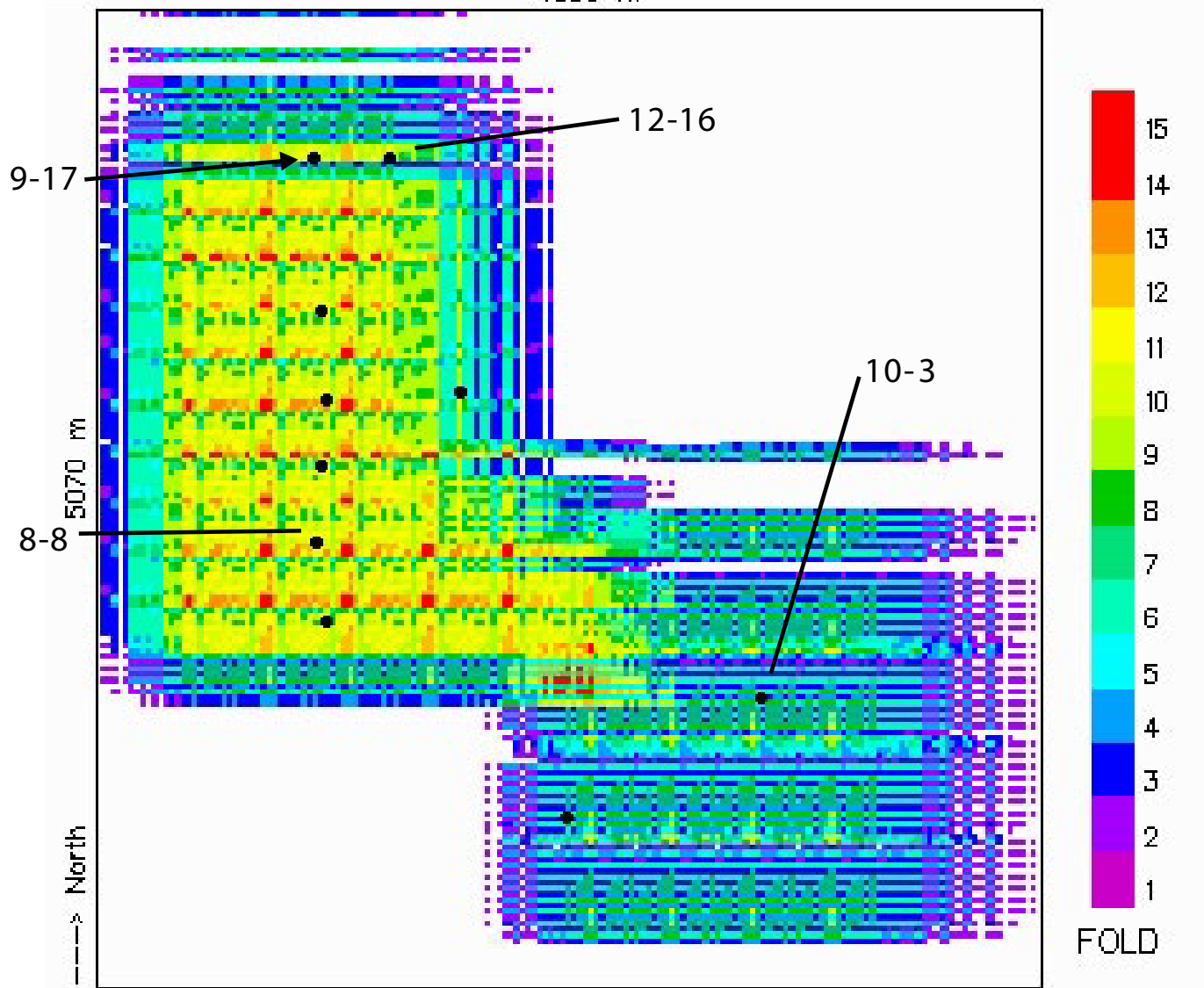


BLACKFOOT 3C-3D DESIGN 2

Figure 21

P-S FOLD, AZIMUTHS 180 - 270 deg., OFFSETS 300-1700 m

4950 m

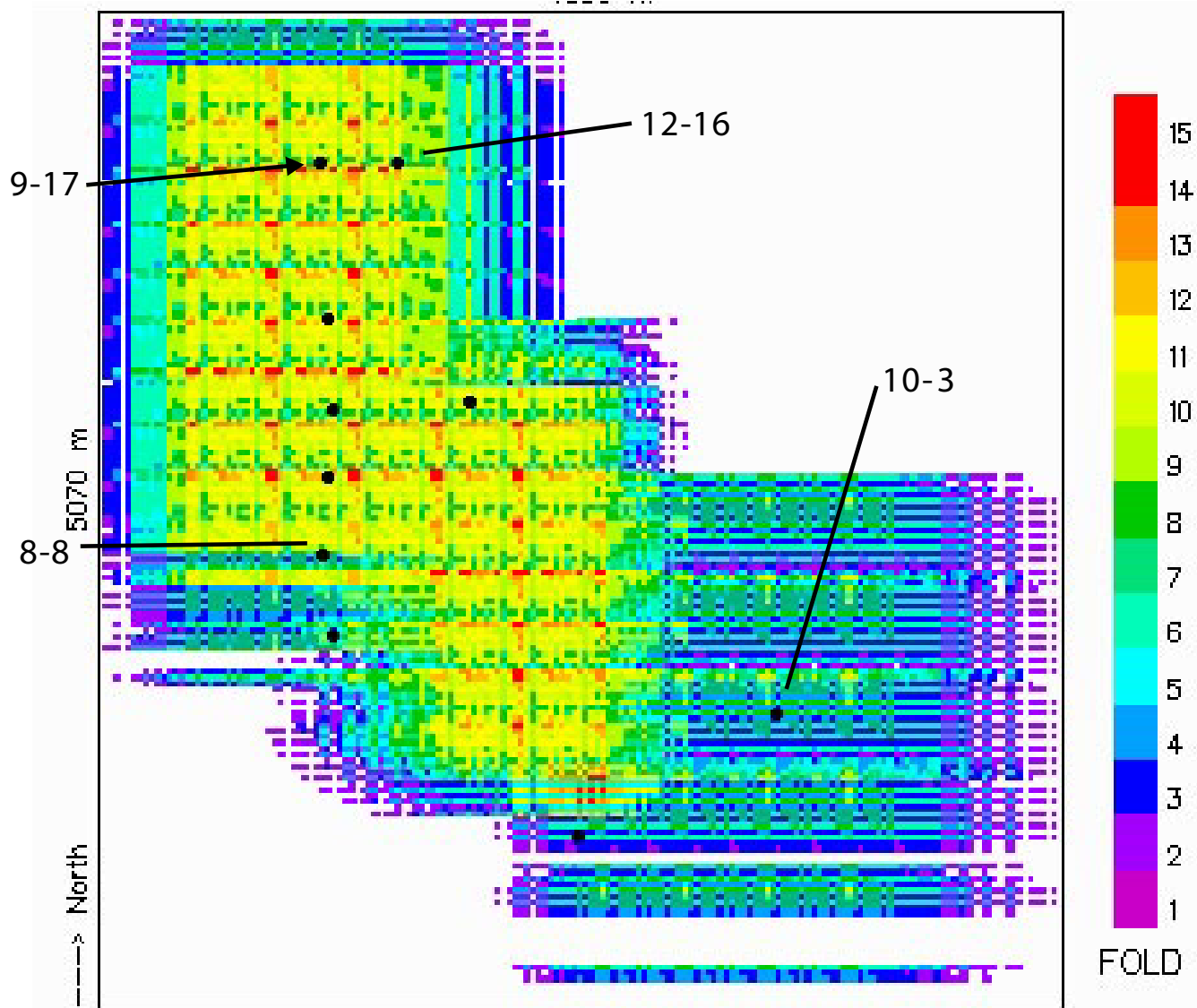


BLACKFOOT 3C-3D DESIGN 2

Figure 22

P-S FOLD, AZIMUTHS 270 - 360 deg., OFFSETS 300-1700 m

4950 m

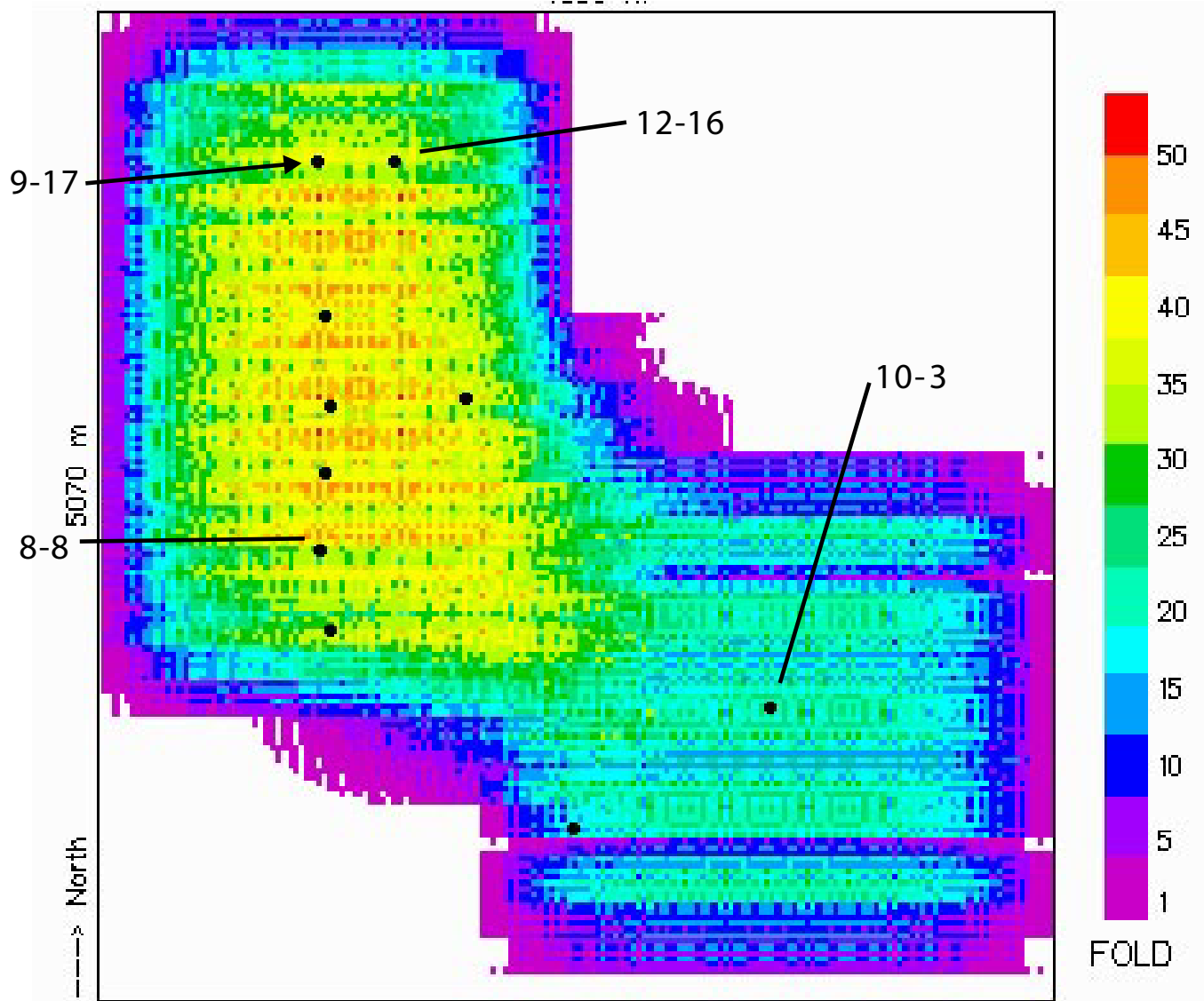


BLACKFOOT 3C-3D DESIGN 2

Figure 23

# DEPTH-VARIANT P-S FOLD, OFFSETS 300-1700 m

4950 m

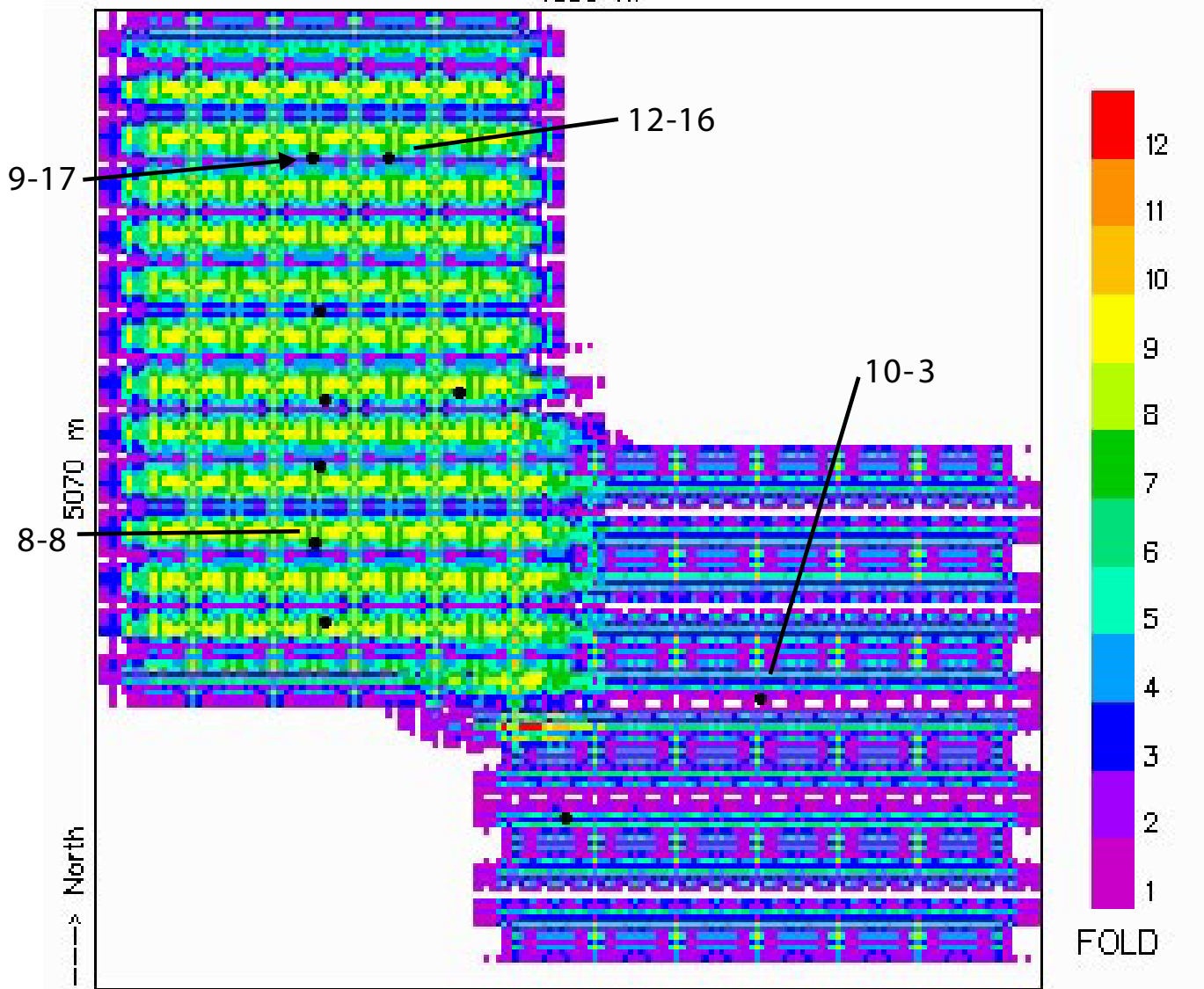


## BLACKFOOT 3C-3D DESIGN 2

Figure 24

# DEPTH-VARIANT P-S FOLD, OFFSETS 300-700 m

4950 m

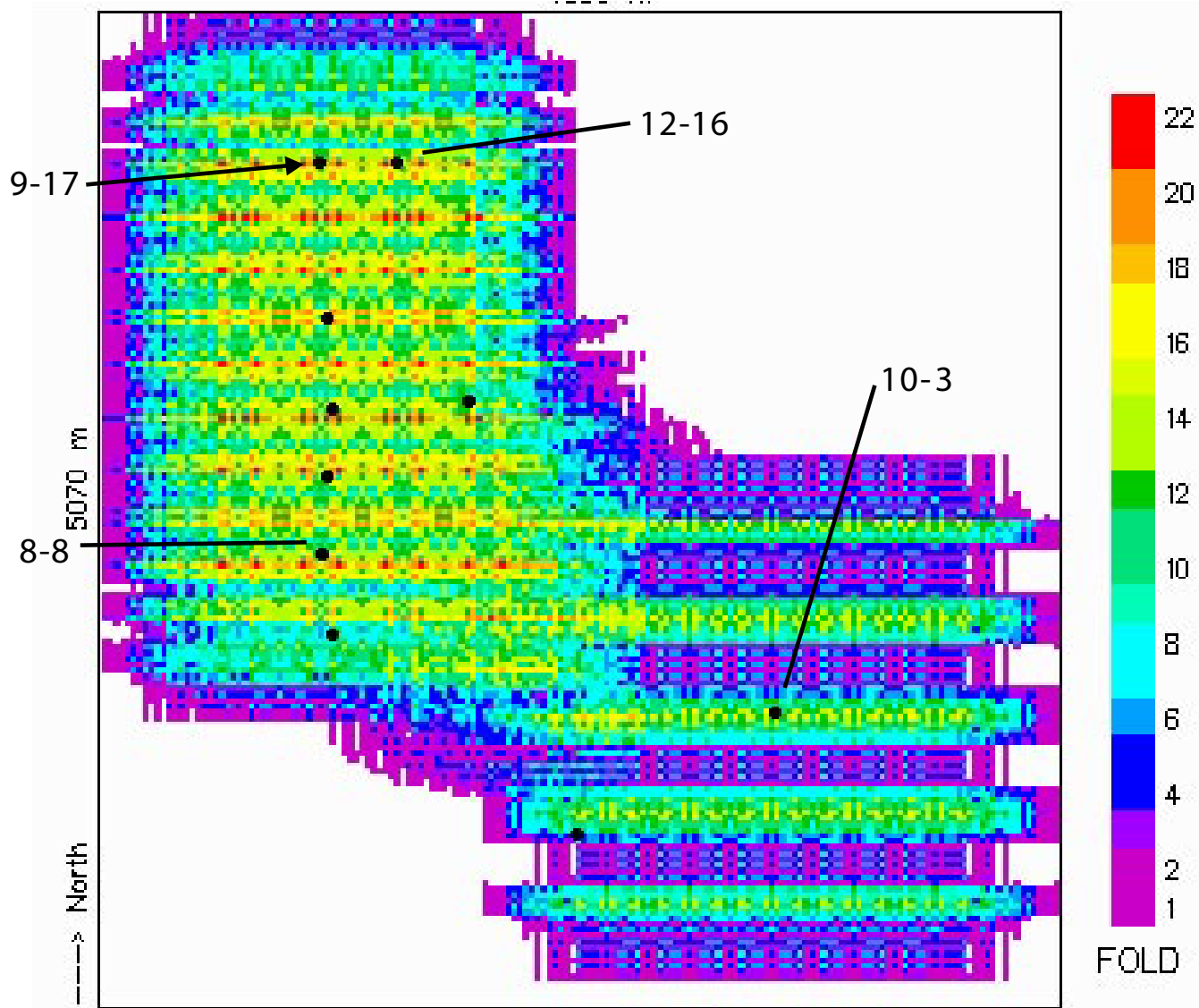


## BLACKFOOT 3C-3D DESIGN 2

Figure 25

# DEPTH-VARIANT P-S FOLD, OFFSETS 700-1200 m

4950 m

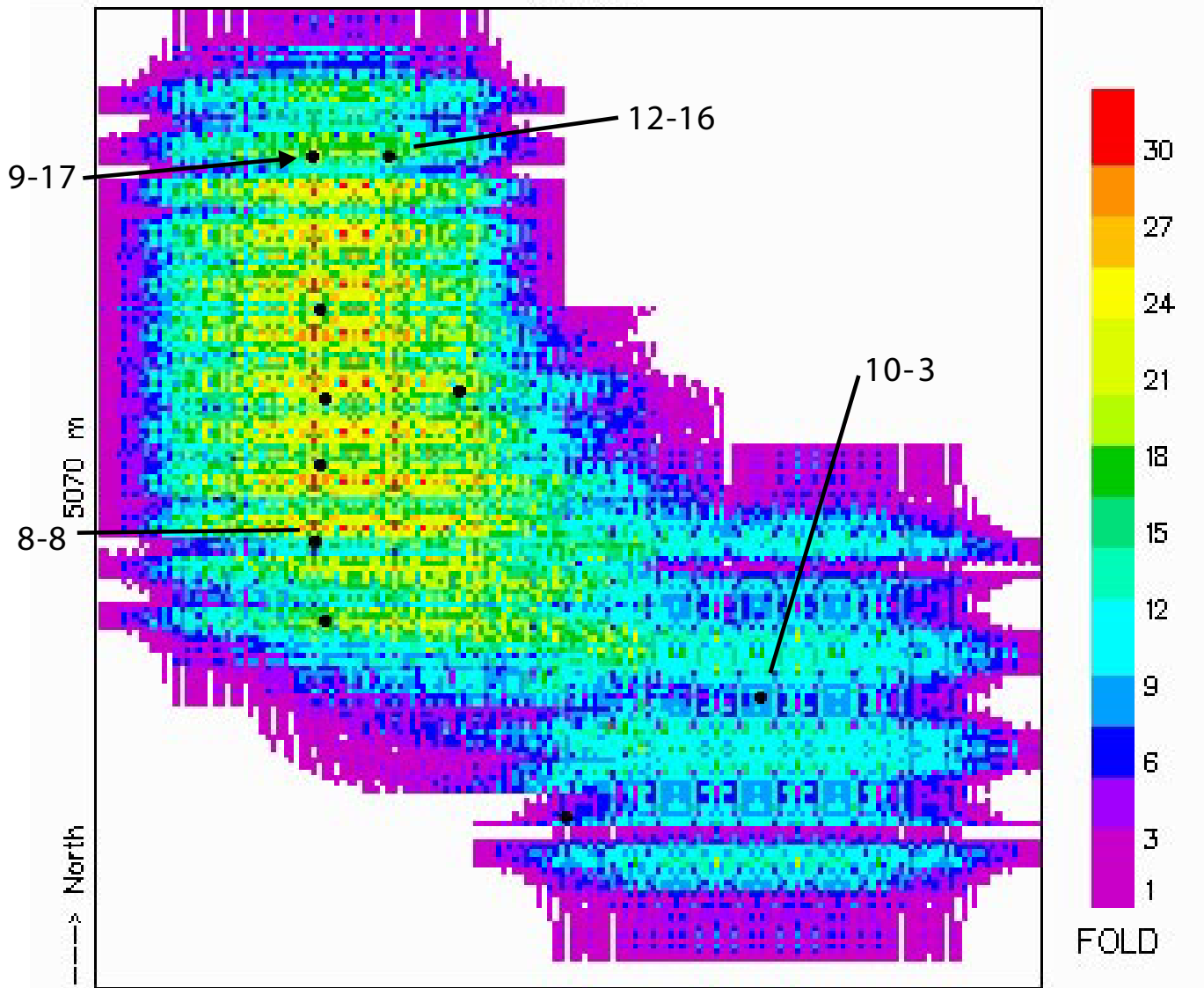


## BLACKFOOT 3C-3D DESIGN 2

Figure 26

# DEPTH-VARIANT P-S FOLD, OFFSETS 1200-1700 m

4950 m

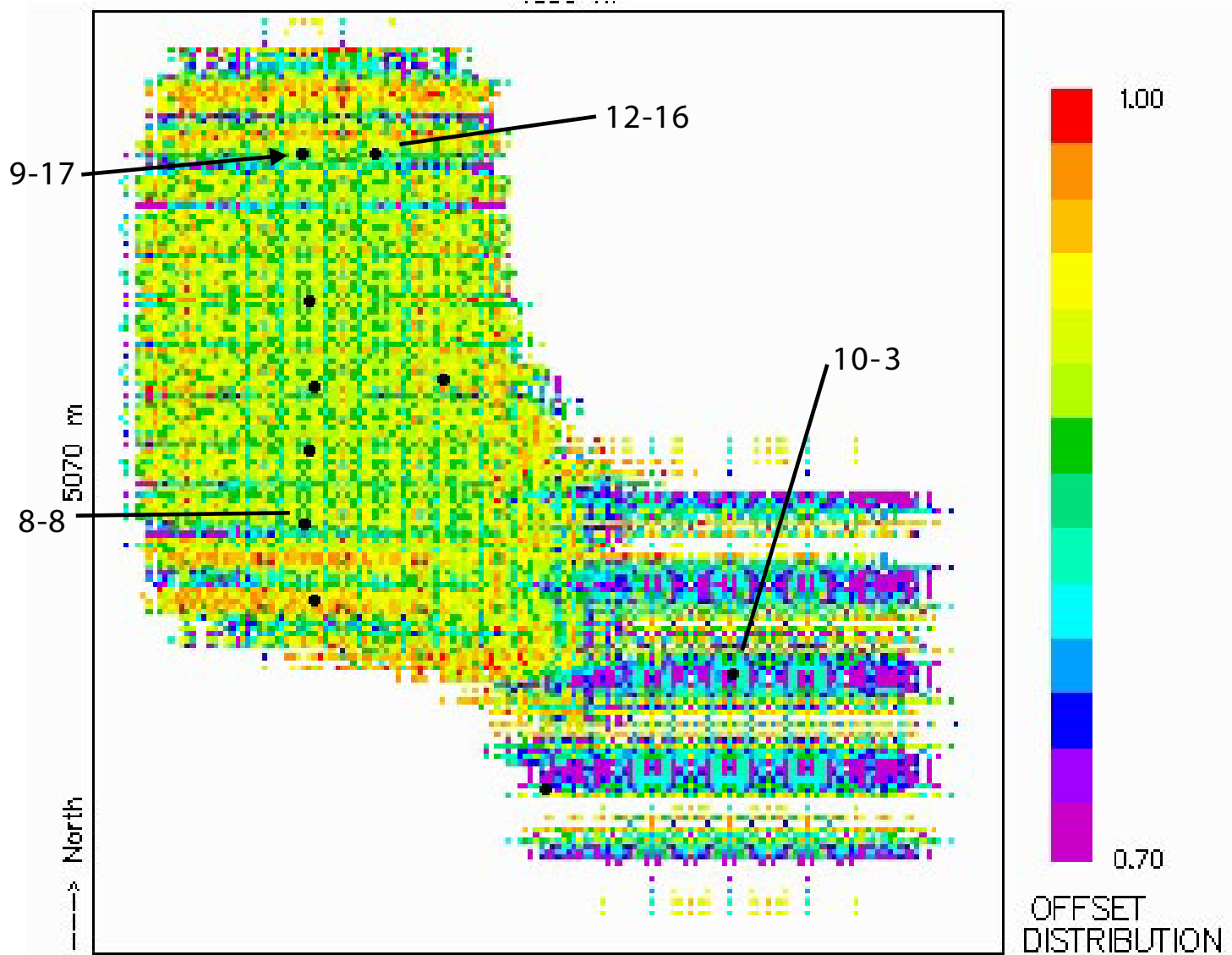


BLACKFOOT 3C-3D DESIGN 2

Figure 27

# D-V OFFSET DISTRIBUTION QUALITY, OFFSETS 300-1700 m

4950 m

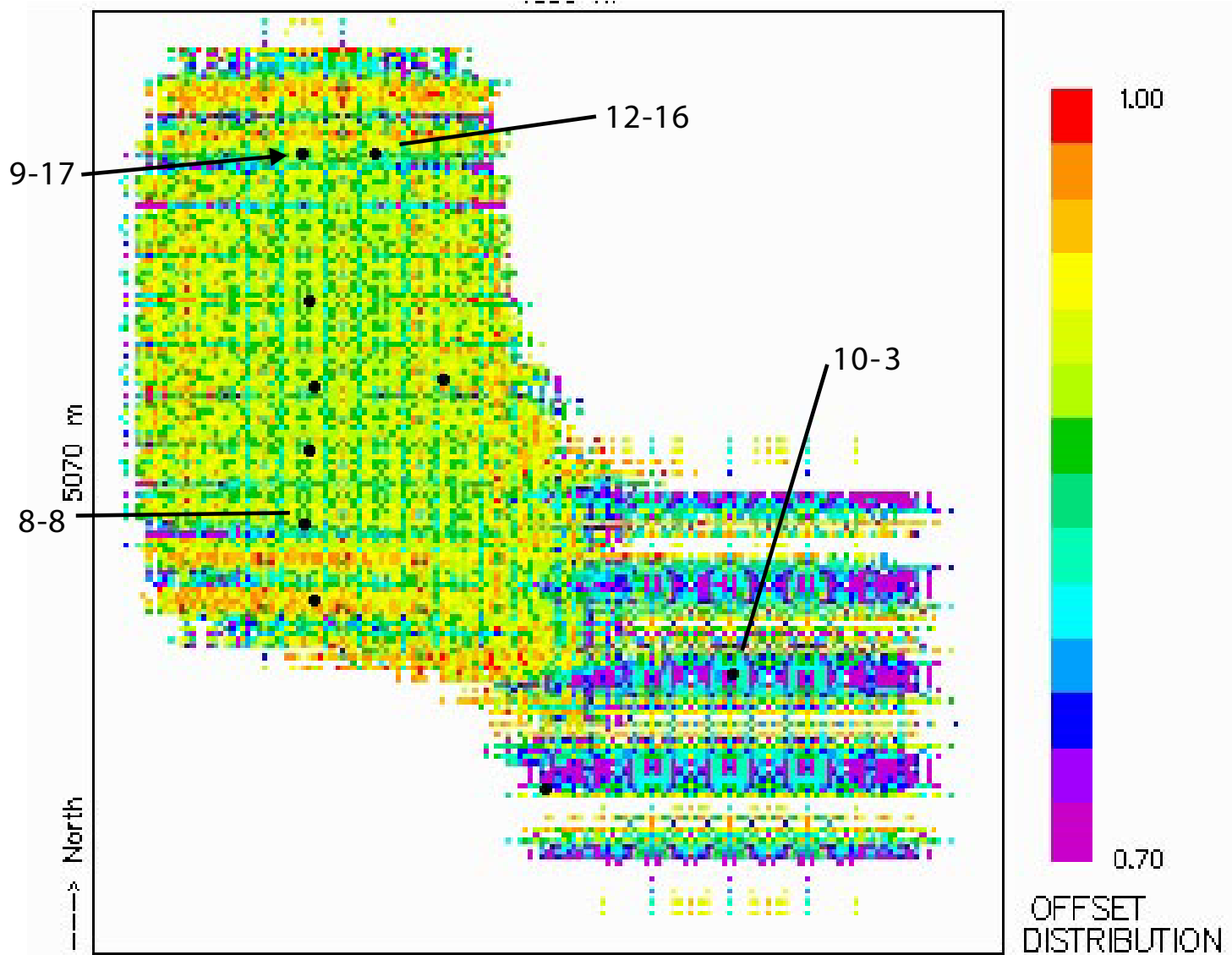


## BLACKFOOT 3C-3D DESIGN 2

Figure 27

# D-V OFFSET DISTRIBUTION QUALITY, OFFSETS 300-1700 m

4950 m

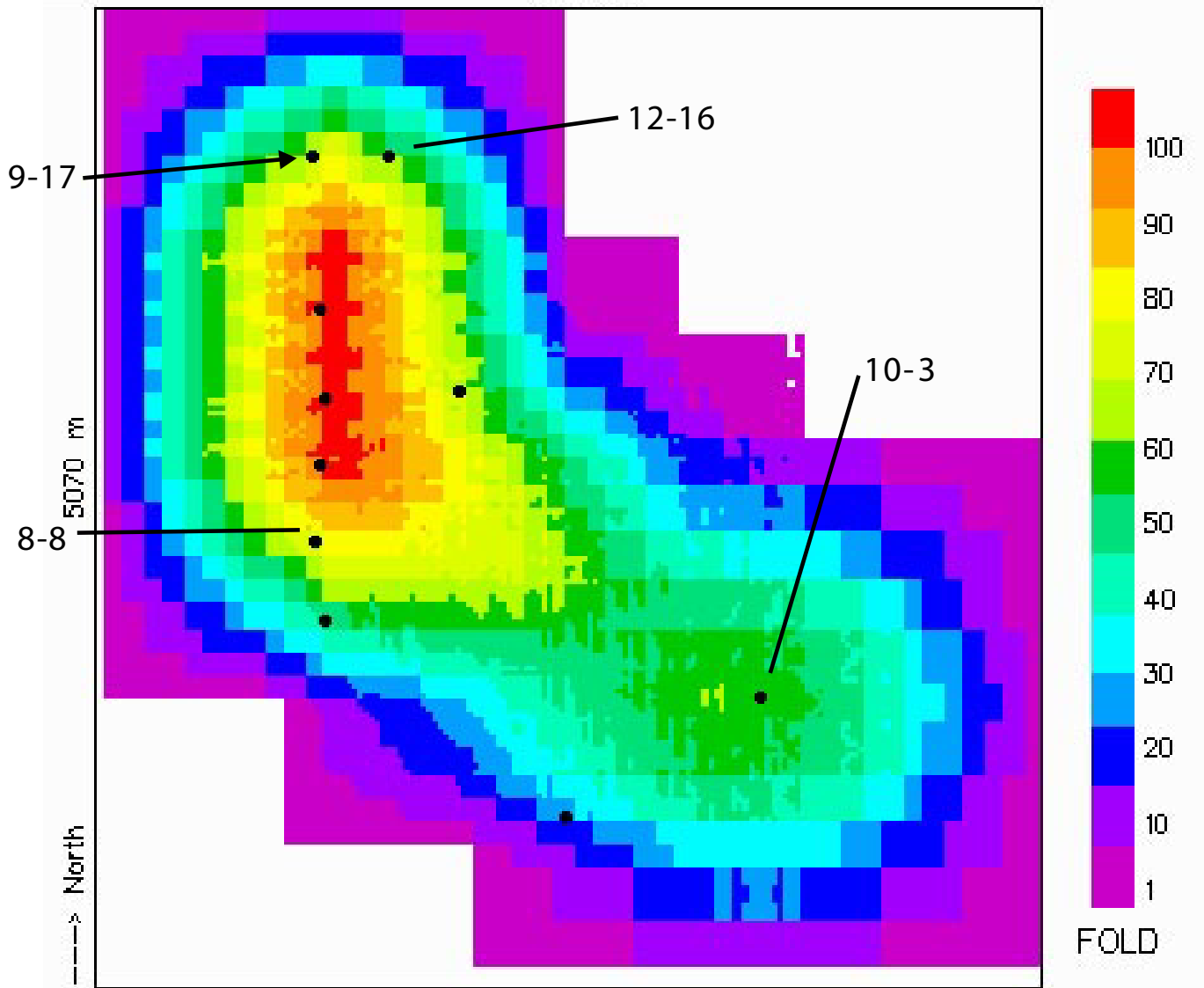


BLACKFOOT 3C-3D DESIGN 2

Figure 28

# P-P FOLD, OFFSETS 0-2700 m

4950 m

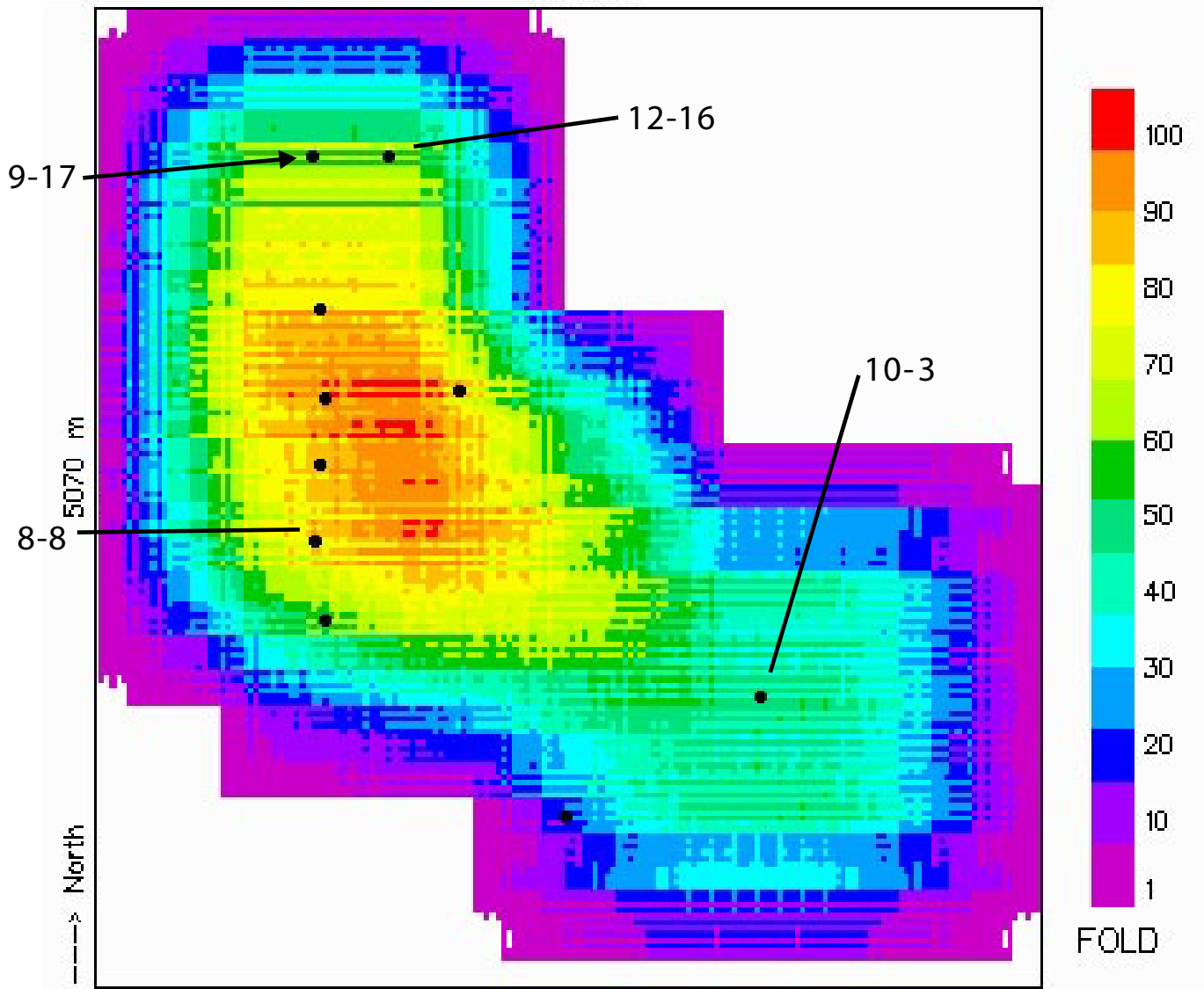


## BLACKFOOT 3C-3D DESIGN 2

Figure 29

# ASYMPTOTIC P-S FOLD, OFFSETS 400-2900 m

4950 m



BLACKFOOT 3C-3D DESIGN 2

Figure 30

# ASYMPTOTIC P-S OFFSET RANGE

4950 m

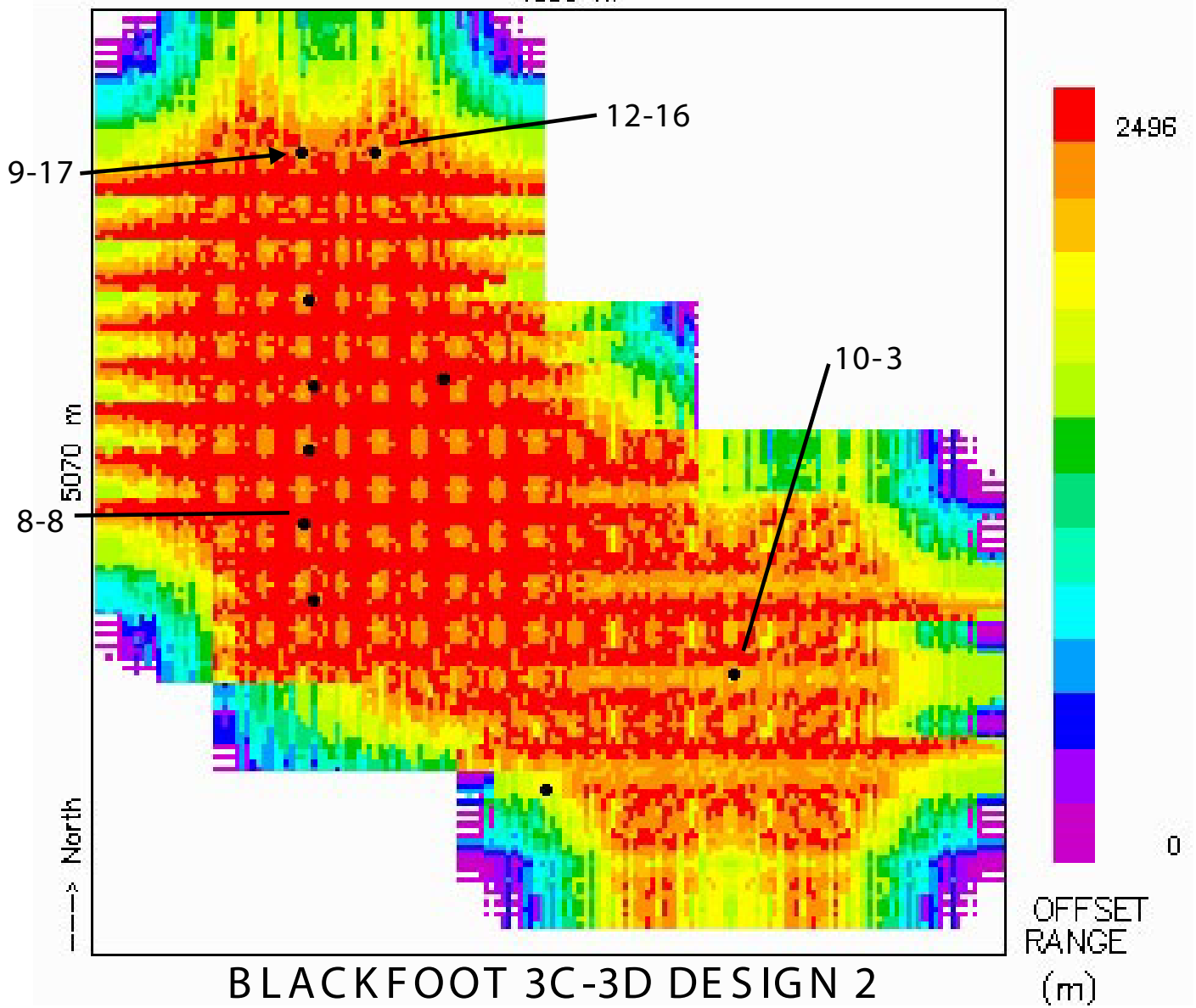
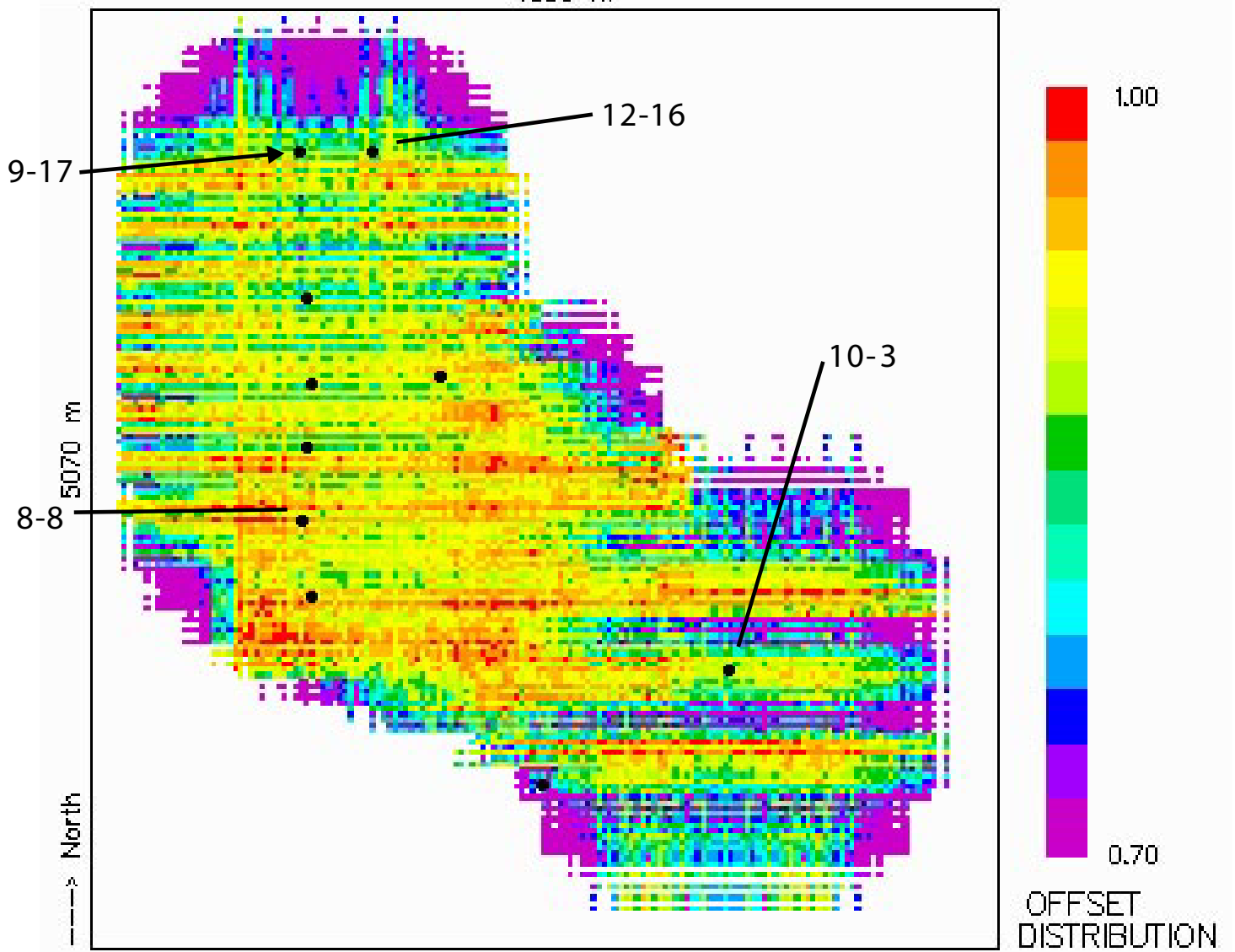


Figure 31

# P-S OFFSET DISTRIBUTION Q.F., OFFSETS 400-2900 m

4950 m

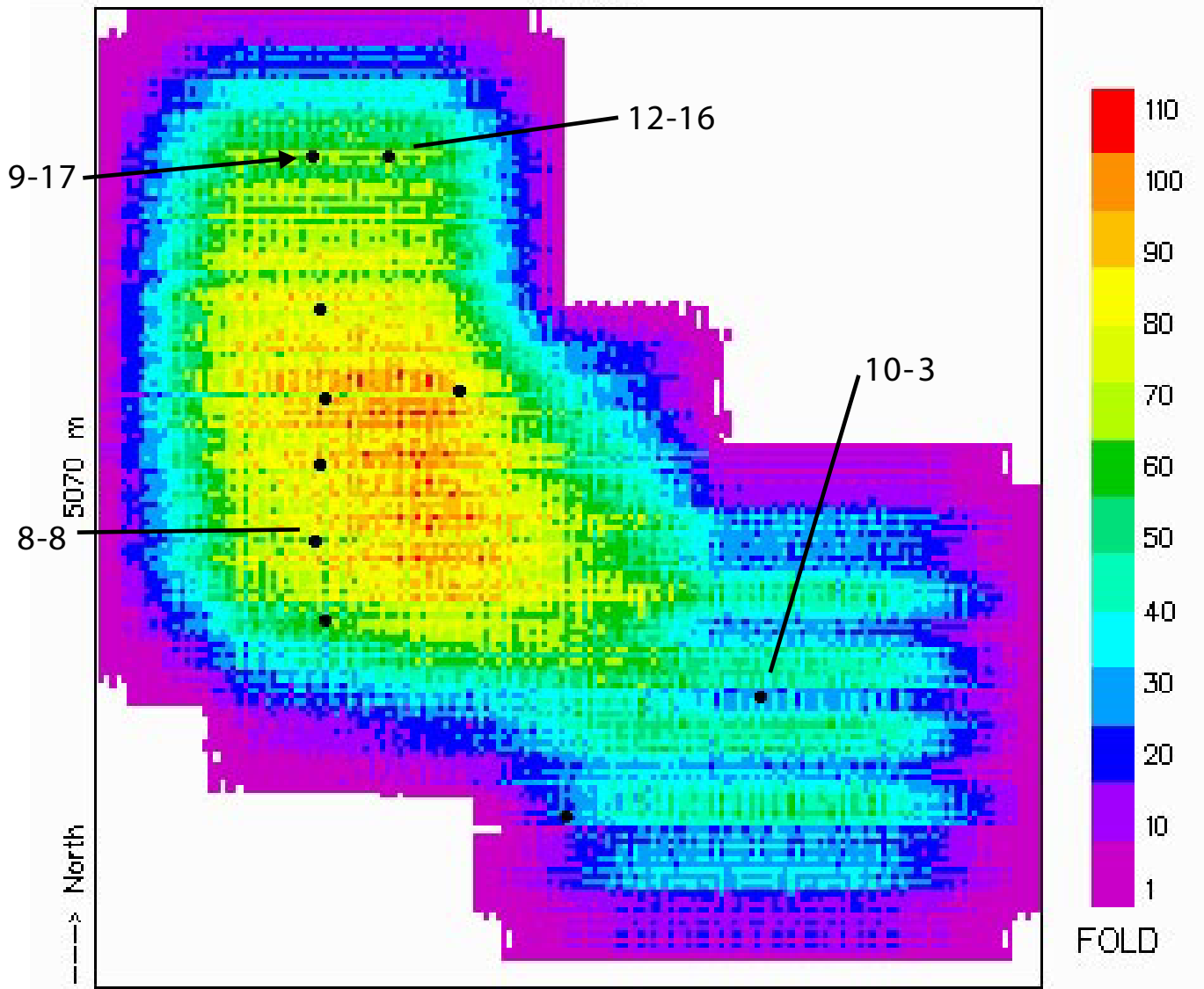


## BLACKFOOT 3C-3D DESIGN 2

Figure 32

### D.-V. P-S FOLD, OFFSETS 400-2900 m

4950 m



BLACKFOOT 3C-3D DESIGN 2

Figure 33

### D.-V. P-S OFFSET RANGE

4950 m

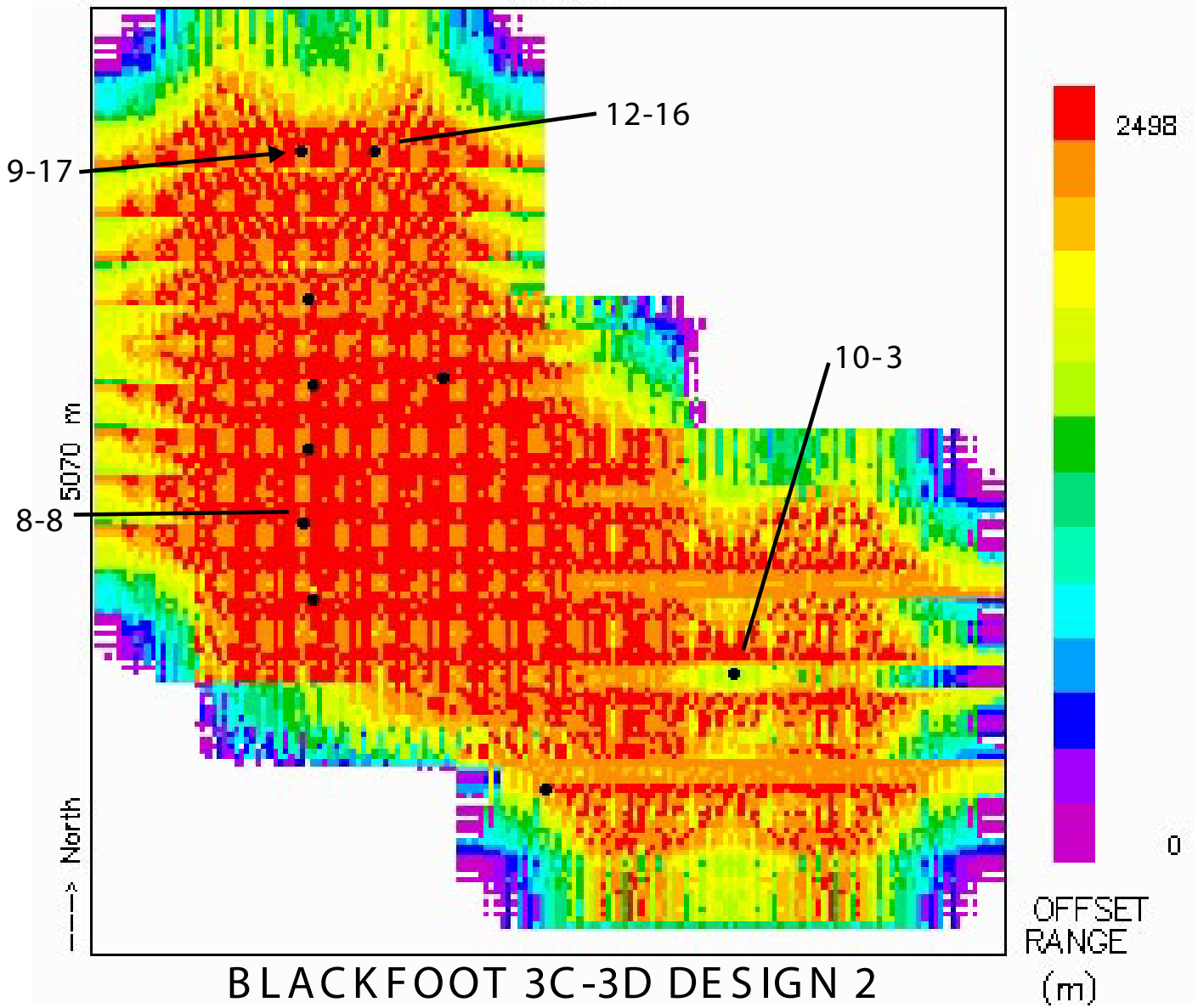
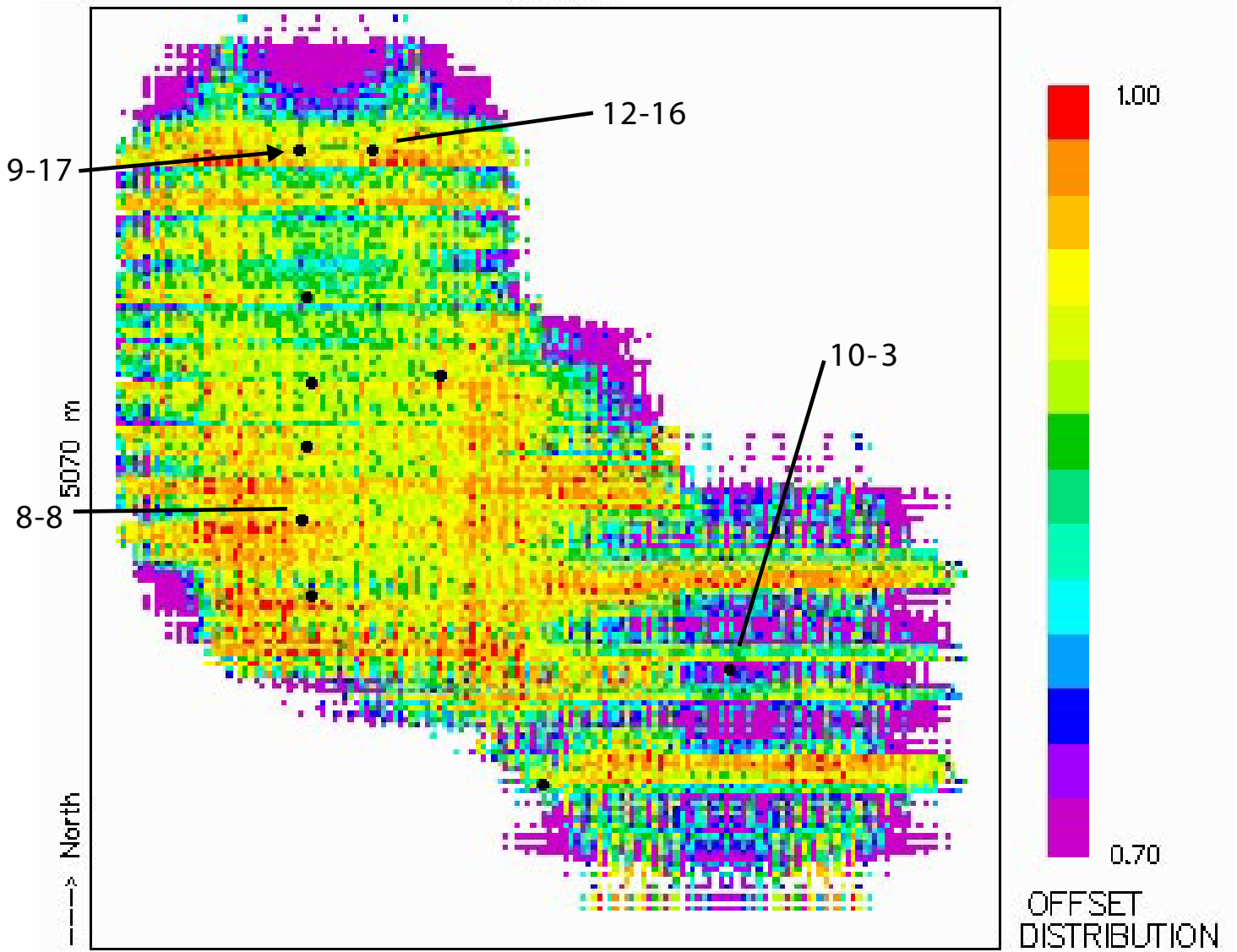


Figure 34

# P-S OFFSET DISTRIBUTION Q.F., OFFSETS 400-2900 m

4950 m



BLACKFOOT 3C-3D DESIGN 2